Alma Mater Studiorum – Università di Bologna

DOTTORATO DI RICERCA IN

INGEGNERIA BIOMEDICA, ELETTRICA E DEI SISTEMI

Ciclo 34

Settore Concorsuale: 09/E2 – INGEGNERIA DELL'ENERGIA ELETTRICA

Settore Scientifico Disciplinare: ING-IND/32 – CONVERTITORI, MACCHINE E AZIONAMENTI ELETTRICI

OPTIMIZATION OF THE POWER ELECTRONICS SYSTEM ASSOCIATED WITH OCEAN WAVE ELECTRIC GENERATORS

Presentata da: Mattia Mantellini

Coordinatore Dottorato

Prof. Michele Monaci

Supervisore

Prof. Luca Zarri

Co-supervisore

Ing. Riccardo Morici

Esame finale anno 2022

Table of contents

List of figures

List of tables

ABSTRACT

The present thesis is focused on wave energy, which is a particular kind of ocean energy, and is based on the activity carried out during the EU project SEA TITAN. The main scope of this work is the design of a power electronic section for an innovative wave energy extraction system based on a switched-reluctance machine.

In the first chapter, the general features of marine wave energy harvesting are treated. The concept of Wave Energy Converter (WEC) is introduced as well as the mathematical description of the waves, their characterization and measurement, the WEC classification, the operating principles and the standardization framework. Also, detailed considerations on the environmental impact are presented. The SEA TITAN project is briefly described.

The second chapter is dedicated to the technical issues of the SEA TITAN project, such as the operating principle, the performance optimization carried out in the project, the main innovations as well as interesting demonstrations on the behavior of the generator and its control.

In the third chapter, the power electronics converters of SEA TITAN are described, and the design choices, procedures and calculations are shown, with a further insight into the application given by analyzing the MATLAB Simulink model of the system and its control scheme.

Experimental tests are reported in the fourth chapter, with graphs and illustrations of the power electronic apparatus interfaced with the real machine.

Finally, the conclusion in the fifth chapter offers a global overview of the project and opens further development pathways.

Preface

World energy situation

In recent decades, following the growth of the world energy demand, the interest in electrical energy production from renewable sources has increased as well. New alternative energy sources have been exploited, gradually abandoning traditional fossil fuels such as oil, coal and natural gas.

Europe's 2050 Energy Strategy has established as a target the reduction in greenhouse gas emissions by 80%-95% compared to the 1990 level, and renewable energy accounting for at least 64% and up to 97% of the electricity consumed: main reasons are not only related to global warming, pollution and environment protection but also to the risk of an availability crisis of traditional sources (their left time is counted in tens of years [1]). As climate changes are modifying habitats at a rate faster than many species can adapt and pollution is becoming day by day a worse problem in every part of the world, a possible future worldwide shortage of energy supply might have devasting consequences, and the uneven distribution of fossil fuels might give birth to conflicts.

Thus, the need for more sustainable energy sources is justified.

According to an estimation by the International Energy Agency (IEA), the world energy consumption stands around 18˙000 TWh per year (i.e., more than 2 TW). Such a demand is due to an increase in the population (ten billion is expected to be reached at the end of the century), energivorous technologies and comforts. Although an analysis conducted from 1973 to 2010 has revealed that the use of renewable energy sources has greatly increased, their incidence nowadays is still low compared to fossil fuels in the world energy balance [2] – [3], as visible in Figure I.

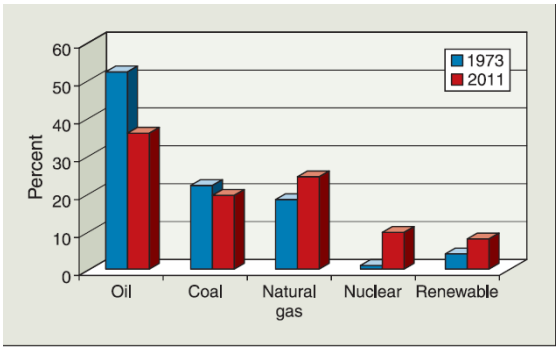

Figure I World energy sources distribution comparison between 1973 and 2011.

Why ocean energy?

Solar and wind energies are the better known and more widespread renewable sources but, with an occupied area equal to 71% of the Earth's surface, the oceanic masses hide a huge amount of energy. IEA studies say that, by fully exploiting ocean energy, a total potential production of 40˙000 TWh per year (i.e., more than 4.5 TW) would be obtained, more than double the necessity.

The IEA Ocean Energy Systems Committee has stated that “ocean energy could have up to 750 GW installed by 2050 with 160,000 direct jobs created by 2030”.

So, marine energy represents a significant resource that cannot be ignored, especially when facing an increasing energy consumption and demand.

Ocean energy can be exploited in many forms. This is why many different technologies have been developed and optimized in different areas of the globe, each one with its own operating principle, advantages and disadvantages.

Above all, differences between various ocean energy generation systems concern the way the energy is captured and converted into electricity, since the other subsystems in the energy harvesting process remain more or less the same with slightly adaptations.

Generally speaking, the great advantage of ocean energy compared to traditional renewable sources lies in the greater constancy, predictability and higher energy density of the former compared to the latter [4].

Although many technical aspects and technology knowledge of marine power harvesting have been known for many years, interest in ocean energy exploitation has increased in the 70’s, following the oil crisis.

An everlasting behavior of human civilization has always been the development of new technologies and, consequently, an increase in energy demand to support activities and comforts. It is not possible, indeed, to stop the scientific progress. Ocean energy can be, together with other well-known renewable sources, an important answer to satisfy the newborn necessities, but the only way to restrain global warming, pollution and the insane exploitation of the natural resources is an higher common awareness, especially in the developed countries.

It is fine to exploit energy sources that have a low impact on pollution and a soft environmental footprint, but it would be a temporary placebo if not coupled to the consciousness that something must change. Energy saving policies must be implemented and an ecofriendly-oriented attitude must be accepted with sacrifices from everyone.

However, ocean energy harvesting systems are not free from environmental impact, although it mainly depends on deployment and construction phases and it is strongly influenced by the chosen configuration, so it can significantly be reduced with prudent decisions.

Chapter 1 Wave Energy Conversion

Ocean energy can be exploited in many ways, depending on which technology is adopted in the generation point. Each technology differs from the others in the way the energy is captured and then converted into electricity. Here follows a list of many different exploitable ocean energy sources.

- **Submarine currents** are influenced by the earth rotation and are highly predictable. They are caused by water temperature differences: water at the Equator, which becomes hotter due to sun rays incidence, moves towards the poles and here it cools, sinks and moves back towards the Equator. Such a waterflow is subjected to speed variations, which occur in a cyclic way with about a ten-year period (the so-called thermohaline cycle). The energy harvesting systems of ocean currents are similar to wind turbines but, since water is denser than air, the size of ocean current turbines is lower for a certain produced power and, from the point of view of the environmental impact, that is better.
- **Tides** are caused by moon gravitational pull. Depending on the location is possible to find different kind of cyclic behavior: semi-diurnal, diurnal and fourteen days cycle have been observed. When the tide rises, a proper reservoir artificially made with barrages is filled and it empties during tide ebb phase. These water transfers can be exploited using a proper water turbine linked to an electrical generator.
- **Tidal currents** are results of tides and, like them, they are highly predictable. In this case, water flow is bidirectional in the same tidal cycle, because the direction at the beginning is the opposite to that at the end of the cycle. Such an energy source can be harvested in particular geographical conditions like narrow waterways, straits, bays or harbors entrances. Energy harvesting systems are similar to wind turbine too, as for ocean currents.
- **Thermal gradient** is a natural temperature gradient as function of depth especially in tropical oceans. Due to its characteristics, it is less weather dependent and more stable with respect to tides and tidal currents. Technologies used to harvest this energy source are based on a low boiling-point material (ammonia for instance), which is vaporized and drives a turbine, followed by a cooling section where this material is restored at a liquid phase.

- **Salinity gradient** is naturally present between freshwater and seawater. Thus, the different chemical potential can be exploited through technics as Pressure Retarded Osmosis, where a permeable membrane separates two solutions with different saline concentration and the generated water flow is easily converted into electricity by a normal hydroelectric turbine.
- **Waves** are caused by winds blowing over the oceans causing water movements. Many technologies to catch wave movements in different ways have been designed and each one differs from the others in the mechanical-to-electrical energy transformation process.

1.1 Qualitative analysis of the waves

The present thesis is focused on the exploitation of the ocean wave energy. Together with ocean currents, they represent the most commercially viable ocean energy sources [3]. Thus, they are very studied and developed, although many limits have still to be overcome.

The waves considered in this work must not be confused with the waves that are seen breaking on the beach. Indeed, in shallows water (i.e., when the water depth is lower than half a wavelength under the assumption of sinusoidal marine waves), waves slow down, their wavelength decreases and they rise up in height before breaking. The major losses of energy are due to breaking and seabed friction, so shoreline waves carry less power that can be extracted.

1.1.1 WAVE ORIGIN AND DISTRIBUTION

Waves are caused by different temperatures on the earth surface due to different heating by the sun. A temperature gradient on earth causes, indeed, a massive air flow with powerful winds which are responsible for wave movement. The amount of energy transferred from air masses to ocean masses depends on the wind speed, time applied and distances: strong winds (also storms) must insist for an extended time over a large distance (i.e. the “fetch”), and such a situation must repeat periodically in order to create an useful energy source and a significant storage (swells) even when wind is absent.

First, waves born as small ripples and they increase in size thanks to the energy extracted from blowing winds. There is a limit in growing due to balance between energy losses and energy input from winds. If this limit is reached (it depends on wind speed and fetch), waves

are fully developed. When the wind stops blowing, waves can travel long distances with little energy losses, becoming “swell” waves. This process is graphically described in Figure 1.1 [1]. Since waves with different periods travel at different speeds, a wave energy harvesting system located at a certain distance from the wave generation point experience first waves with a longer period, then those with a shorter period, thereby permitting a sustained recovery of the high power pulse originated by winds.

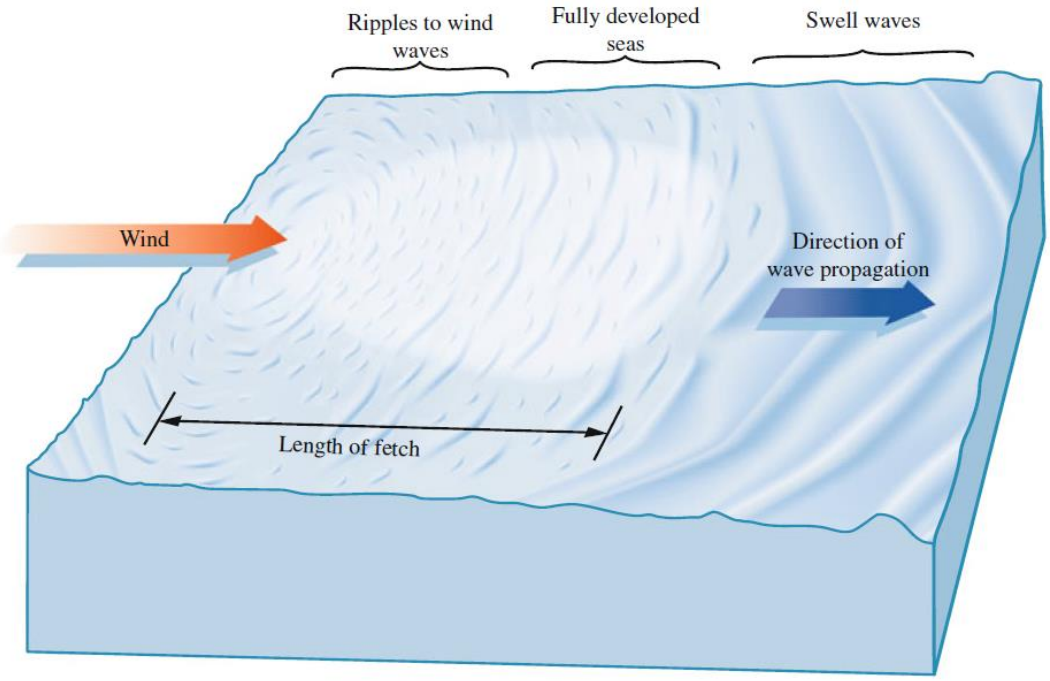

Figure 1.1 Wave generation process.

Thus, the distribution of wave kinetic energy is not uniform but is influenced by winds distribution: it is mainly concentrated between 30 and 60 degrees of latitude in both hemispheres and, due to the greater force of the western winds, it has greater intensity in the western coasts of the continents. Average wave power varies also seasonally: in winter levels increase up to 6 times compared to the summer season. The following regions offer the highest wave energy potentials over the globe: coasts of the Western Europe, Canada, United States, the south-western coast of Australia, New Zeland, South America and South Africa [3] – [4].

In Figure 1.2 an overview of the global wave force distribution is shown. To make a quantitative analysis, values in kW/m (which is the amount of available power per wave crest meters called “power per meter of wave front” or “average omni-directional wave power”) are given and reported in the figure.

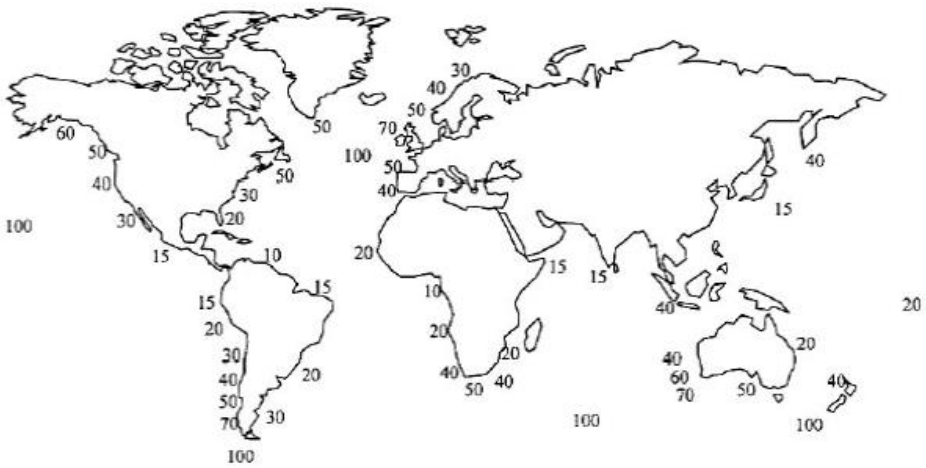

Figure 1.2 World wave force distribution.

The set of all characteristics, which identify a certain wave environment, is called "wave climate". The main parameters related to wave climate are period, height, wavelength, occurrence and total mean water depth. This information is very important in order to perform a proper and optimized design of a wave-energy conversion system at a certain location, especially when choosing the right motion device responsible for catching the mechanical energy of the waves.

1.1.2 WAVE ENERGY REPRESENTATION

Power per meter of wave front expressed in [kW/m] corresponds to an important indicator for the assessment of wave-energy capability but, when considering just this simple parameter to compare different wave sites, information regarding directional, temporal and spectral characteristics lacks, resulting in an incomplete evaluation about the real average power potential.

Another issue is that average omni-directional wave power takes into account energy contributions from all events irrespective of their exploitability. The power rate of the storms, for instance, which is a very relevant contribution to the total power amount, is usually unexploitable due to severe stresses experienced by energy conversion systems.

In order to compensate such a distortion, other information is necessary when evaluating a certain site and this data are still not sufficient to make a complete analysis, because power capture also depends, for instance, on the interaction between the energy conversion system configuration and the waves, which is barely predictable.

Thus, although the power per meter of wave front is a useful datum to understand wave uneven distribution, it is not the only one to be taken into consideration when choosing an ocean wave energy production site [1].

Usually, after the identification of a possible site of interest for ocean wave power exploitation, a scatter diagram is produced in order to make a preliminary characterization. As reported in Figure 1.3, a scattered diagram reports occurrence frequency for a certain wave as a function of a representative period *Tz* (peak period, zero-crossing period or energy period) and a representative height *Hs* (typically the significant wave height which is the average wave height of the highest one-third of the waves). These last two parameters are put in the vertical and horizontal axes and the resulting grid is filled with the occurrence probability.

Scatter diagram

Hs \ Tz	3.5	4.5	5.5	6.5	7.5	8.5	9.5	10.5	11.5	12.5	13.5	14.5
0.25	0.0066	0.0056	0.0030	0.0023	0.0011	0.0007	0.0003	0.00005				
1	0.0453	0.1650	0.0906	0.0347	0.0131	0.0047	0.0019	0.00069	0.0001	0.00004	0.00007	0.00005
2	0.0018	0.0368	0.1604	0.0650	0.0229	0.0099	0.0032	0.00121	0.00009	0.00005	0.00005	
3		0.0003	0.0187	0.1084	0.0335	0.0071	0.0033	0.00171	0.0004	0.00007		0.00002
4			0	0.01021	0.05565	0.01163	0.00209	0.00052	0.00034	0.00021	0.00005	
5				0.00002	0.00729	0.02391	0.00301	0.00069	0.00031	0.00014	0.00005	0.00005
6					0.00012	0.00603	0.00691	0.00052	0.00007			
7				0.00002	0.00009	0.00026	0.00352	0.00152	0.00016	0.00005		
8							0.00062	0.00288	0.00017			
9								0.00086	0.00073	0.00002		
10								0.00002	0.00043	0.00016		
11									0.00011	0.00014		
12										0.00004		

Figure 1.3 Example of a scatter diagram.

Thanks to scatter diagrams, more detailed information with respect to average omni-directional wave power are available, but the precision of such a table depends on the resolution of vertical and horizontal characteristics.

A negative issue related to scatter diagrams is the lack of temporal/directional or spectral information.

1.1.3 COMPARISON WITH OTHER ENERGY SOURCES

The potentially exploitable wave power all over the world is estimated to be more than 1 TW [4].

It is not easy to list positive and negative aspects of such an innovative technology at the present stage of development. However, considerations can be done about general common aspects of renewable energy harvesting in comparison with other generic energy sources.

When comparing wave energy with other traditional renewable energy sources, some advantages of the former with respect to the latter can be highlighted:

- **constancy**: waves are present 24 hours a day for seven days a week even during the night, in cloudy conditions and in low speed wind conditions (swells);
- **predictability**: intensity can be predicted several days before the arrival;
- **little energy losses**: waves losses are virtually zero while travelling very long distances (this is a unique feature),
- **high power density**: many studies say that the available energy per square meter provided by the wave motion is 15-20 times higher than either wind or solar source [5] (about 1 kW/m^2 for photovoltaic source and 1 kW/m^2 for wind at 12 m/s speed).

Furthermore, because of higher constancy, the utilization factor, i.e., the ratio between produced energy per year and rated installed power is, for a certain plant, two time higher in the case of wave compared to wind technology.

Moreover, while a power generation plant based on a conventional either fossil or renewable source needs to occupy a certain area removed from the earth soil, a wave energy production plant of the same power would occupy half of the territory, moreover in parts of the ocean not exploitable in other ways. Obviously, it would be a bad idea to cover all the coasts with energy harvesting machines, above all due to environmental and marine wildlife issues, but the difference in occupied area is relevant in order to make a choice for a certain renewable power mix depending on the location.

1.2 Wave energy quantitative analysis

Even if it's difficult to give a mathematical representation of phenomena related to ocean waves due to the great variability, this section offers a simple model to understand behavior of the wave. Although a stationary sea state can be described with average parameters (height and period), individual wave description can be significantly hard.

It is important to say that linear theory, illustrated in section 1.2.1, is just an approximation and a more complicated spectrum analysis must be done to fully define sea states.

1.2.1 WAVES LINEAR DESCRIPTION

Energy is stored in waves as both potential and kinetic energy, due to water masses motion and displacement with respect to the mean sea level.

When generated, waves appear complex and irregular, but they continue travelling even after wind have expired with minimum energy losses, becoming progressively more regular and smoother (swells).

Thus, for an initial analysis, the linear theory is applicable with a relevant simplification in the process description.

Sea waves can be simply described as sinusoidal waves with the characteristics shown in Figure 1.4.

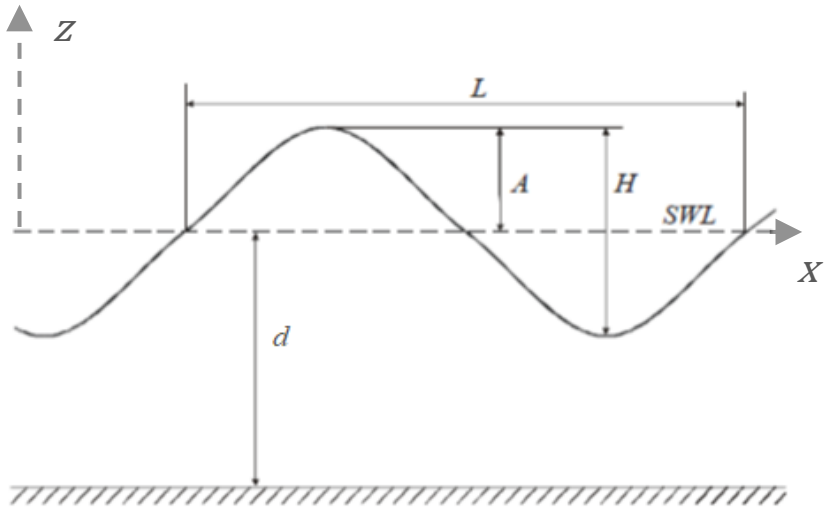

Figure 1.4 Wave representation according to the linear theory.

The water surface elevation, standing the linear theory, is given by (1.1):

$$z = \frac{H}{2}\cos\left[2\pi\left(\frac{x}{L} - \frac{t}{T}\right)\right] \tag{1.1}$$

where L is the wavelength, H is the double of the amplitude, T is the period and SWL is the mean seawater level, at a distance d from the seabed, as visible in Figure 1.4.

In addition, other wave parameters can be defined:

- wave steepness $s = H/L$;
- wave number $k = 2\pi/L$;
- wave frequency $\omega = 2\pi/T$.

The parameter that can distinguish between linear and non-linear waves is steepness s. Typically, for steepness values lower than 0.01, linear relationships are valid, while for higher steepness values, the linear theory is less accurate and higher-order wave models are more

suitable. Since, however, using higher-order wave model is very difficult, the linear theory is often used for regular waves even with steepness values higher than 0.01 [1].

1.2.2 MICROSCOPICAL ANALYSIS

Microscopically, wave movement is due to the elliptical motion of water particles, which extends also below the surface decreasing in radius with depth, as visible in Figure 1.5:

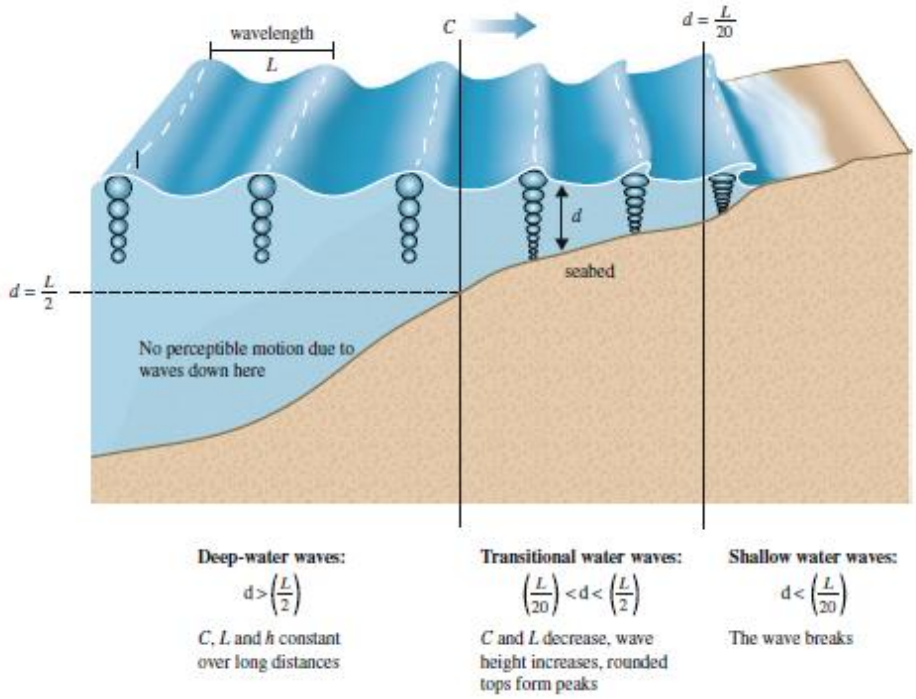

Figure 1.5 Microscopical behavior of ocean waves taking into consideration the ratio d/L

Taking into consideration a single water particle, its vertical and horizontal displacement can be described as shown in (1.2) and (1.3) respectively [1]:

$$\zeta_v = \frac{H}{2}\cos\left[2\pi\left(\frac{x}{L}-\frac{t}{T}\right)\right]\frac{\sinh[2\pi(z+d)/L]}{\sinh[2\pi d/L]} \tag{1.2}$$

$$\zeta_h = -\frac{H}{2}\sin\left[2\pi\left(\frac{x}{L}-\frac{t}{T}\right)\right]\frac{\cosh[2\pi(z+d)/L]}{\sinh[2\pi d/L]} \tag{1.3}$$

where z and x represent vertical and horizontal direction respectively.

As the water depth d decreases with respect to the wavelength L, (1.2) and (1.3) become more and more different, resulting in an elliptical motion.

Thus, three regions can be defined considering the ratio between the wavelength L and the depth d:

- in deep water, where the ratio d/L is higher than 1/2, the seabed does not affect the wave motion;

- if *d/L* decreases down to 1/20, depth starts influencing particles motions;
- in shallows water (i.e. *d/L* lower than 1/20), wave motion is subjected to strong modifications due to the ocean floor, resulting in dissipative phenomena.

Thanks to this analysis, it is clear that it is not possible to use the absolute depth as a meaningful variable and it must be considered in relation to wavelength *L* in order to understand consequences on the motion of the waves.

1.2.3 WAVE DISPERSION, ENERGY AND POWER

The dispersion relationship (1.4) states the relation between *L* (wavelength), *T* (wave period) and *d* (depth) [1]:

$$L = \frac{gT^2}{2\pi}\tanh\left(\frac{2\pi d}{L}\right) \tag{1.4}$$

Equation (1.4) means that, at a certain depth, *T* and *L* are dependent on one another. Furthermore, *L* decreases more or less while *d* decreases, assuming *T* constant.

From equation (1.4) is possible to determine the speed *c* of a wave crest:

$$c = \frac{L}{T} = \frac{gT}{2\pi}\tanh\left(\frac{2\pi d}{L}\right)\left[\frac{m}{s}\right] \tag{1.5}$$

That means that, for a given *d*, the greater the period, the greater the wave profile speed (that is the origin of swells phenomenon).

The energy density of a ocean wave is defined as the energy of the water resulting from the potential and kinetic energies below a square meter of ocean surface.

$$E_{density} = \frac{\rho_{water} g H^2}{8} = \frac{\rho_{water} g A^2}{2}\left[\frac{kJ}{m^2}\right] \tag{1.6}$$

The wave energy propagates at a certain speed, defined as the wave group speed c_g [1]:

$$c_g = \frac{1}{2}\left[1 + \frac{4\pi d/L}{\sinh(4\pi d/L)}\right] c\ \left[\frac{m}{s}\right] \tag{1.7}$$

An important indicator used for instance in Figure 1.2 to characterize the world exploitable wave distribution is the power per meter of wave front (already introduced in section 1.1.2), which can be calculated by multiplying the energy density (1.6) by the wave energy propagation speed c_g in equation (1.7).

$$P_{wavefront} = c_g E_{density}\left[\frac{kW}{m}\right] \tag{1.8}$$

All previous equations have been calculated at the Sea Level (SWL). By taking into account the value *d/L*, it is possible to consider the power decrease below the SWL through

an exponential decay by a factor $-2\pi d/L$. Such an approximation is valid if $d > L/2$, where seabed does not affect wave motion.

In general, it can be said that, since wave power level changes at any scale (seconds, days and years), wave energy conversion output will follow the envelope profile of a certain wave group so energy storage becomes very important from the point of view of the integration of the power plant into the electrical grid to smooth out energy peaks.

Previous considerations have been carried out taking into account the simple linear theory. In fact, waves behave as irregular oscillations, namely a Fourier series of harmonic components, with a more complex analysis which is beyond the scope of the present work.

1.3 Wave dissipative effects

In order to make a connection between waves considered in this thesis and common waves we usually see nearshore, this section offers an analysis of coastal processes that are responsible of waves modifications and energy reduction.

As waves approach the shore and arrive in shallows waters (i.e., where $d < L/2$) indeed, many attenuation and modification effects arise [6]:

- **Shoaling**: waves height H first slightly decreases and then increases more rapidly, as shown in Figure 1.6.
- **Bottom friction**: waves lose a certain amount of energy due to friction with ocean bottom when water becomes shallower.

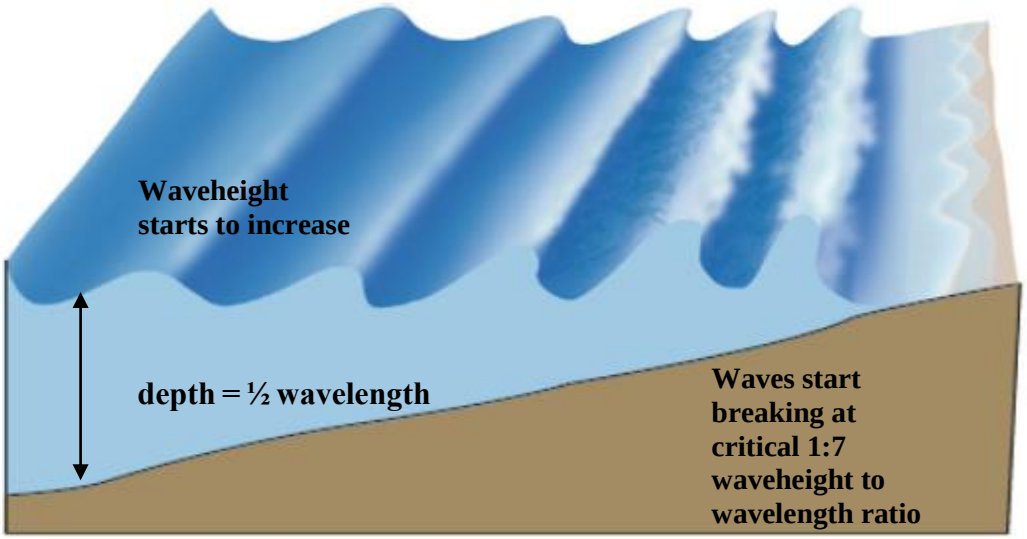

Figure 1.6 Shoaling process and eventually wave breaking.

- **Wave breaking**: waves can break due to increasing steepness caused by shoaling. When the wave height *A* is greater than about 0.8 of the water depth *d* (or about 0.14 of the wavelength *L*), then the waves break.

  Particularly, the cause stands in the difference between horizontal wave particle velocity and wave celerity. When the first becomes higher than the latter, the wave will spill energy in the form of breaking.

  Depending on the wave and the seabed steepness, three different types of breaking can be listed: spilling, plunging and surging as shown in Figure 1.7.

  From the point of view of some nearshore or shoreline wave energy harvesting systems, wave breaking is a positive factor because it limits the largest energetic storm waves from far away which can damage the systems.

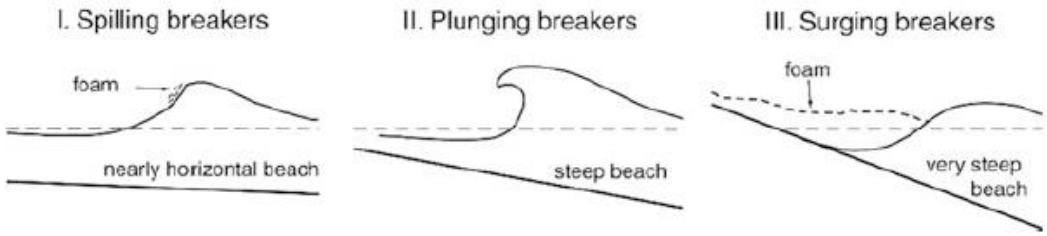

Figure 1.7 Three different kind of wave breaking.

- **Refraction** and **diffraction**: waves can undergo to an energy density redistribution following irregular ocean bottom.

  Waves are focused by refraction, caused for instance by submarine ridges. Refraction can be commonly observed from the beach because waves always appear to come from the same direction orthogonal to the coastline. The direct proportional dependence of the wave celerity *c* on depth is responsible for this phenomenon. Since the lower the depth *d* becomes, the slower *c* becomes, if the direction of the waves is not perpendicular to the shore, it will start to bend because the farther part of the wavefront will have an higher velocity than the nearer one (see Figure 1.8). Although refraction results in a concentration of waves (especially in presence of submarine ridges), it is an energy conserving process, and consequences on a certain energy harvesting system can be good or bad depending on other factors, such as the directional behavior of the wave catching system.

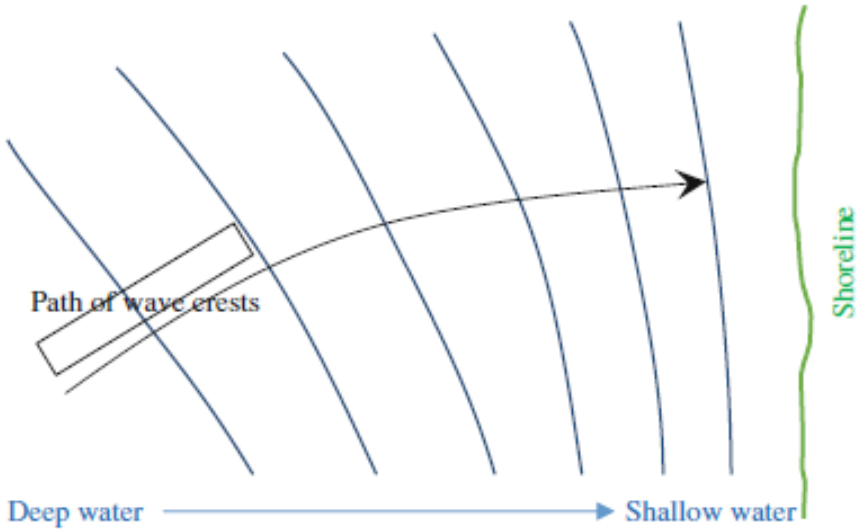

Figure 1.8 Schematic representation of wave direction bending due to refraction.

Waves are, instead, dispersed by diffraction, caused for instance by submarine canyons, in a very similar way to refraction. In particular, diffraction can be observed in presence of an obstacle. Waves would continue to travel ahead the obstacle leaving a region of calm water in the lee of the obstacle, but with diffraction waves are seen to be present even behind the obstacle. The explanation stands in the deviation in wave direction due to different depth (which is originated by the presence of the obstacle itself).

1.4 Wave observation and measurements

Although interest in ocean energy is quite recent, visual observation has been archived by meteorological organizations since the mid 1850s.

Visual analysis has given satisfactory results in wave direction and height observation, but not very reliable results in wave periods. That is why visual observation is considered more appropriate for comparative studies of wave climate in different locations.

Wave measurements is achieved nowadays using many different devices, which can be either placed in situ or work remotely.

The first issue to deal with, when approaching a wave measurement system, is that the measurement time is very relevant in order to define the wave climate of a certain place. Shorter sampling duration results, indeed, in larger uncertainty, while longer sampling duration would smooth out extreme sea states caused by varying wind fields (those variations

can be also very relevant and they can lead to dangerous sea state for wave energy harvesting machines).

Typically, a 15-30 minutes sample duration is considered to be a reasonable compromise between these factors [1].

Other problems arise concerning battery life and deployment time of measurement systems, which can introduce limits to the measurement procedure.

The following paragraphs list current well-known measurement systems:

- **Surface-following buoys**: a buoy slackly moored to the seabed can follows ocean waves movements and convert them in useful measurements by means of an accelerometer (however, GPS systems are becoming more diffused). This measurement system is the most common and known, although it is quite expensive and strong currents and steep waves reduce the measurement accuracy. In Figure 1.9 a typical application is shown.

Figure 1.9 Surface-following buoy type wave measurement system.

- **Seabed pressure sensors**: by measuring the water pressure variation from the bottom of the oceans, water surface elevation value can be obtained. Devices exploiting pressure difference are however suitable for shallow waters due to depth-induced attenuation in wave pressure. Moreover, these devices are more indicated to measure swell waves, since high frequency waves suffer more from the attenuation phenomenon previously reported. In order to gain also directional information, they can be organized in arrays. A picture can be seen at Figure 1.10.

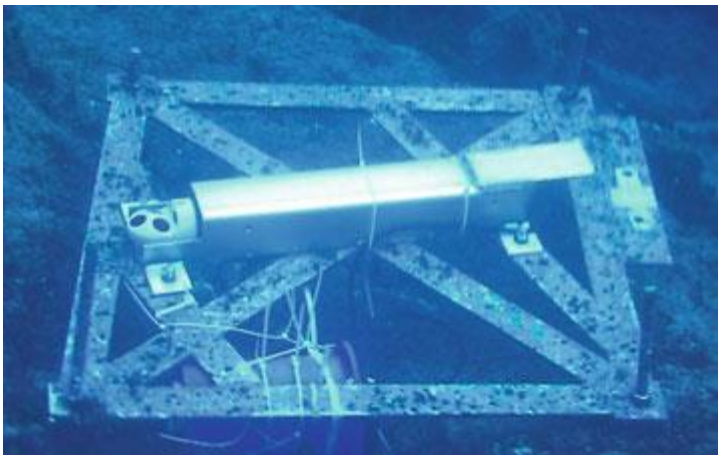

Figure 1.10 Seabed pressure type wave measurement system.

- **Acoustic current profiler**: recently developed, acoustic profilers exploit the concept of red/blue shift in acoustic pulses. A time series of different water velocities is composed and combined to obtain a 3D model of waves. These devices are usually placed in the seabed where can be subjected to less damages (see Figure 1.11). Similar problems with respect to seabed pressure sensors arise, in particular concerning the lower effectiveness, which decreases with the depth due to attenuation. Another common problem of these two devices is that they have to store data locally and this can be a problem for projects that need data for the development. Among their advantages, they can provide information also on ocean currents.

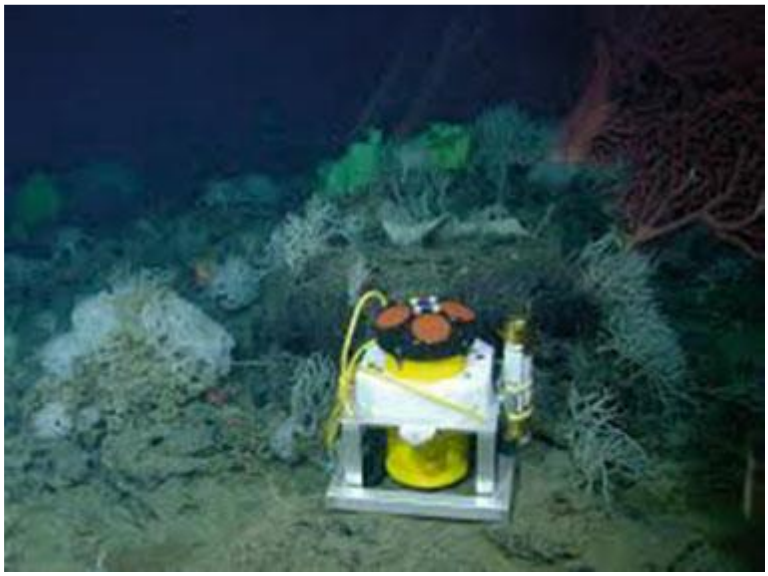

Figure 1.11 Acoustic current profiler type wave measurement system.

- **Radar (land-based and satellite)**: measurements can be performed also remotely via radar sensors. In this way, the system is protected against harsh marine environment, it does not need safety systems and deployment is usually easier, so the total cost is

typically lower. Moreover, data are readily available. Particular radars are those on satellites, which can provide estimates of significant wave height along the satellite track. Temporal resolution with satellites can be low (depending on satellite passages) but data can be provided from a large geographical area.

1.5 Wave Energy Converters

In this chapter, basic information about Wave Energy Converters (WECs) is given. First, when talking about WECs, the whole wave energy conversion chain, from the wave-motion catching device to power-harvesting system including energy transformation, conditioning, control and safety system is meant. Many different WECs have been studied and designed over the past 30 years and in this section a general description and characterization are given, while the next section illustrates a classification.

1.5.1 BRIEF WECS STORY

Although wave energy has always been an interesting source to be exploited with many ideas and designs (the first patent dates back to 1799), researches have been intensified for the last 30 years. An important pioneer was the Japanese navy in the sixties, with a marker buoy able to catch waves energy to light on its lamp. The real turning point was the publication in 1974 of an article in the scientific journal Nature by prof. Stephen Salter from the University of Edinburgh. The article, as a reply to the general oil crisis, presented an innovative and highly efficient cam-shaped floating body (the so called Salter Duck visible in Figure 1.12) to harvest energy from ocean waves.

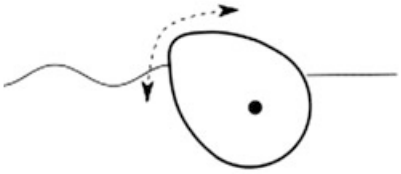

Figure 1.12 Illustration of the Salter's Duck working principle.

Unfortunately, energy policies turned their interest in large power capacity plant, avoiding arrays of smaller units, although many scientists disagreed with this position. Thus, due to low interest and funding lack, wave energy harvesting research had been halted.

As an answer to the oil crisis started in the 70s, wave energy came back as a possible renewable energy source with an interesting overall potential to be exploited.

In order to reply to the energy demand, many WECs prototypes have been developed, optimized and commissioned since the mid-1990s. Due to uncommon knowledge in the wave energy fields, many studies are going on, and several different approaches are being developed. Thus, it is not completely clear nowadays which WEC technology will be the future commercial application of marine wave energy conversion [5].

1.5.2 WECS CHALLENGES

Although the knowledge of WEC devices is at a pre-commercial stage, it is clear how important wave energy conversion can be for our energy market. It represents another sustainable and endless energy source, which can increase the amount and the diversity of renewable energy mix, with the purpose to increase the availability and decrease the dependence on traditional fossil sources. The creation of a new market sector carrying innovation and employment has also to be considered as a positive aspect of wave energy conversion field development [1].

Of course, many challenges have to be faced and that is why various technologies have been studied and developed. Here follows a list of difficulties that must be overcome.

- **Reliability problems**: given the difficulty and the cost of maintenance interventions, reliability becomes very important for a WEC. Failures can occur and the difficulty of repairing increases, since spaces are often not freely manageable during the WEC design. Interventions must be rare and as easy as can be, in order not to be forced to bring an offshore converter back to the harbor. WEC components must be easy to purchase, maintain and replace (and so wide commercial development is a necessity).
- **Survivability**: since the WEC load in extreme weather conditions can be 100 times higher than normal condition load, WECs needs to be oversized or equipped with reliable safety systems, better if passive (i.e., safety mechanisms that can be activated without need for external interaction or energy). However, those systems and strategies increase the total cost of the device.
- **Conversion efficiency**: due to high irregularity of incoming waves, it would be usual, for a certain WEC, to operate out of maximum power extraction rated condition. That is why high efficiency (of the whole conversion chain, which is, sometimes, very long) is necessary over a large range of incoming waves in order to exploit as much as possible conditions different from the rated one.

- **Operating range**: as stated above, due to varying source conditions, the range of operation must be as extended as possible.
- **Output electrical energy quality**: although the generation is very irregular, using wave energy becomes an interesting alternative path for renewables. However, electrical power output must respect normal standards in order to be acceptable to the utility network. To do so, energy storage systems of many different types can be designed, also integrated in the WEC operative principle itself, as well as particular operating configurations of WECs array.
- **Scalability**: in order to be an economically viable renewable energy source, a WEC must be capable of further enlarging its dimensions (like offshore wind turbines) and produced power as well. Unfortunately, many WECs reach their optimal dimension at too low power levels. Arrays of multiple WECs are not considered in the analysis because no advantages would be obtained in the total cost with respect to the total produced power.
- **Environmental footprint**: since the importance of renewable energy harvesting systems stands not only in the renewable characteristic itself but also in the lower environmental impact, WECs must have the lower impact possible on marine ecosystem and ocean wildlife. Unfortunately, this characteristic is at the opposite with respect to cost effectiveness and power catching efficiency and that explains why research and optimization are so important in this field.
- **Production cost**: moving wave energy conversion from pre-commercial phase to commercially viable energy harvesting solutions is difficult due to lack of standards and of a consolidated industry supply chain. In particular, difficulties rise about the production cost, especially for such systems that needs to face harsh and aggressive marine environment. Unlike military or medical applications, where the reliability and accuracy are main issues with no compromises, energy production requires in general effective but low-cost technologies, both in terms of production and maintenance.
- **Fluctuations**: due to the nature of waves, the absorbed power is subjected to fluctuations (few seconds timescale); moreover, waves travel in groups, so energy absorption follows also a timescale of few minutes. These fluctuations lead to a both electrical and mechanical oversizing necessity, since extracted power is not constant but has many peaks, each one far from the others. Unfortunately, oversizing is also an obstacle to the economic optimization for the beginning of a commercial phase.

Those are essential aspects in which a WEC must excel in order to demonstrate a long-term economic and energetic potential and find a place in the renewable energy harvesting prospect.

Since their development has begun recently, the full market commercialization is a future objective, which must be aimed following a trajectory with initial successes and failures.

1.5.3 WEC SITU CHOICE

When choosing a wave energy conversion site, subsequent steps must be followed, in order to make the best characterization possible for an irregular source like the ocean waves [6].

First of all, it is important to investigate the wave energy resource magnitude and commercial viability in a certain region by means of existing wave data. In this first phase, an initial assessment is done and then further developed. Typically, the analysis starts with the review of existing oceanographic and wave atlases.

Then, wave measuring devices can be placed in the exact project site to collect data for a certain period. It is recommended to perform direct measurements for at least one year or longer.

A numerical analysis is also performed, calibrating wave model with existing measured wave data.

Inspections and verification must consider the site also from a geological point of view (for moorings calculations), depending on the WEC technology that would better suit all the characteristics of a certain location.

Thus, it is clear how many considerations other than strictly marine must be done in order to properly choose an ocean site suitable for a certain WEC application. In particular, an omnipresent consideration must be done regarding the environmental impact, which cannot let be relegated at the end of the evaluation process.

Due to its geographical uneven distribution, a wave energy harvesting system solution is not always applicable and a widespread exploitation of all the coastal areas is neither sustainable nor environmentally feasible. Specialized applications that make sense are those that rely now on auxiliary polluting system to obtain the energy needed: for instance, a wave energy converter can power an oceanic research center, avoiding the need for cables from the shore or diesel generators; wave energy can be useful for islands or some particular coastal

areas; wave energy conversion, finally, can power auxiliary systems of a ship which, for some reasons, has to stop far from the shore.

Another important consideration about the installation of a wave power capturer device is that, due to waves high variability, during the design, an important trade-off must be done between under-utilization of installed capacity and excessive shedding of absorbed power. For instance, due to seasonal difference, a wave power plant well designed for winter conditions (also able to undergo strong conditions) can be too oversized and can work with lower efficiency during summer. Thus, the so-called seasonal load match is good in regions where utility peak demand is dominated by heating and lighting, while in locations where peak demand is driven by fresh air conditioning, the seasonal load is much poor.

1.5.4 STRUCTURE OF A WEC

From a generic point of view, it is possible to spot similarities in all WECs, although they operate according to different operating principles.

Main subsystems that are present in all WECs are:

- **Hydrodynamic subsystem**: it is the primary wave absorption system, i.e., the first passage through wich wave force and motion are transferred to the power take-off. There are different technologies, designed to better suit a particular wave occurrence.
- **Power take-off (PTO)**: it converts the energy captured from the hydrodynamic system into electricity by means of one or different transformation stages. It also can be of different types, according to the chosen operating principle. Any PTO can be defined by three parameters:
    - the force produced against an external acting thrust;
    - the stroke along which the PTO moves to produce the force;
    - the speed of the PTO motion.
- **Reaction subsystem**: it is the system that maintains the WEC in an optimal relative position with respect to the seabed. It offers a reaction response to the PTO while the hydrodynamic system is acting. For instance, it can be a mooring system. The PTO becomes more efficient while wave motion is harvested against a fixed reference point, because relative motion is optimized.
- **Control subsystem**: it drives the system by applying a proper control algorithm taking feedback measurements. Sensors, actuators, control electronics and a power maximizing algorithm are included in this section.

- **Electric conditioning system**: in order to correctly interface a generation system with the grid, a power electronic section must be present to operate all the adaptations needed and the proper energy flux management. Regardless of the operating principle of the conversion system, the power electronic apparatus is very similar to the one in a wind power generation system [7]. In the simplest form, it consists of a back-to-back conversion system, where a first converter (let us call it Generator Side Converter, GSC) apply the proper voltage to the generator windings in order to extract the power and the other converter (let us call it Grid Tied Converter, GTC) linked to the grid, keeps the voltage across the common bus DC as constant as possible. It is also necessary to provide a storage system located on the generator side in order to keep the auxiliary services of the WEC (lights, bilge pumps, sensors, valves, regulation systems) active even without electricity generation.

Although many of the conversion stages, in particular the power electronics interface to the electric grid, are similar to many others energy-capture technologies, substantially changes stand in the generator control mode, in the motion capture device and in the design concept.

1.5.5 WEC CONCEPTS

The description of WECs behavior, advantages and disadvantages can be done by defining some key parameters:

- the **wave-to-wire efficiency** is the overall efficiency of the system that delivers the absorbed wave energy to the grid. It is the ratio of the output power to input power;
- the **capture width ratio** (**CWR**) measures the capacity of the converter of exploiting waves. At a given frequency, it is the ratio of the total mean power absorbed by the PTO to the mean power per width unit of the crest of the incident wave train;
- the **utilization factor** (or capacity factor) as described in section 1.1.3 is the ratio between the average produced power (or energy as well) and the installed power, and it represents the utilization rate, which means the return on its initial cost.

A proper WEC dimensioning starts from the wave analysis. In particular, peak and period of the wave with the highest **annual energy contribution** must be taken into account, where the annual wave energy contribution corresponds to the product of wave energy and occurrence annual probability.

1.6 WEC classification

Presently, due to research status of marine energy exploitation, there are many competing WECs technologies based on different concepts and designs. The European Marine Energy Centre provides a comprehensive list updated in February 2017 of 226 wave energy generation technologies sorted in different categories.

Not every WEC can be inserted in a certain classification since a great variety of wave energy harvesting technologies exists, and many new researches and studies are introduced every day. Also, new challenges are continuously overcome with innovative new technologies, sometimes very different from their precursors. Then, many different classifications are possible and new kinds of sorting logic can be implemented. As a result, unlike for wind energy industry, it is not easy to converge onto a winner technology concept (three blade horizontal axis for wind energy), because of the great variety of WEC with respect to wind energy systems.

1.6.1 DISTANCE FROM THE SHORE

A first distinction is possible according to the distance from the shore.

- **Shoreline**: shoreline systems present various environmental problems, for both the marine ecosystem and the view, but low maintenance cost and few problems related to energy transmission have to be considered even if the catchable power diminishes as the water level goes down. They can be placed at the bottom of the sea, integrated in breakwater-like structures or fixed to rocky cliffs so mooring systems are not required, but suitable sites are not so diffused and their exploitation must be careful.
- **Nearshore**: for nearshore systems (usually from hundreds of meters to few kilometers from the shore), issues concerning mooring in shallows waters or fixing to the bottom arises, with the necessity to bear great stresses. Captured energy is higher than shoreline systems but not as high as offshore devices.
- **Offshore**: at a greater distance, it is possible to catch waves with higher energy density and the visual pollution is less important, but problems of energy transmission and greater exposure to adverse atmospheric phenomena arise in very far installation (the energy transfer uses submarine cables and the machine must be very reliable) and maintenance costs for the difficulty of intervention. There are floating or submerged

devices, and they represent the most promising class of WECs since they can exploit wave power before it deteriorates because of the dissipation effects.

1.6.2 DIRECTIONAL CHARACTERISTICS

Another classification among floating WECs (most diffused kind of installation) can be based on the directional characteristics [4]. An absorption system is indeed designed for a certain incident wave direction, thus it is possible to identify these families:

- **point absorber**, which can be floating or submerged and absorbs energy in all directions, since the horizontal physical dimensions of the device are small with respect to waves length;
- **terminator**, which extends perpendicularly with respect to the wave direction and absorbs the energy by terminating the waves;
- **attenuator**, which is, unlike the previous one, aligned in parallel with respect to waves direction (experiencing less force than a terminator) and ride the waves that attenuates while the power is extracted.

1.6.3 ENERGY CAPTURE PRINCIPLE

Finally, some categories can be defined according to the principle of wave energy capture, essentially how the device exploits the wave force and the PTO layout [3] – [4] – [8]

- **Oscillating Water Column (OWC)**: in these systems a particular kind of double-hole chamber is used to convert oscillating wave movements into an air flow, which is easily exploitable thanks to a mature wind energy technology.

  From the underwater lower hole, wave oscillations come and induce an air pressurization inside the chamber (rising and falling water level increases and decreases air pressure respectively). Passing through the top hole, the air moves a bidirectional turbine, generating electricity.

  Since in one wave cycle the air flow changes its direction, the turbine must be designed to rotate in one direction independently from the incident airflow direction. For this purpose, a Wells turbine has been typically used for more than 20 years but further optimization can be done in order to increase its efficiency.

  The chamber profile must be calculated to concentrate air flow through the turbine.

Another important design issue is the risk of mechanical resonance of waves within the chamber causing a net zero air flow thorough the turbine. Thus, it is important to take into account the particular wave characteristics (wave height, length and period) of the chosen location in order to make a proper design.

OWC WECs can be shoreline (in this case they usually exploit landscape conformation like cliffs), nearshore and offshore. Although a firmly fixed system can harvest more energy since the chamber does not move with incoming waves, it can also be damaged in rough seas because it has no flexibility. Thus, mooring systems must be a compromise between higher energy capture and flexibility, i.e., rigidity and slackness when facing extreme sea conditions.

The simplest control system for PTOs of this kind is a bypass valve, which can prevent the turbine stalling by releasing possible extra air pressure and also perform a turbine rotational speed control by limiting the main air flow.

With valves, the control of the air pressure and flow can be achieved, resulting in an improvement in the response time and captured energy optimization, but other solutions, such as turbine blades pitch control, can be used.

Examples of such a technology in existing applications, shown in Figure 1.13 and [1], are Pico in Azores (Portugal) and OceanLynx in Australia; another famous plant of this category (Figure 1.14) is located on Islay Island (UK) and is called LIMPET.

Figure 1.13 Top: Pico in Azores (schematic and actual plant). Bottom: OceanLynx in Australia (schematic and actual plant).

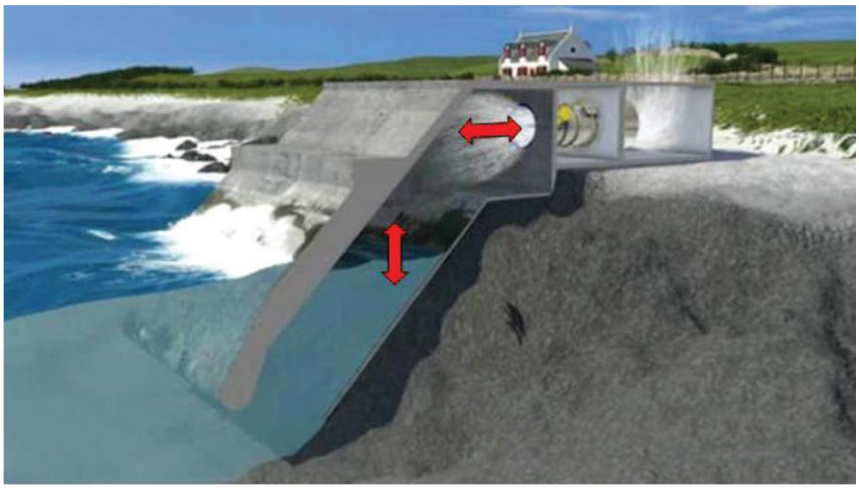

Figure 1.14 LIMPET (drawing) on Islay Island.

- **Overtopping Device (OD)**: in these devices, waves are stored in a reservoir located few meters above the sea level. Then, the collected water flows back into the sea through a low-head hydroelectric turbine (unidirectional flow). Usually, physical collecting systems are used to concentrate ocean waves through the reservoir.

  Mooring issues are the same as OWC devices, and ODs are typically nearshore systems. ODs are not as common as OWCs.

  A famous real application of offshore overtopping WEC technology is the Wave Dragon (Denmark). Typical characteristics of the Wave Dragon are two long deflector wings used to lead waves toward the front of the device, where a ramp is present to direct water in a reservoir. Its mooring system is a slack chain, which allows the system to orientate in the wave direction. Pictures are shown in Figure 1.15 and Figure 1.16.

Figure 1.15 Wave Dragon, Nissum Bredning, Denmark.

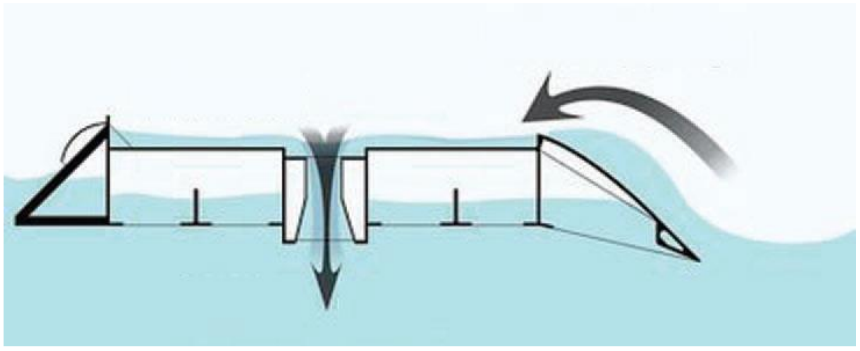

Figure 1.16 Wave Dragon operating principle and water flow direction, from wave collecting to water discharge through hydroelectric turbine.

- **Wave-Activated Body (WAB)**: it is convenient to classify different systems in this category, since it encompasses a large field of WEC concepts that work in a similar way converting energy from relative motion into electricity.

  In general, WABs systems are made up of different (at least two) floating bodies able to move independently, which follow the wave oscillations. The energy of this relative motion is converted into electricity (for example by high pressure oil pumping or with a particular electric generator).

  A famous WAB WEC is the Pelamis (Figure 1.17), composed by cylindrical sections each one moving with respect to the others. Its mooring system is designed to allow Pelamis to orientate and follow the ocean waves in order to adapt to their wavelength. Directionally speaking, this device is a terminator. Its functioning principle is based on high pressure storage: energy is accumulated (hydraulic accumulation) in order to smooth irregularities in power fluctuations and, in a second section, converted into electricity by hydraulic motors connected to generators.

Figure 1.17 Pelamis in Orkney, Scotland.

Other systems are based on the movement of a flapping body with respect to a fixed part, as the Oyster (Figure 1.18).

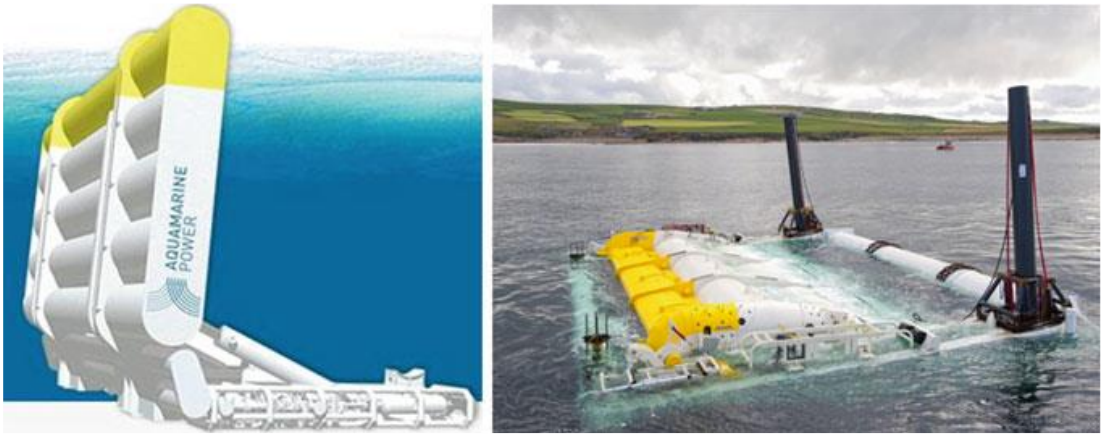

Figure 1.18 Oyster in Orkney, Scotland.

Finally, it is important to mention the WEPTOS, composed by several moving bodies with the same shape of the Salter's Duck, as shown in Figure 1.19.

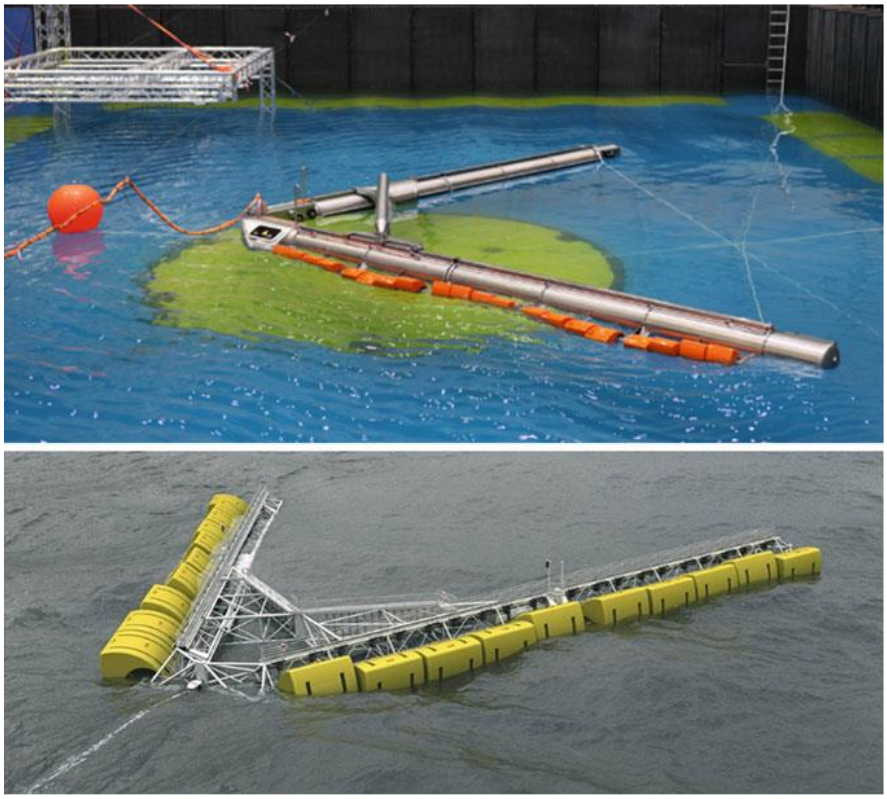

Figure 1.19 WEPTOS model (top) and real (bottom) in Cantabria, Spain.

An important WAB configuration corresponds to the point absorber. The next section will provides a detailed description of this kind of system, which is useful later in this thesis.

1.6.4 POINT ABSORBER

The point absorber WAB is a particular kind of WEC. It can harvest wave energy from all directions in one point of the ocean, basically following wave movements.

Due to their characteristics, they are optimal for offshore and nearshore applications, in ocean water depth ranging from shallow to very deep.

Various shapes are possible for this type of WEC.

- The buoy type (or float type) works thanks to a floating device and its relative motion with respect to either a mooring or a high inertia part.
- The semi-submerged hollow cylinder configuration allows water to flow between its ends due to the established pressure difference caused by wave movement. Then, such a water flow can be captured by a proper turbine.
- Floating pistons at different heights move while following the wave oscillations thanks to some floaters.
- Flexible hoses manage to pump water through a turbine thanks to their stretching movements due to the heaving of a buoy, which follows the ocean waves.

In general, the more restricted in motion, the more efficient a WAB PTO is. If only one degree of freedom is left, the WAB WEC cannot choose to orientate in the direction of the lowest wave resistance (where the PTO interaction would be limited and so the energy extraction would be low).

The most common solution (around 33% of the WEC devices) adopted is the buoy-type (float type) point absorber system, thanks to its simplicity, omni-directional behavior and ease of deployment.

Figure 1.20 shows the working principle of the buoy-type point absorber WAB WEC.

The yellow section is the floater, which follows the movements of the ocean waves. The green part, which houses the electric generator for the mechanical-to-electrical energy conversion, ends with a high inertia plate, which remains stable with respect to ocean waves (a little motion is of course possible in order to avoid serious damage when high stresses occur). As visible in Figure 1.20, the movement of the floater produces a relative motion of the yellow part with respect to the green part, resulting in a heaving oscillatory motion of the PTO inside the green spar.

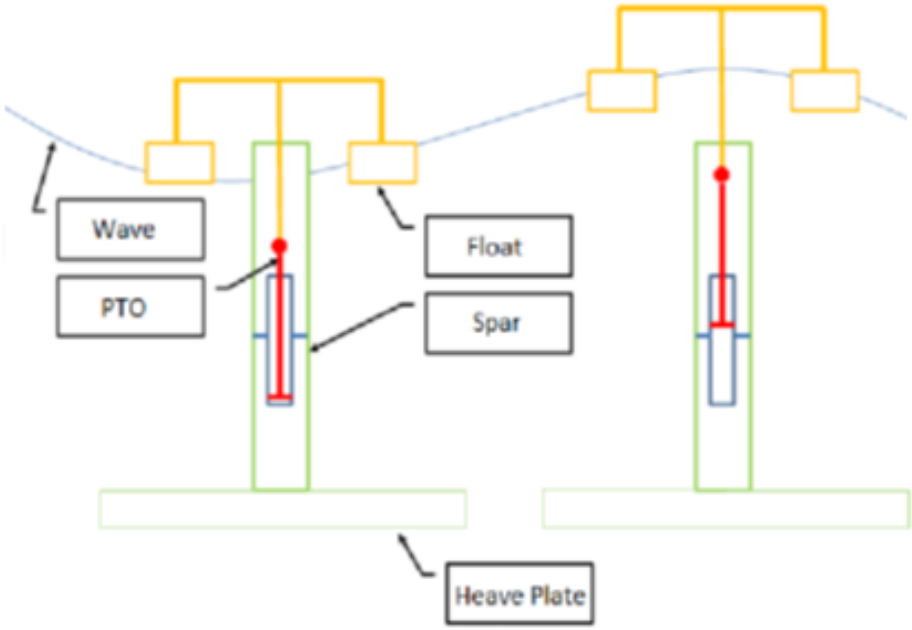

Figure 1.20 Schematic view of a Float Type (Buoy Type) - Point Absorber WAB WEC

A real example of an existent application of a buoy type point absorber is the Wedge Global W1 tested in Gran Canaria at PLOCAN site in 2014, depicted in Figure 1.21.

Figure 1.21 Wedge Global W1 ready for sea tests.

1.7 Direct-drive PTO

As said, the PTO is the system which superintends the energy conversion from a mechanical form (wave movement) to electricity.

The power conversion to electrical energy is usually achieved by means of a two-step process, which can be, for instance, as follows: wave → pneumatic system → electric generator or wave → hydraulic system → electric generator or wave → mechanical system → electric generator.

Given the difficulty of control, low reliability and low efficiency especially due to delays and inertia of traditional PTOs (mechanical or pneumatic systems), a direct-drive PTO is a preferable solution [9].

1.7.1 CHARACTERISTICS OF A DIRECT-DRIVE PTO

Since an higher number of conversion stages brings low efficiency (in a series system all efficiencies must be multiplied), low reliability (the overall reliability depends on the reliability of all the components) and high control difficulties (more systems have to be controlled and coordinated), it is a good idea to reduce the conversion chain to a single step.

In a direct-drive PTO, the movement of the waves is directly exploited and converted into electricity with no intermediate energy transformation stages. Due to direct conversion, this technology gets greater efficiency, as well as higher reliability and lower need for maintenance, since the number of moving mechanical parts used is reduced and common failure sources (hydraulic/pneumatic/mechanical components) are eliminated. Also, controllability gets many advantages and simplifications, and more efficient control strategies can be implemented to increase the energy that can be harvested from the waves.

When using a direct-drive PTO in ocean wave electrical power generation systems, the main drawback is that forces must be very high to produce high power levels, since the speed of the motion involved is small (1 m/s as order of magnitude) and there is no interposed system able to amplify it. If the speed of the moving part matches the speed of the waves, the resonance condition is achieved: the relative speed between the moving parts of the WEC is increased, and lower forces are needed to get the same output power.

1.7.2 DIRECT-DRIVE PTO ELECTRICAL MACHINE

An important aspect that must be clarified is that the electrical part of the WEC as well as the control apparatus cannot be seen isolated from the whole wave power conversion system.

This mean that the electrical system cannot be added at the end of the WEC design and the design of the PTO is a key feature as well as the chosen location.

A change in the electrical and control system could indeed influence the overall cost and performance, survival rate and can make the difference between success and failure.

There are different types of electric machines used as generators for different types of WECs.

When talking about a direct-drive PTO based on the technology of the buoy-type point absorber, the only possible choice is an electric linear generator (Figure 1.22).

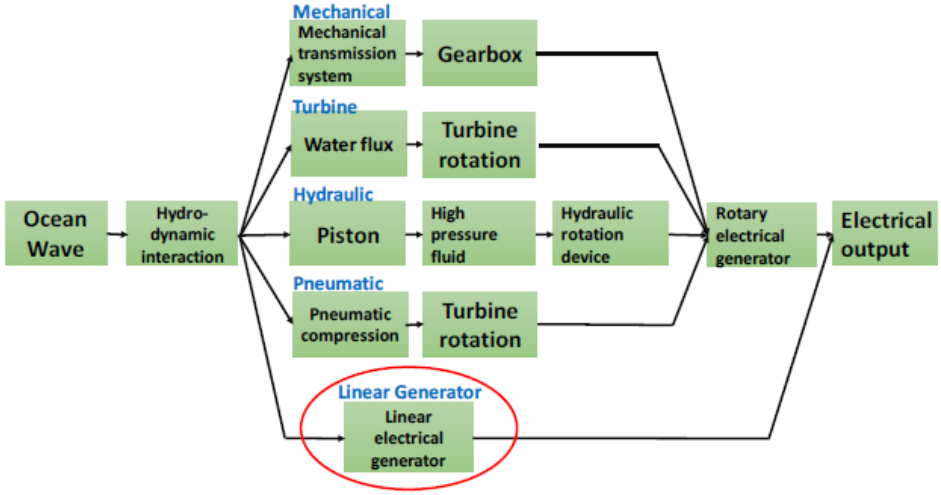

Figure 1.22 Different kind of PTOs, the last one is the direct-type PTO.

Since the wave motion for a heaving point absorber consists of vertical swings, a linear electric generator with a proper control strategy can represent an effective direct-drive PTO. Unlike traditional rotational electric generators, the stator part in linear generators is coupled to a translator device, which moves with respect to the former along the common axis, usually oriented as the major dimension of the system.

So, the direct-drive PTO consists of an electrical energy conversion system able to manage the input mechanical power from wave heaving movements without transforming it.

Of course another electricity conversion is required to correctly interface the electrical power generator and the final users, for example through the electric grid.

1.7.3 DIRECT-DRIVE PTO STATIC CONVERSION

The power electronic conversion system associated with a buoy-type point absorber direct-drive PTO must be bidirectional, so as to allow the generator oscillations to damp by returning part of the power to the machine, in order to maintain control of the maximum power that can be produced. The damping control, very relevant for systems with irregular generation such as the wave-energy harvesting systems, can be obtained mechanically using pumps and valves. While these solutions can properly act for large scale oscillations, transient forces are better managed by the generator itself, with a power electronics configuration capable of a bidirectional energy flow [10].

1.8 Standardization framework

The relatively young life of marine energy has not already seen a dedicated standardization apparatus that specifically refers to situations related to energy extraction (many references, indeed, come from other aspects of sea environment exploitation, and some of them can be properly adapted).

Since wave energy conversion systems are quite new to the authorities and also to scientific world and the public, they tend to be administered with already existing legislation, which was created with no particular references to ocean-energy conversion systems.

Many attempts have been pursued by the International Energy Agency-Ocean Energy Systems (IEA-OES) to coordinate several technical annexes with participants from many countries with the purpose to provide main guidelines for ocean energy devices standards.

Also the International Electrotechnical Committee (IEC) has set up the TC114 committee to draft ocean energy conversion standards, managing several aspects.

Anyway, the path is not easy and many work is still to be done to create a dedicated legislative apparatus.

Another problem is that the development of ocean energy systems straddles many competencies within different responsibility levels, thereby resulting in multiple consents from multiple authorities, causing many bureaucratic delays. The same problems arise when an offshore plant comes ashore.

Usually, consenting take into account aspects such as sea space and sea bed occupation, environmental impact, electrical connection, decommissioning.

The ideal process would see the development of wave energy systems going hand in hand with the development of specific legislation.

The advantage is that since legislative systems usually are not full flexible and responsive to change, by reflecting in real time the experience gained in many projects directly in the law apparatus, a proper standardization framework can be developed [5].

The main effect of the legislation development is to allow the beginning of a commercial phase for wave energy production plants, with a reduction in purchasing costs and the creation of a strong industrially developed supply chain, as well as a permanent place in the renewable energy market.

1.8.1 LEGISLATION SPATIAL LIMITS

First, it is important to introduce some remarkable issues. Although each state has sovereignty on the land and it can regulate all activities, this authority is limited on the sea, in accordance with international law. The official framework in this field is the United Nations Law of the Sea Convention (LOSC) (often referred as "Constitution for the Oceans" as it covers many marine issues) and it prescribes nature and extent of state's rights in relation to coastal boundaries by defining some specific jurisdictional zones. For issues that cannot be solved by simply taking into account maritime jurisdictional zones, the LOSC provides elements to ensure an international cooperation, including straddling and highly migratory fish stocks, scientific research, marine pollution and protection of the environment [11].

Internal water lie landward of the baseline from which territorial sea are measured. There, a state can exercise full sovereignty by applying its own laws and exploit any resources, including energy harvested from waves.

Territorial water extends till 12 nautical miles from the baseline outward from the shore.

To date, wave energy systems are all located in either internal or territorial waters, and a future development of a technology to be used outside these areas, is likely possible.

The Exclusive Economic Zone (EEZ) refers to the sea space beyond and adjacent to territorial waters, spanning 200 nautical miles from the baseline. In this aera is possible to produce energy from water, currents and winds. Obviously, any abandoned or disuses installation or structure must be removed.

All states are, moreover, allowed to lay submarine cables and pipelines on the continental shelf and they can authorize and regulate drilling activities for all purposes.

Beyond the 200-miles EEZ, there are the high seas, which are characterized by freedom of navigation, overflight and laying of cables and pipelines, as well as artificial islands and other installations. Fishing and scientific research are allowed too.

1.8.2 ENVIRONMENTAL ISSUES

An important aspect which is often misconsidered is the environmental impact. Although such important considerations cannot be neglected, environmental legislation requirements are still in progress in many countries [5].

According to the European Union (EU) Directive on Environmental Impact Assessment (EIA) (Directive 85/337/CE), all EU member states must present an environmental impact analysis to evaluate environmental consequences for projects as power stations, before obtaining the building permission.

In 1992, the United Nations Convention on Biological Diversity (CBD) presented a specific program on marine and coastal biodiversity safeguard, significantly reinforced by the Jakarta Mandate in 1995. It asserts that parties involved in projects regarding ocean environment must require an Environmental Impact Assessment (EIA).

Other EU legislation have been published (Directive 97/11/EC, Directive 2003/35/EC) and they have been adopted in the national legislation of the member states: in general, coastal states must measure, prevent, reduce and control pollution.

The first European Commission ocean laws collection was launched in 2007. The Integrated Maritime Policy (IMP) recognizes that all issues regarding oceans are linked and sea policies must develop joining up.

Moreover, in order to support marine sector sustainable growth, the Blue Growth Agenda has been launched in 2012. Among its five focus areas (aquaculture, coastal tourism, marine biotechnology, seabed mining), also ocean energy harvesting is present, with the purpose to enhance this sector, to enlarge the range of possible energy sources and reduce pollution by greenhouse gas emissions.

Nature conservation legislation comprises the Birds and the Habitats Directives, which protect EU biodiversity.

Regarding Environmental Impact Assessment, the legislation incorporates the Environmental Impact Assessment Directive (2011/92/EU) and the Strategic Environmental Assessment Directive (2001/42/EC), with the purpose to carefully think about environmental consequences (including human beings, flora and fauna, soil, water, air, climate and landscape, but also material assets and cultural heritage and interactions between all factors) for big projects taking into account any possible implication regarding the surrounding ecosystem. The important innovation is to involve also the public participation in the process of decision making, in order to improve the strength of decisions quality.

It is easy to imagine why WECs devices must be subjected to an EIA. Since they harvest energy from oceans in a more invasive way with respect to offshore wind turbine, they introduce new and unknown interactions with the marine wildlife.

The analysis methods of environmental consequences are various, and due to the low level of knowledge of wave energy devices, it becomes difficult also to compare the obtained results even if they are evaluated by a common EU legislative base.

On the other hand, the Strategic Environmental Assessment (SEA) Directive acts in accordance with public plans and programs. Its objective is, above all, to integrate the environmental considerations in an early phase of design of marine energy harvesting project, in order to promote real sustainable development.

In this way, since it is performed when the project is being created, the development can be led in areas where environmental negative effect can be avoided or reduced.

1.8.3 DECOMMISSIONING

Regarding decommissioning, two main legal frameworks can be described:

- UN Law Of Sea Convention (LOSC) describes, in article 60, that any abandoned installation in the EEZ must be removed for navigation safety reason.

  The removal must be performed as soon as reasonably practicable after the abandonment. Some evaluations must be taken into consideration:

  - effects on navigation safety;
  - material deterioration and their impacts;
  - effects on marine environment and wildlife;
  - risk of displacement from original position;
  - cost, personnel risks and technical feasibility of the removal process;
  - determination of a new possible use or other justification.
- London Convention on the Prevention of Marine Pollution by Dumping of Wastes and Other Matter (1972) has been an important regulation against deliberate dumping at sea to better control of the pollution of marine environment.

Although legislation in decommissioning and abandonment matters are present and well diffused, the procedures involved remain difficult and slow.

Aspects concerning decommissioning legislation, in any case, can improve as the diffusion of WEC technologies would increase.

1.8.4 TECHNICAL ISSUES

The project focused in this thesis aims also at creating a set of standards in order to properly prepare the terrain for a future solid growth of the wave energy market sector with the establishment of a consolidated industrial supply chain and a strong theorical and experimental background.

Some of the actual standards can be adopted for the project. A list for design and installation is the following:

- The International Maritime Organization (IMO) Resolution A.89 (21) Recommendations on Training of Personnel on Mobile Offshore Units (MOUs)
- IEC 60092 Electrical installation in ships;
- EN 50110-1_2013: Operation of electrical installations: General requirements;
- IEC 60529_1989: Degrees of protection provided by enclosures (IP Code);
- IEC 60204: Safety of machinery - Electrical equipment of machines;
- NEN 1010: Safety Regulations for Low Voltage Installations;
- IEC 61892 Mobile and fixed offshore units - Electrical installations - ALL PARTS;
- IEC publication 60533 - Electromagnetic compatibility of electrical and electronic installations in ships.
- IEC TS 62600-2: Marine energy systems - Design requirements
- IEC TS 62600-102: Wave energy converter power performance assessment at a second location using measured assessment data
- IEC TS 62600-103: Guidelines for the early stage development of wave energy converters – Best practices and recommended procedures for the testing of pre-prototype devices

1.9 Environmental impact

Generally speaking, ocean power can be considered virtually a non-polluting source and, obviously, less environmentally degrading than most other forms of power generation.

With reference to negative effects of fossil energy sources exploitation, indeed, wave energy sources appear to be clean, although they may hide some negative drawbacks that have to be highlighted in order to better concentrate the development in appropriate locations that maximize positive effects and minimize the environmental drawbacks.

The main problem stands in the limited knowledge about possible negative impacts on marine wildlife and environment, which are also specific for each different site. So far, tests

have been done considering small scale deployments, usually single units which are either scale prototypes or full scale versions, but wave energy devices are likely to be deployed in arrays, so acquired data are not reliable at all.

It would be great to predict drawback effects of deploying a wave energy capture device far aside the deployment, via models and simulations for instance. With a deep knowledge of all possible phenomena that can occur and of relevant physical and biological processes which can affect the ecological stability, side effects can be predicted in advance with accuracy by using a high resolution model.

Unfortunately, areas considered for wave energy systems deployment are typically subjected to high energy natural phenomena (mainly but not only waves) and physical disturbance is very high (ecologically they are classified as exposed o extremely exposed). Thus studying the environment and the predictability of anthropogenic impact on natural processes is very challenging for ecologists.

Impact of shoreline devices is expected to be higher compared to offshore devices, since usually a shoreline device needs invasive works in the coastline such as excavations or landscape modifications, especially for an array.

1.9.1 POLLUTANT EMISSION

When referring to typical pollutant emissions, Wave energy devices produce no emission in normal operation compared to traditional fossil sources. However, deployment, installation, commissioning, operation and decommissioning phases of a wave powered plant can carry some emissions.

For any device, both shoreline and offshore, there are concrete problems of generating water turbidity during installation. Emissions of pollutants such as hydraulic or other type of oil or lubricants can occur too, also as a result of bad maintenance practices. Moreover, dissolving antifouling coating and other paint agents, which may be toxic to some species, can be diffused in the water.

Finally, amounts of any number of substances can be released by devices used for the deployment, commissioning and maintenance, such as boats, machines or instruments.

Emissions are in general very low in comparison to traditional fossil energy sources, and they can be reduced and controlled with careful choices and attentions, since the most dangerous consequence is represented by bioaccumulation in the food chain [12].

1.9.2 SEDIMENTS AND ORGANISMS TRANSPORTATION

There is concern that wave height is subjected to a reduction of 10-15% behind a wave energy plant and a re-establishment of the original height occurs within 3-4 km behind the plant, thanks to diffraction phenomenon. The height reduction can alter the marine currents and, above all, it may reduce sediment (both inorganic such as silt, clay from ground runoff, sand from rocks and minerals, and organic such as calcifying microalgae or calcium carbonate from mollusks shell) transportation, thereby altering the erosion processes of the coasts, beach morphology and seabed stability for devices located within 1-2 km from the shore.

The alteration of sedimentation processes can cause marine biological balance disturbance, with an impact on nearshore biological communities and microscopic mixture.

Sediment distributions influences indeed reef associated organisms, and any modification of sedimentation rate affects turbidity, salinity and water temperature with consequences on suspension feeders distribution and an inhibition of the algae and benthic organisms growth rate.

Regarding organism transportations, it can be said that plankton distribution as well as larvae spreading is highly regulated by waves motion over vast oceanic distances, providing food source for fish and whales. These dispersal patterns could change as per effect of changes in hydrodynamics due to the presence of a wave energy capture device.

The consequences drive the primary producers (phytoplankton) to change, with a knock on effect on the whole food chain of which it is the basis.

Changes will occur also to wave climate and, as a consequence, to bed shear stress and wave climate setup.

Of course, changes will be less likely for large water depths and in this case sediment transportation will be likely remain undisturbed.

Other negative consequences may arise after submerged cables installation, forming a disturbance impact corridor, although it should be rapidly colonized [12].

1.9.3 IMPACT ON MARINE WILDLIFE

On one hand, the deployment of wave energy harvesting devices will reduce fishing in the surrounding area, thereby producing a positive impact on marine wildlife, especially if the new introduced artificial habitat will be suitable for colonization by algae and marine animals, being a sort of sanctuary area for threatened or vulnerable species (as it is thought for abandoned drilling platforms).

On the other hand, one of the main sources of concern regarding disturbance to marine mammals and fishes is represented by underwater noise and vibrations resulting from operation, maintenance, commissioning, installation and decommissioning phases, which may be a problem depending on their frequency range. Even if airborne noise (emitted for instance by systems involving air turbines) would be likely masked by surrounding noise generated by wind and waves, a potential issue is determined by noise transmitted underwater.

Low frequency sounds generated by offshore wind turbines, for instance, can be detected by marine mammals, with negative effects on short term behavior and orientation, and it is reasonable to think that so it would be for wave energy catching devices. Also migratory routes can be influenced.

Another concrete risk for marine mammals and fishes is the physical contact, meaning a collision with installations.

Finally, the electromagnetism resulting from wave-energy harvesting systems (submarine cables, for instance) can cause interference and disturbances to the orientation and feeding mechanism of marine mammals and elasmobranchs, if they are very near to cables themselves. Otherwise it is not so relevant, as per electronics ships equipment, radios or GPSs.

Birds and pinnipeds are also attracted by artificial spaces constituted by wave energy devices. They can provide artificial protected surfaces for seabird nesting, resulting in a growth rate undesirably greater than it would be without the structure. Finally, another negative issue for birds is the collision with devices, especially at night, since birds seems to be attracted by artificial lights sources [12].

1.10 SEA TITAN Project

SEA TITAN is a European project in the framework of Horizon 2020, which aims to design, build, test and validate an innovative ocean wave energy harvesting system based on a direct-drive PTO solution to be used with multiple types of WECs.

A simpler, stronger, multi WEC-compatible and more cost-effective PTO technology would indeed significantly improve the wave energy market, thereby moving out from research early stage to a commercial phase, with a good standardization program.

Designing a crosscutting PTO means focusing all the efforts of the industrial world on a unique solution independent of the WEC, thus increasing the possibility of further development and improvement.

The project counts many participants from all over the Europe, from both the academic and the industrial world, with a strong know-how on technology.

SEA TITAN takes advantages from its precursor, namely the W1 WEC by Wedge Global, based on the first-generation PTO, deployed at PLOCAN site in Gran Canaria in 2014 as per Figure 1.23.

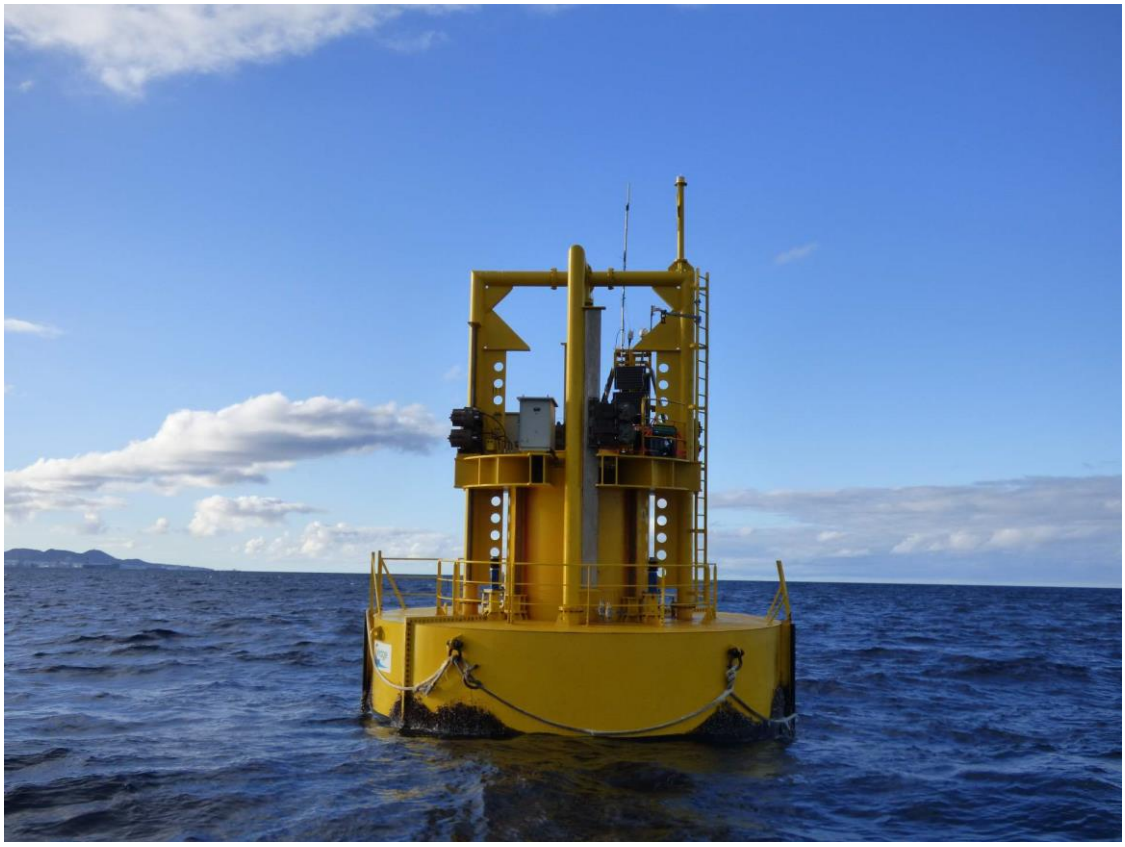

Figure 1.23 WEDGE W1 prototype during sea tests, starting point for SEA TITAN project.

1.10.1 WEC AND PTO

The chosen WEC device type has been the buoy-type point absorber (among wave-activated bodies), due to its simplicity, easiness of deployment and omni-directional behavior (as visible per Figure 1.24). It can also be easily boosted via smart PTOs, increasing the energy capture capability with positive effects on energy density (kWh/kg) and costs related to power extraction (LCOE €/kWh). These characteristics make the heaving point absorber WEC the ideal system to grant efficiency, high force and crosscutting features.

In order to maximize the efficiency and improve the control of the overall WEC, a direct drive PTO has been chosen, to avoid the conversion of the wave mechanical energy into electricity in two steps (usually pneumatic-electrical, hydraulic-electrical, mechanical-electrical). With a heaving movement due to the chosen hydrodynamic system, the PTO is a linear generator coupled to a proper power electronics converter and control apparatus.

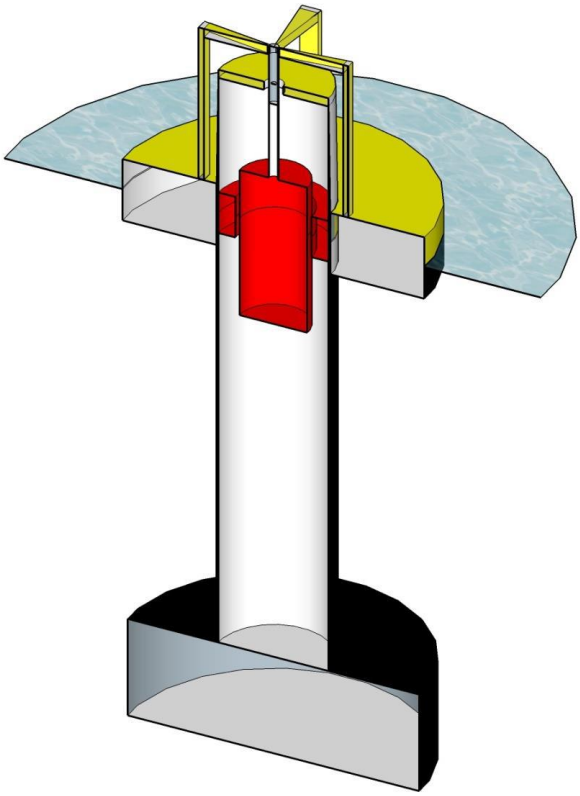

Figure 1.24 SEA TITAN WEC schematization.

The idea of a direct drive PTO offers many advantages: the overall efficiency is improved and most of the common failure sources are eliminated, moreover the controllability gets better, allowing the implementation of more efficient control strategies.

In order to better analyze the basic idea of SEA TITAN, some parameters are introduced:

- the Integrated Power Capture Ratio (IPCR) makes a comparison between the relative captured energy with a real PTO and the relative captured energy with an ideal PTO (with no force limitations and 100% efficiency);
- the Levelized Cost of Energy (LCOE) is the total cost of the device over its whole lifetime divided by the overall produced energy. It stands at about 85 c€/kW, ranging from half this value when the resource is very good up to about 140 c€/kW if the resource is very poor;
- the Capital Expenditure (CapEx) is the total cashflow used to build, operate and maintain the WEC;
- the Float-to-Wire Efficiency (FtWE) indicates the ratio between incoming mechanical energy from ocean waves and output electrical energy fed into the grid.

Particularly, regarding economic evaluations, a techno-economic model for LCOE estimation has been developed. Real condition sea states have been used to simulate wave input and all the energy conversion chain from the incident mechanical wave energy to the electrical energy integration within the grid (wave-to-wire model). A risk analysis of the key parameters has been done, and the model has been validated via a comparison with data acquired during 36 months at the PLOCAN site.

1.10.2 ELECTRIC LINEAR GENERATOR CHOICE

In order to design a direct-drive PTO, since waves cause an heaving oscillatory movement, the only solution is to use an electric linear generator.

Different types of linear machine have been evaluated and three possible candidates have been selected:

- Linear Permanent Magnet Synchronous Machine (LPMSM);
- Variable Reluctance Machine (VRM) or Switched Reluctance Machine (SRM);
- special machine based on the combination of the previous ones, such as the Vernier Machine (VM), and the Transverse Flux Permanent Magnet Machine (TFPMM).

In order to make a choice, there are some issues that must be taken into account.

First, the stroke length is defined not only by the wave height, but also by the resonance condition, because, in such a situation, the elongation can be large even for small waves. Anyway, it must be limited due to mechanical issues.

Then, to make an effective comparison, stator and translator dimensions can be analyzed introducing the shear stress σ N/m^2, which is the force produced by the electrical machine

per unit of its airgap surface. The shear stress is proportional to the electric load of the machine (A/m) and the magnetic load (T).

Regarding the comparison between PMSM and VRM, the main difference stands in the way the magnetic field is produced: while in the first case it is produced via permanent magnets, in the second type of machine it is generated by current in copper coils. Thus, the usage of material is different: in a permanent magnet machine, a certain amount of permanent magnet material is needed in order to produce the field.

With modern rare-earth magnets it is possible to generate magnetic fields up to 1.3 T with about 75 kg of material per square meter of airgap surface. In summary, a PMSM would require from 0.025 to 0.05 m^2 air gap per kN of required force and from 1.9 to 3.8 kg of magnetic material per kN of required force.

Talking about Saturated VRM (SVRM), the magnetic load must be expressed in terms of saturation flux density to define the shear stress. Although magnetic load can be higher, electric load is usually smaller than permanent magnet machine, and so the shear stress ranges in similar values with respect to PMSM.

Thus, the great advantage of SVRM is, above all, the winding spatial concentration, which allows more efficient cooling and cheaper fabrication cost. Moreover, no permanent magnet material is required, avoiding high costs and issues regarding the protection against the harsh marine environment (to which magnets are very sensitive). Additionally, in emergency cases, permanent magnets can lead to uncontrolled generation or be demagnetized, so they are quite delicate to be managed [13].

Regarding economic arguments, the main issue stands in the price of materials, in particular permanent magnet material, which runs the risk of being very volatile and can significantly increase the total cost of a generator, thereby introducing also other expensive manufacturing processes, delays and maintenance costs.

A little disadvantage comes from the acoustic noise and the copper losses resulting from high-force demanding operations (most likely when the speed is slow as for a swelling wave).

In conclusion, the choice of the Swithced Reluctance Machine type has been seen as the most effective standing the previous techno-economic considerations. The challenge has been to maximize the airgap surface with respect to the overall mass and volume and it has been reached working on the geometry [14].

1.10.3 AZIMUTHAL GEOMETRY

One of the most relevant aspects for the project is an innovative direct-drive PTO composed of a second-generation linear electric generator which is the Azimuthal Multitranslator Switched Reluctance Machine.

This new development is based on the configuration and geometry of a first generation Rectangular Multitranslator Switched Reluctance Machine (RMSRM) already developed by Wedge Global (W1 prototype) and tested in Gran Canaria at PLOCAN site in 2014. Efforts and studies have been done in order to increase its specific force density (both continuous and peak) and efficiency with the purpose to extend catchable energy range, in order to become a suitable and crosscutting solution for many different WEC applications.

These enhancements are also a solution to one of the key issues with WEC PTO systems, namely achieving sufficiently high peak force to limit hitting end-stops during large waves, while maintaining high efficiency and low cost for the average waves.

Technical details of this shape choice are discussed in chapter 2.

1.10.4 OBJECTIVES

SEA TITAN project pursues many objectives regarding innovation and implementation of new technologies. Here follows the list of the main focuses.

- Starting from the first-generation linear electric generator PTO RMSRM, an innovative second generation AMSRM is developed with improved characteristics, as:
    - doubled stator force density (referred to the stator mass, since he translator is modular and can be of different lengths), from 15.2 N/Kg to more than 30 N/Kg;
    - doubled IPCR, from 19% to 38%;
    - increased FtWE by a factor of 10%, up to 80%;
    - 25% lower CapEx per kW;
    - at least 30% lower LCOE, because reliability and energy production will increase while system mass and need for materials will decrease.
- A modular and crosscutting PTO is designed to allow an easy adaptation to different WEC technologies. By introducing a crosscutting PTO technology, a solution to the lack of a dedicated standard apparatus and supply chain is found, in order to find a common secure research path with lower development costs and make the purchasing less hard. A certain desired PTO can be made by one or more stacked modules, sharing

the same passive part, thereby being adaptable for many power levels. To become a suitable technology, requested forces and speed are up to 500 kN and up to 3 m/s.

- An innovative open hardware business model is created, developed and validated along the SEA TITAN project. It basically consists of opening the innovation process to the community in order to accelerate the advent of wave energy and to take advantage from external comments, ideas and further developments. Such a business model aims to enhance technology developments providing free use of patents by other competitors (WEC developers for instance). One of the goals of the project is to widely spread the wave-energy generation, but wave-energy research and development programmes of either major utilities or independent power producers are very small (far less than 0.1% of total R&D resource). So, the open hardware model aims at quickly improving quality and technology and promoting the diffusion of such a crosscutting PTO technology, collecting back each suggestion of improvement.
- A solid set of standards to address the world of wave-energy conversion is also created. The whole research activity around SEA TITAN allows introducing a certain level of standardization through the collaboration with international standardization technical committees. Standardization is very important to guarantee the respect of existing practices and reach a better market operativity and world visibility. One of the key issues that can make the ocean energy a viable renewable source also from a commercial point of view is indeed the existence of a structured standardization apparatus. Standardization platform constitutes an effective and fast way to transmit information and knowledge, since every piece of information is able to reach a widespread dissemination focusing on interested stakeholders.

In general, all the objectives have the common will to introduce an optimization of the project. The optimization implies high performance levels, reliability and lower costs, which are characteristics requested nowadays by wave-energy harvesting systems, and not met by most of common available off-the-shelf components that industry offers, or met by components too expensive to allow the beginning of a commercial phase for this kind of renewable-energy generators.

1.10.5 METODOLOGY

The proposed methodology of development for SEA TITAN can be detailed in four stages:

- Stage 1: **requirements**. The relationship between the PTO force and energy-capture capability is investigated for different technologies operating in different sites. For each technology, it is possible to evaluate the optimum PTO force and force density, the IPCR and its impact on the LCOE. Thus, it is possible to present a conceptual preliminary proposal for adapting the AMSRM to each WEC technology.
- Stage 2: **prototyping**. AMSRM prototyping is performed standing the results from stage 1 and the geometrical restrictions. The prototype can provide consistent information on technological issues, performance and costs. Many modifications and improvement are done and, finally, drawings and schematics are produced. The fabrication of each block (including power electronics and control system) is followed by Factory Acceptance Test (FAT) and then the integration of the complete PTO.
- Stage 3: **testing**. After the installation of the PTO and the first reception tests, both the device static and dynamic analysis are performed, in terms of force and efficiency. In the second phase, a PTO for different WECs sites is emulated with proper control strategy and selected sea-state(s). The test system consists of a generator and an actuator and tests are performed for different WEC technologies and sites to assess a realistic evaluation of the PTO performance, which is also compared to the results predicted by the available WECs models.
- Stage 4: **projection**. This phase extends the work to future activities, immediately before a ready-to-market product or the standardization phase. The main passages are:
    - calculation and design by updating tools and models to achieve a desired performance;
    - documenting all the fabrication procedures and technical solutions in the prototype in order to simplify fabrication methods and improve reliability;
    - building a new prototype cost model (thanks to experience) to extrapolate costs for bigger machines and perform a better and detailed LCOE analysis of a complete WEC;
    - improving the predictability of PTO and WECs models by taking advantage of experimental results;
    - integration and of AMSRM to different kind of WEC technologies.

1.10.6 ESTIMATED ADVANCEMENTS

In this section, the advancements of SEA TITAN are summarized:

1. Sea Titan develops a PTO suitable for many kinds of WEC, by pursuing principles of modularity and adaptability with operating values of force, stroke but also dimension and shape.
2. The PTO solution based on a switched reluctance linear machine is robust, reliable, cost effective and less demanding for maintenance. Since the direct drive solution is used, there are less moving parts, and reliability and controllability get better, as well as maintenance needs. Expensive materials like magnets are avoided.
3. In order to maximize the energy capture and conversion, force density level (from 17.5 N/kg of the RMSRM to a minimum of 30 N/kg for AMSRM) and efficiency have been increased, by acting on the control system and on the geometry of the machine. The velocity of the machine has been boosted too, reaching values up to 3 m/s thanks to the control system.
4. With the advantages gained, IPCR will increase from 19% to around 38% by acting on both force and efficiency.
5. CAPEX decreases by acting on the size of the system, in order to reduce LCOE, since CAPEX gives a significant contribution to the value of LCOE. The reduction in the CAPEX passes through some improvements:
    a. With the improvement in force density and efficiency, end-stops and brakes are limited and their contribution to CAPEX can be reduced.
    b. The symmetry of the machine facilitates keeping an easier manufacturing process and reducing the structure manufacturing costs.
    c. The modular approach and design determine a reduction in assembly and installation costs because processes are made simpler and can be serial.
6. Basing on models, LCOE would be reduced to 38 c€/kWh, to be confirmed with the optimized PTO cost model developed with information acquired during the experimental tests.

1.10.7 CONTRIBUTION

The main innovative aspects of the projects concern the versatility of the proposed energy harvesting machine and the simplicity of the power electronic apparatus as well as the auxiliary components, which make the overall system a suitable solution adaptable to many different locations.

The expected future impact of SEA TITAN project is spread over time:

- The next development projects of this innovative WEC and PTO will start from a consolidated basis, optimized in terms of performance and technical simplicity.
- Inside renewable energy sector, life cycle environmental impact will be reduced, not only because of the particular energy source, which can help stabilizing renewable production in the renewable energy market thanks to its predictability, but also because
    - noise is reduced by 60% since no gearboxes or hydraulic systems are used;
    - much material is saved and the footprint decreases if the geometry is chosen and adapted to the specific case;
    - no rare-earth materials are required.
- Nowadays, off-the-shelf components are not common or too expensive to meet SEA TITAN requirements. The industrial capacity can benefit from the necessity of standardized components, inaugurating commercial phase with a stabilized supply chain.
- Industrial growth and jobs can be created in Europe by increasing the wave energy sector. Since the prognostic is to deploy 100 GW of ocean energy power in Europe by 2050, around 250000 new high-quality jobs could be created, indirectly and directly, above all in the Atlantic coastal areas that suffer from high unemployment. Energy independence for Europe coastal areas will be granted too, breathing new life into peripherical harbours in Europe [15].
- SEA TITAN is a contribution for the solution of climate change issues and environment protection.
- Regarding the standardization, two standards are produced (namely two CEN Wokshop Agreements CWAs), which contribute to spread the knowhow of the project:
    - CWA 50271:2021 - Recommendations for a modular and cross-cutting Power Take-Off for wave energy direct drive linear solutions.

- CWA 50272:2021 - Methodology, procedures and equipment required for the laboratory testing of a modular and crosscutting Power Take-Off for wave energy converters.

The hope is that SEA TITAN design, which is adaptable to many WEC and different wave climates, versatile in shape and component arrangement, simple and robust, becomes a viable solution to start a commercial phase for ocean wave energy extraction systems, moving out from research and development stage.

Thanks to the standards, which have been developed by each participant in the project, both the design procedures and the testing methods are explained, in line with the open hardware business model on which the project is based.

Chapter 2 AMSRM and control

Although the central focus of this thesis is the design of the power electronics section, Chapter 2 is dedicated to the innovative aspects of SEA TITAN project concerning the electrical machine and the control system.

The reason why it has not been possible to commercially purchase all the power electronics elements stands in the particular characteristics of the system, starting from the electrical machine and its control.

Basis requirements and starting inputs come from those parts of the system.

2.1 Thrust and Efficiency

The name SEA TITAN stands for Surging Energy Absorption Through Increasing Thrust and efficieNcy. The innovations introduced to obtain a competitive wave-energy harvesting device lead to an increase in continuous and peak thrust force and efficiency.

Due to the slow wave heaving, which is various in waveform and energy carried, the need to increase thrust and efficiency to raise up the collected power is completely justified.

The main choice is the use of a direct drive PTO. With no mechanical, hydraulical or pneumatic intermediate energy conversion, the wave swelling is directly acquired, and the wave velocity become the system velocity, which is, thus, quite low. This slow motion must be coupled to high forces, i.e., thrusts in order to develop high power output. For a given wave height and period, there is a theoretical limit to the power that can be harvested from wave motion, depending on the control strategy that calculates the force that the machine must exert for each incoming wave. To ensure a wide range of wave periods, a wide range of thrusts (forces) is needed, and so it is theoretically impossible to harvest power from all sea states. Instead, it is preferable to work near the sea states with high occurrence.

Also, since the input energy source is variable, and rated conditions are not always met, an high-efficiency conversion is needed in order to exploit as much power as possible even when favorable conditions are not present. Furthermore, for real common PTOs, working in a wide range of forces to catch all the available power means showing a decrease in efficiency due to energy losses.

Finally, a higher peak force helps the system to survive against harsh wave conditions or storm mechanical stresses. Thanks to the limitation of end-stopping events, the WEC can operate in safety also against severe impacts, thereby reducing maintenance interventions.

It is now clear why an increase in efficiency and thrust (force) is necessary to produce a new generation of PTO to harvest a bigger amount of energy from ocean waves.

The requirements stated above need an high level adaptability and versatility.

2.1.1 MODEL ANALYSIS

For better understanding the need to reach higher thrust and efficiency, an analysis based on a theoretical model is hereafter shown.

The adopted model is based on the electrical representation of an heaving point absorber excited by wave movements. For the sake of simplicity, only the swinging movement of the floater is considered.

As visible in Figure 2.1, the whole system on the right is represented as a simple electric circuit on the left. Two external forces act on the floater in Figure 2.1a: they are the force exerted by the waves on the floater, highlighted in red, and the resistance force applied by the PTO to extract power from incident waves, highlighted in green. These two forces act on the floater and turn into a certain velocity profile through the inertia of the body, as the second principle of dynamic says. In Figure 2.1b the wave excitation and the PTO force are modelled as voltage generators $|U_W|_0$ and $|U_{PTO}|_\alpha$, coupled through the mechanical impedance of the floater $|Z|_\varphi$ (including radiation, inertia and buoyancy coefficients) [16]. As visible, if the Kirchhoff Voltage Law is applied to the circuit, the two voltages of the generators are opposite as the two corresponding forces. Additionally, to take into account the non-ideal behavior of the PTO, a parallel resistance $|R_{PTO}|_0$ is added to consider copper losses and efficiency in general. The $|R_{PTO}|_0$ is put directly across the $|U_{PTO}|_\alpha$ meaning that the chosen PTO force has also consequences on the losses of the machine and on its efficiency.

In such a schematization, the currents (i_1, i_2 in the scheme) correspond to the velocities.

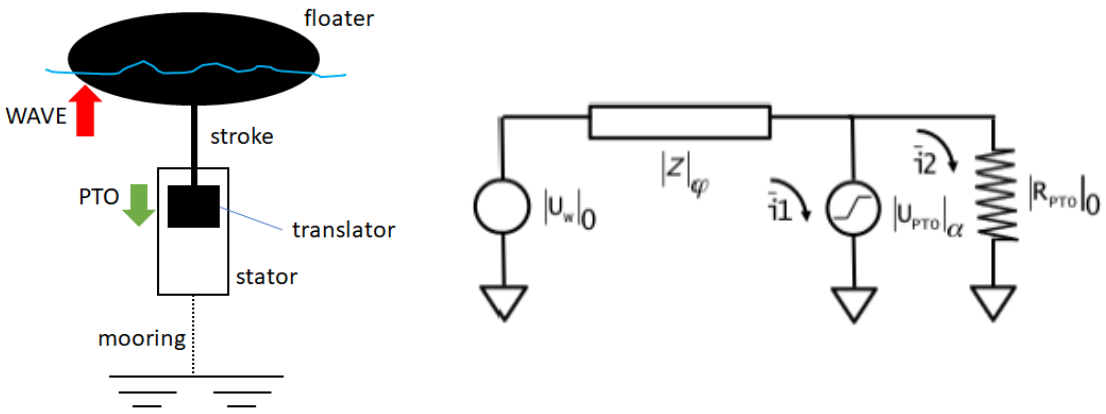

(a) (b)

Figure 2.1 Electrical parallelism to the mechanical model.

Starting from certain input data, the results obtained from this model have been compared with experimental measurements from the W1 prototype (see Figure 2.2).

Tests in Las Palmas, both at the harbor and at the PLOCAN facility, have been done on W1 prototype, considering a wide range of wave periods.

As visible, trends reported in Figure 2.2 (considered for a regular wave height of 1 m) show that the model can well predict the real behavior of the system, thereby allowing us to simply study the characteristics of the PTO.

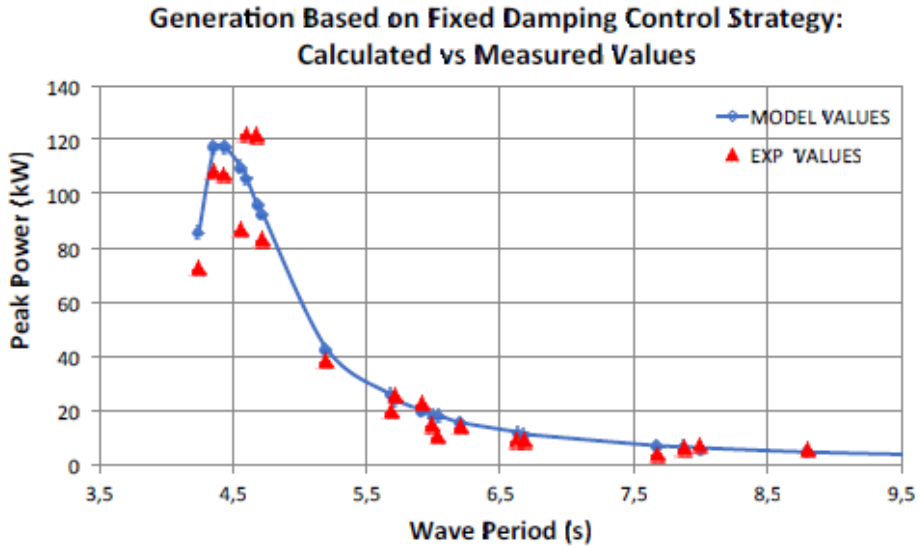

Figure 2.2 Comparison between the electrical model and experimental data for W1 prototype.

In order to understand the behavior of the system and the impact of thrust and efficiency on the catchable wave power, let us consider the model in Figure 2.1b with specific control strategies.

First, it is necessary to understand that, for each wave period (which means wave velocity), a certain value of applied force is required for the PTO in order to extract the maximum power in a certain wave climate. This means that, in order to harvest wave power, it is necessary to calculate the proper thrust that the PTO applies in opposition to the wave force and this thrust leads to a certain velocity value of the floating buoy and the translator as well.

If the calculation is correct and the machine mechanics allows high velocities, the power extraction improves with the same exerted thrust.

Figure 2.3a and Figure 2.3b shows a red curve (PTOXX) and a blue curve (FPTOX), which are, respectively, the maximum power that can be extracted from waves as a function of the wave period, and the corresponding force that the PTO must exert in order to extract the power in a limitless condition.

Conversely, the orange curve (Preal) and the green curve (Fava) represent the power and force extracted by the WEC under the constraint of a limited force.

Two different models of PTO are examined, resulting from the electrical equivalent model of Figure 2.1b in the ideal and real cases.

The ideal case (Figure 2.3a) assumes a control strategy that maximizes the generated electrical power for incoming regular waves, a high value of maximum applicable force corresponding to 1 MN (10^6 N) and 100% efficiency (which means that R_{PTO} is infinite, i.e., an open circuit).

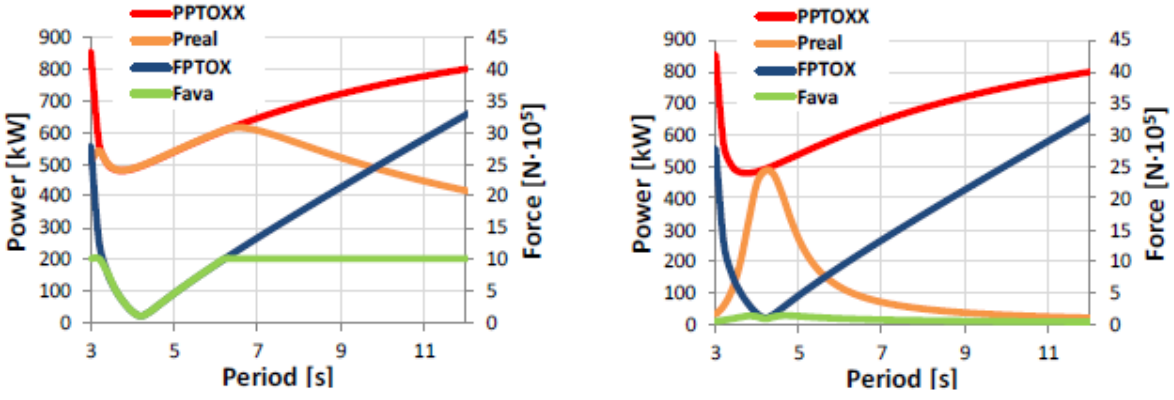

Figure 2.3 Comparison between ideal PTO (left) and real PTO (right).

In Figure 2.3a the orange curve represents the actual extracted power thanks to a certain force applied by the PTO (green curve) with the control strategy and the limits listed above. The maximum extractable power with no limits (red curve) requires a force (blue curve) which overcomes the imposed limit of 1 MN (10^6 N). Only when the green and blue traces

coincide, the actual power (orange curve) coincides with the maximum harvestable power (red curve).

The real case is shown in Figure 2.3b, where the red and blue curve are the same as before, since they represent a condition with no limits at all. In the real case, energy losses are also taken into account (differently from previous "ideal" case), thus, although the force limitation is the same as the previous "ideal" case (10^6 N), the WEC control strategy uses a lower force than the available one to maximize energy production, since losses grow for higher level of the force. In this case, the actual force (green curve) follows the maximum limitless force (blue curve) just in a narrow range of periods of the incoming wave. As a result, the actual power (orange curve) is much smaller than the maximum power that can be extracted with no limits (red curve).

It is now clear how real conditions (force limitations and lower efficiencies) tend to reduce the amount of harvested power.

Thus, when considering a real PTO (in the electrical model in Figure 2.1b it means that an $|R_{PTO}|_0$ of a certain value is considered), force restrictions and limited energy conversion efficiency occur and the amount of harvested energy drops down with respect to an ideal lossless PTO with unlimited force.

2.1.2 IPC AND IPCR EVALUATION

WECs are typically designed on a certain wave period (the most common in the chosen location) and the design tries to match the maximum extracted power and the period with the higher probability of occurrence. Since, indeed, it is impossible to find sites with constant daily or seasonal period heights, a certain level of flexibility in the values of force density is required and that is why increasing force density can lead to an increase in power capture.

An index which is very useful to quantify the advantages of a higher PTO force and efficiency is the Integrated Power Capture (IPC), which can be graphically represented as the area enclosed by the generated electrical power curve for a certain range of wave periods. As visible in Figure 2.4 (left), the ratio between the IPC for a real PTO (yellow area) and an ideal one (read area plus yellow area), both calculated on the entire period range chosen, is defined as IPCR (Integrated Power Capture Ratio).

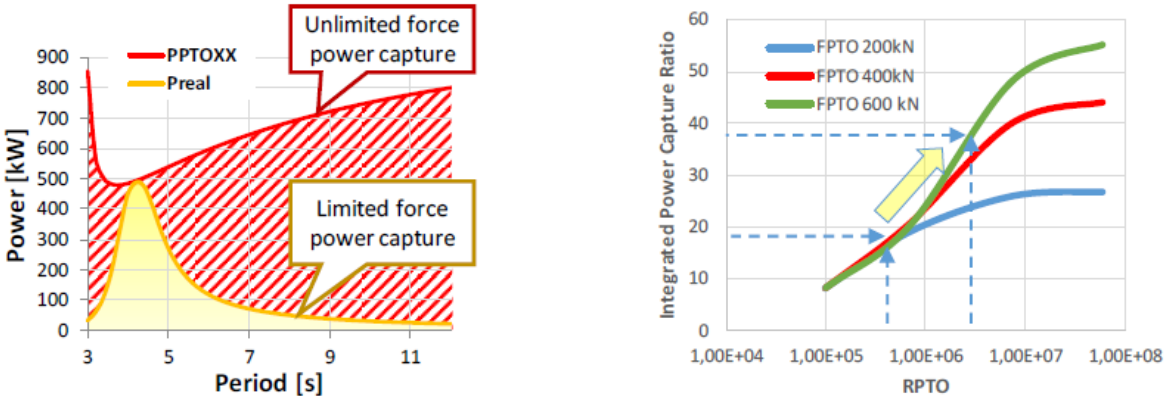

Figure 2.4 Graphical IPC and IPCR concepts on the left and IPCR dependance on thrust and efficiency on the right.

It is clear that the IPCR represents an ideality factor, which must be kept as high as possible. The graph in Figure 2.4 (right), shows that the IPCR can be increased by acting on:

- force capability, i.e., the force constraints that maintain the green curve below the blue curve in Figure 2.3;
- efficiency, represented by $|R_{PTO}|_0$ in the equivalent electrical circuit (Figure 2.1). The higher the resistance value, the more efficient the PTO is.

The best way to achieve a high level of extracted power is to increase both previous factors, and that is why SEA TITAN project aims to increase thrust (force) and efficiency.

Of course, to gain more power it is necessary to have an higher efficiency, otherwise no good effect is gained just by extending the thrust range.

SEA TITAN project aims to increase the IPCR value from 19% (W1 prototype) to 38%.

2.2 Linear electrical machine

The main innovation of the project stands indeed in the chosen type of PTO. To simplify the control and get efficiency benefits, the WEC is a Heaving Point Absorber type and in order to get the maximum advantages the PTO is a direct type one, which keeps high efficiency and low cost for the average wave case while reaching high peak force for larger waves. The lack of subsequent energy transformation stages determines high efficiency, high reliability and better control capability.

The electric generator must be than a linear generator due to wave vertical swing movement. In chapter 1.10.2, the choice of a switched reluctance machine as linear generator has been justified thanks to its simplicity, robustness, cost effectiveness and controllability.

An important innovation introduced in the project is the shape of the machine, which is substantially different from its precursor W200 (housed in the W1 prototype).

2.2.1 RMSRM

SEA TITAN PTO is based on Wedge Global Rectangular Multitranslator Switched Reluctance Machine (RMSRM), called W200 prototype, housed in W1 WEC developed through many R&D stages since 2007 and deployed in 2014 in Gran Canaria (PLOCAN site). The hydrodynamic system of W1 is a wave-activated body too (specifically an heaving point absorber type).

If the rectangular shape has been kept in order to maintain a certain level of simplicity and mechanical robustness, the multitranslator configuration finds its motivation in the necessity for a higher thrust level.

The basic idea has been to increase the airgap surface per unit volume, i.e., an increase in the total force with limited impact on the total volume. By keeping the same shear stress (force density calculated per unit of airgap surface), in order to obtain an higher resulting force, a wider airgap surface is necessary.

Thanks to the multitranslator layout, this becomes possible without increasing the total volume, thereby avoiding extra costs for material, transportation, deployment and maintenance and benefiting from the modularity.

While the simplest configuration of a Linear Swithced Reluctance Machine (LSRM) consists of one translator in the center and one stator all around, the first main important configuration improvement is the introduction of a second stator in an intermediate position, with the so called double-sided machine, a configuration which allows improving the overall force density and erasing the transversal force, with lower mechanical stress on moving element (see Figure 2.5).

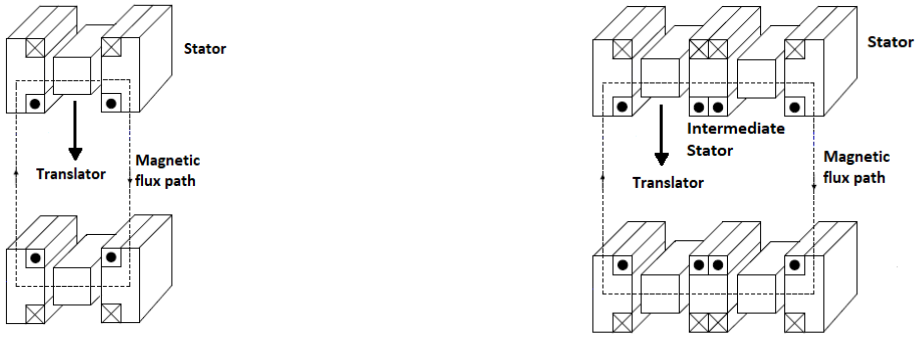

Figure 2.5 Comparison between single translator (left) and multitranslator (right) configuration.

Moreover, since high forces are necessary because low speeds are involved (sea waves heaving movements are slow), a need for more force has been achieved doubling the airgap, which results in a relevant surface with limited impact on the volume and the mass of the

system. The machine has been built, tested and then validated at the harbour of Las Palmas (Gran Canaria) and at PLOCAN site with the name of W1 prototype (shown in Figure 2.6

Figure 2.6 W1 WEC prototype on the left and W200 RMSRM on the right.

and Figure 2.7). The sea tests have allowed to collect over 3000 hours of operational data, covering a relevant amount of wave heights (from 0.3 m to 1.5 m) and periods (from 4 s to 11 s). The delivered power was in the expected range, showing good agreement with predictions.

Figure 2.6 W1 WEC prototype on the left and W200 RMSRM on the right.

Figure 2.7 Detailed picture of the multitranslator configuration for the W200 WEDGE Global prototype.

2.2.2 AMSRM

The SEA TITAN AMSRM is a non-patented Wedge Global linear electrical machine with many innovative aspects: the solution is compact, robust and cost-effective since permanent magnet materials are not used.

The multitranslator topology leads to a higher force density, but the main innovation in comparison to the precursor RMSRM stands in the azimuthal shape, which brings many advantages:

- the concept of multitranslator machine is enhanced and the airgap surface is increased by maintaining the same volume;
- the resulting exterior shape is cylindric and it can be easily adapted to many ocean-wave harvesting applications, where the cylindrical shape is often used;
- the particular shape allows compensating the lateral force, thereby reducing both the need for balancing systems and increasing the stability and robustness of the whole machine;
- no end coils are present since the flux close in the azimuthal circular shape: a certain amount of material is saved.

Such a particular geometry has the advantage of increasing the volumetric force density and the efficiency without using permanent magnets, so that power scaling increases with the volume instead of the outer surface as happens in traditional rotating machines or traditional linear machines.

Moreover, the force balancing improves and, in general, less material is used for a certain thrust level, reducing the mass and any other cost related to the weight.

In order to better understand the layout innovation and the comparison between RMSRM and AMSRM geometry, they are both represented in Figure 2.8

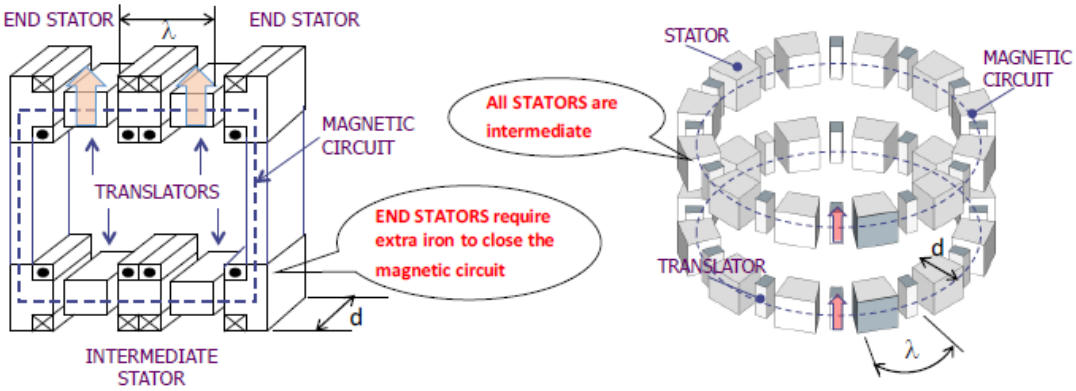

Figure 2.8 RMSRM on the left and AMSRM on the right.

As visible, in the RMSRM the magnetic flux path is displaced in a plane parallel to the direction of motion, thereby resulting in the necessity of a closing magnetic circuit on both sides due to the presence of end stators.

With the AMSRM layout, the magnetic flux path closes on a plane which is perpendicular to the direction of motion (this concept is highlighted in Figure 2.9). Each stator is identical to the others and no extra iron for magnetic circuit closures is necessary.

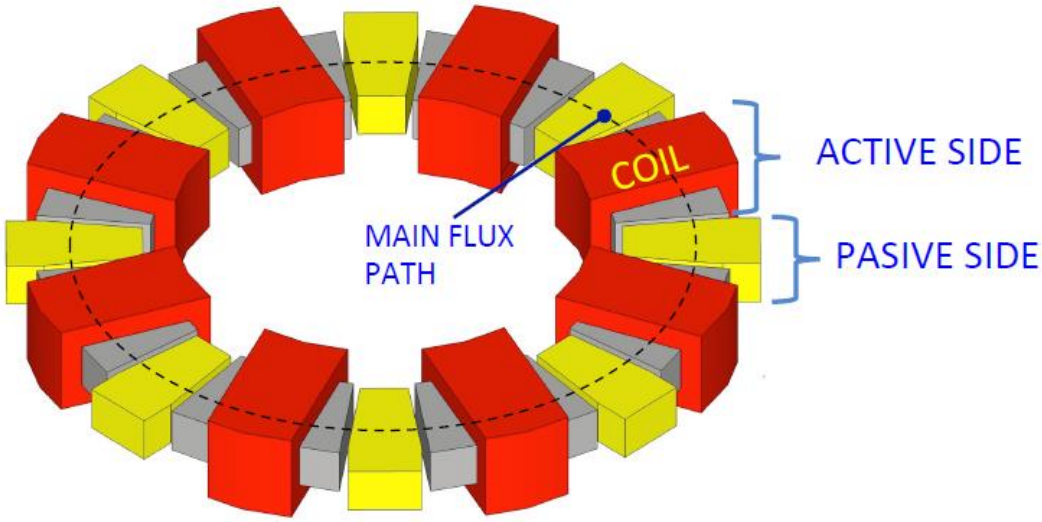

Figure 2.9 Highlighted magnetic flux path in an AMSRM portion.

Furthermore, an improved balancing in the two directions perpendicular to the moving one is introduced, with less stress on mechanical components.

Besides the advantage of eliminating end stators, there are other benefits in the AMSRM geometry.

An azimuthal layout indeed can be simply organized in a circular shape, favouring not only the design of marine-energy extraction systems but also the modular purpose of the solution. Due to fluid dynamics requisites, for pressure distribution reasons, the cilindrical shape is preferred when designing a system intended to be submerged. Therefore, the machine has a strong crosscutting behavior, because it can be adapted to many WEC solutions and external geometries.

Moreover, the resulting “donut”, as visible in Figure 2.10, is extremely modular, since more of these systems can be easily stacked one on another to reach the desired output power level.

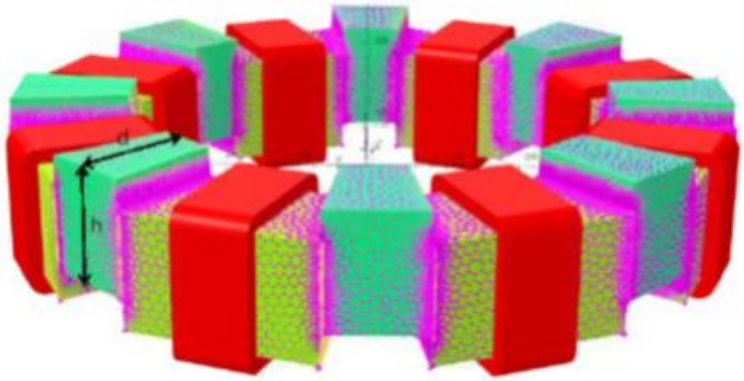

Figure 2.10 3D rendering of the AMSRM configuration.

Finally, also cooling issues gets benefit from this configuration, since the overall geometry offers a better behavior in heat dissipation and forced cooling. The main consequence stands in a larger electric load (flowing current) in comparison to RMSRM with limitations due to heat extraction problems.

2.2.3 STATOR AND TRANSLATOR ROLE CHOICE

Regarding the structural characteristics of the machine, two main parts can be spotted: the stator and the translator.

While the stator is coupled to the external carter and solidly linked to it in order to stay virtually stable (actually some motion can occur anyway), the translator moves up and down, maintained in position by proper bearings.

Even if the distinction about the moving features is clear, each part can be arranged according to different solutions, although not all of them are convenient.

Both stator and translator indeed differentiate regarding:

- the role: coils and windings define the active part while the passive one is composed only of ferromagnetic material, but no restrictions are considered, at the beginning, on which role would be better to assign to each part;
- the position: in this case, considering the stator as a fixed point, the translator configuration can be either inside or outside the stator, thereby resulting in a significant difference in the electrical interface layout;
- the length: particularly referred to the relative length between stator and translator, a factor that strongly influence the required space, material and cost.

Standing these considerations, it becomes clear that the choice of the machine configuration is quite a complicated issue and it must be intelligently elaborated.

First of all, it is better to elaborate in a graphical way all the possible geometries in order to understand the various situations. In Figure 2.11 all the configurations are present.

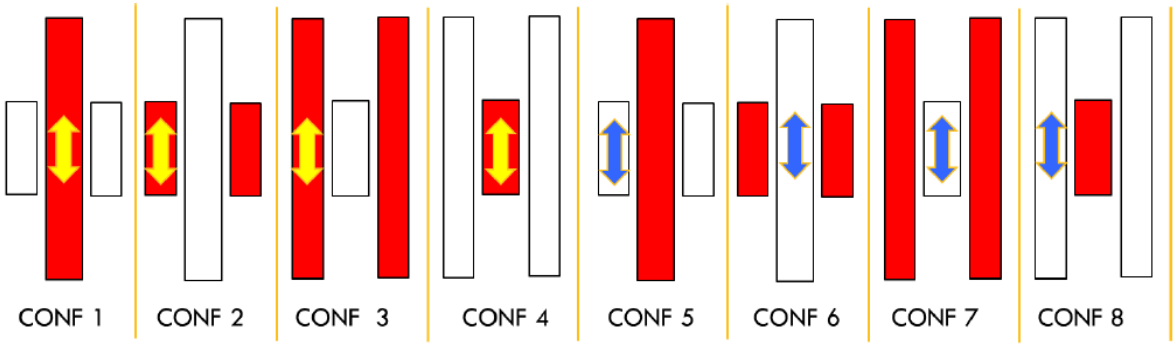

Figure 2.11 Translator and stator possible configurations. Arrows (blue or yellow) for translator, Red for active unit.

In details:

- Configuration 1: the translator, which is the active part, is inside the stator and it is longer.
- Configuration 2: the translator, which is the active part, is outside the stator and it is shorter.
- Configuration 3: the translator, which is the active part, is outside the stator and it is longer.
- Configuration 4: the translator, which is the active part, is inside the stator and it is shorter.
- Configuration 5: the translator, which is the passive part, is outside the stator and it is shorter.
- Configuration 6: the translator, which is the passive part, is inside the stator and it is longer.
- Configuration 7: the translator, which is the passive part, is inside the stator and it is shorter too.
- Configuration 8: the translator, which is the passive part, is outside the stator and it is longer.

With the purpose to make the better choice, it is possible to observe that:

- With a longer translator, some spacing problems arise, in particular the required housing would be doubled in space, as well as in material and costs, with issues concerning the transportation and deployment.
- The translator can assume the role of the active part, but it is necessary to foresee flexible cabling in order to connect to a moving part.

- If the translator is external, it may become necessary an additional prime mover for the translator interfaces.
- With a longer active part, more active material is needed, resulting in an increase in the cost due to construction, maintenance and total weight (due to copper high density)

Standing these suggestions, the combination which are considered to be the best are configuration 4 and configuration 6.

For each of them benefits and drawbacks are reported in Table 2.1 considering both a real application and alco consequences on laboratory tests:

Table 2.1 Benefits and drawbacks of stator/translator configuration 4 and 6.

	Configuration 4	**Configuration 6**
Benefits	• The stator can be integrated in the external carter structure, with no need for extra space and a cheaper solution which easily maintain high stiffness. • In a laboratory test, it is easy to fix the whole machine solidly to the ground via the external firm carter.	• The passive translator is lighter since it is internal and smaller. • There is no need for flexible cables and the access to electrical wiring is facilitated. • During laboratory tests, it becomes possible to move the stator shorter part with a motor.
Drawbacks	• Flexible cabling is necessary and the access to the active part is difficult. • During laboratory tests, the issue of supporting the active part must be solved.	• A space longer than the longest of the two part is required to correctly let the machine work. • The moved weight is higher and guiding systems are more solicitated. • The stiffness of the passive translator is not easy to achieve and, during a laboratory test, it's necessary to use intermediate supports.

On the basis of the wave climate in the application site, the material, money, suppliers availability, the space and instrumentation used for laboratory tests and the characteristic of the interface between the PTO and other part of the WEC, it becomes possible to take a decision.

Regarding SEA TITAN project, the chosen configuration is Configuration 4, as visible in Figure 2.12.

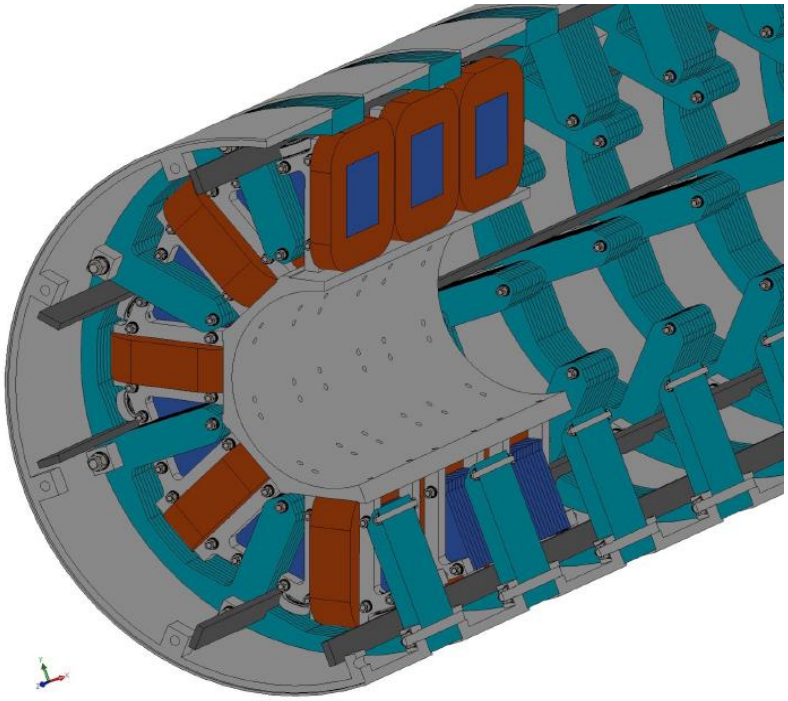

Figure 2.12 3D rendering of SEA TITAN PTO.

2.3 Electrical and mechanical design of the AMSRM

Since the main features of the active part play an important role in the definition of the PTO modular design, it is necessary to illustrate the design procedure of the active parts in order to better understand the constraints of the whole system.

The winding characteristics must take care not only of the force and power requirements, but also voltage limitations and stray fields as well as Lorentz forces must be considered.

Starting from the initial parameters, the design process passes through the calculation of magnetic field, ampere-turns, geometric size of the pole, Lorentz force and, finally, the total active part weight. After that, it becomes possible to determines the characteristics of passive part under specific configuration.

2.3.1 POM

A PTO Optimization Model (POM) has been developed in order to better understand the behaviour of the whole WEC system. Thanks to the POM, which integrates a wave-to-wire (W2W) model into an optimization algorithm, the basic characteristics of a WEC system, tailored to a given location, such as stroke, speed and thrust are obtained.

The POM approaches the design issue as an optimization problem, passing through the W2W model. Basically, it takes into consideration two search-space variables (rated thrust and stroke) and two target functions (average produced electrical power and cost), which must be maximized and minimized respectively.

The optimization problem is then solved by means of differential evolutionary algorithm.

At the beginning of SEA TITAN project, the analysis has been conducted for eight cases, including the Wedge Global W1 prototype location, whose analysis is shown in Figure 2.13. Optimum values of thrust and stroke are 109.26 kN and 2.664 m respectively, which maximises the power per unit of cost.

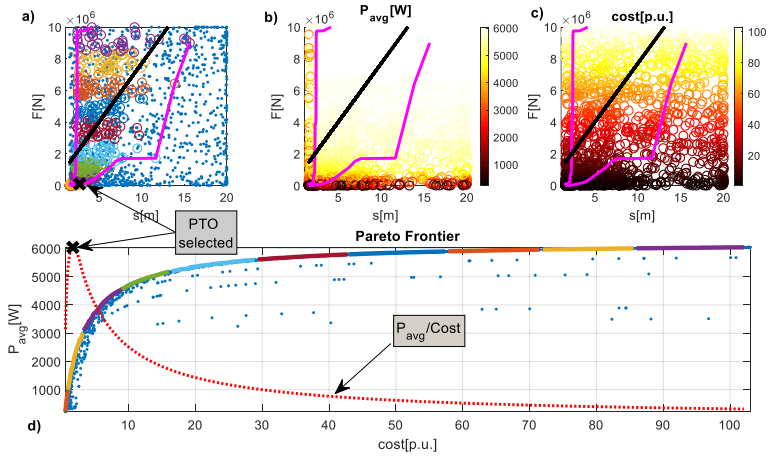

Figure 2.13 Pareto Frontier of Wedge Global's W1 at PLOCAN: a) b) c) with respect to the search space variables; d) with respect to the optimisation functions.

At this point, the aim has been to find a trade-off between simplicity and resulting thrust. A bigger AMSRM module would lead to a low number of modules for each configuration but, since the number of modules must be an integer number, the resulting thrust would be more easily controllable with a smaller module.

Taking advantages of a parametric study, the best compromise solution has been found for a 40 kN module, as shown in the graphical analysis of Figure 2.14.

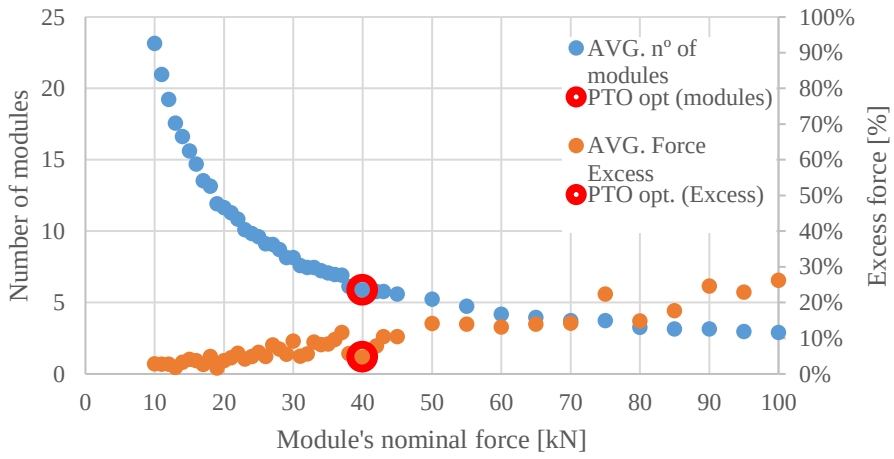

Figure 2.14 Average number of PTO modules (for all the 8 cases studied), and excess force for different PTO configurations of PTO (different values of rated force of the AMSRM module).

Regarding the rated speed, a compromise solution has been found at 3 m/s as it is a wave speed value suitable for many ocean conditions in most of the analysed cases.

2.3.2 *SEA TITAN STATOR AND TRANSLATOR DESIGN*

Regarding the SEA TITAN project, the copper coils of the active part (translator) are wound around an electrical steel core (940-100A) and supported by a non-conductive stainless-steel (AISI 304) star structure. The active unit is modular and each module consists of 3 phases, 8 coils per phase. A 3D rendering of the active part is visible in Figure 2.15.

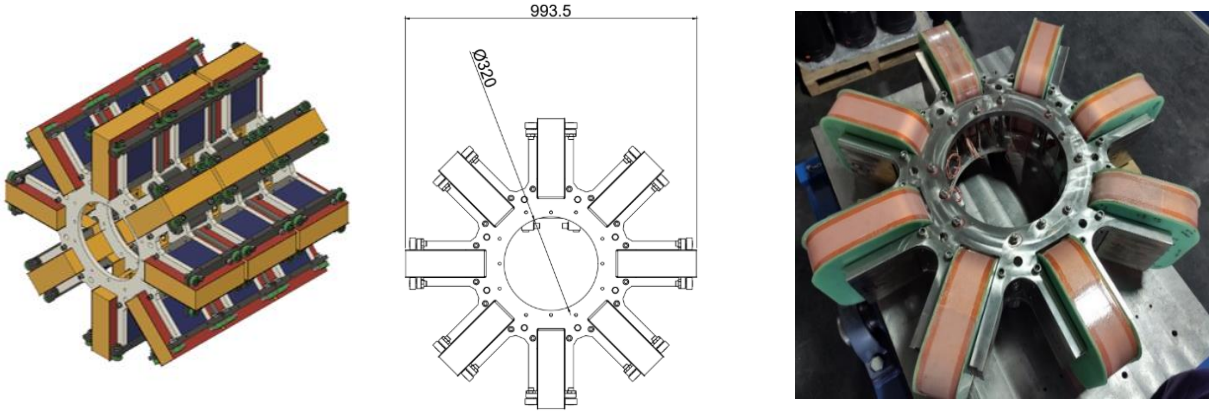

Figure 2.15 PTO translator. 3D model (left). Star support, including coils, front view (right).

The stator unit (passive part), shown in Figure 2.16, is made of electrical steel laminations (940-100A), with a support structure made of non-alloy steel (EN 1.0420). A total of fifteen stator modular units are present.

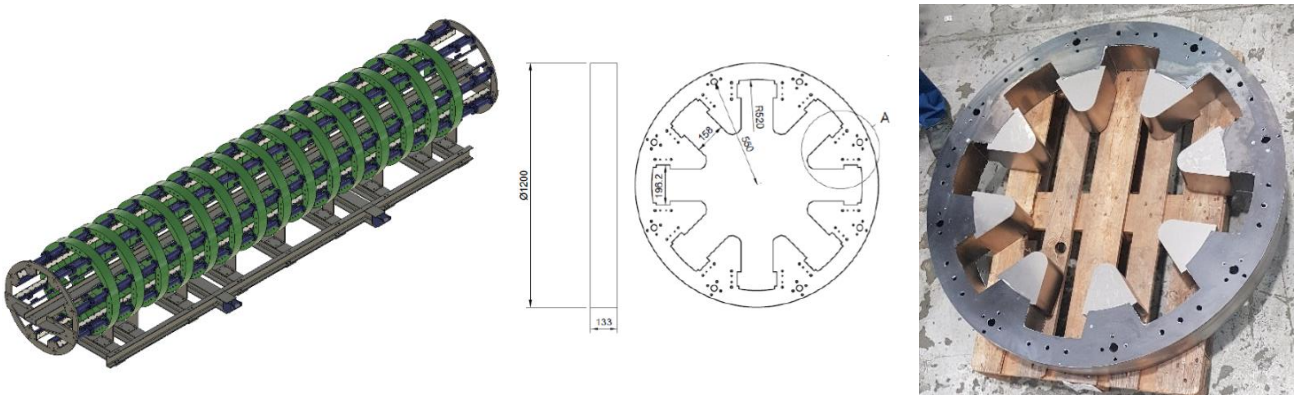

Figure 2.16 PTO stator and main frame. 3D model (left). Stator modular unit: Lateral view (center), front view (right).

The main frame used for laboratory test is also visible in Figure 2.17. It lets the whole machine stay fixed to the ground.

Figure 2.17 Main frame of the machine for laboratory tests.

Initially, the project aims to develop a laboratory application, in order to explore and validate the new technology, so many features, not only related to the machine design, are meant to be tested in a safe laboratory facility. Nevertheless, this situation does not affect the general structure of the system, and proper choices to run the machine in a marine environment have been faced and validated as well via shrewd design also for the power electronics section, which will be discussed in details in chapter 3.

Finally, it is worth saying that the force variation with the relative position of the stator/translator as well as the maximum peak value of the force is strongly influenced by the external aspect ratio of the pole itself. In particular, the wider the pole, the more triangular

the force profile. Let us consider two kinds of poles, each one with a coil with the same current and cross section area (Figure 2.18), but different values of width and height.

An higher height/width ratio corresponds to an higher peak force and a steadier plateau (Figure 2.19).

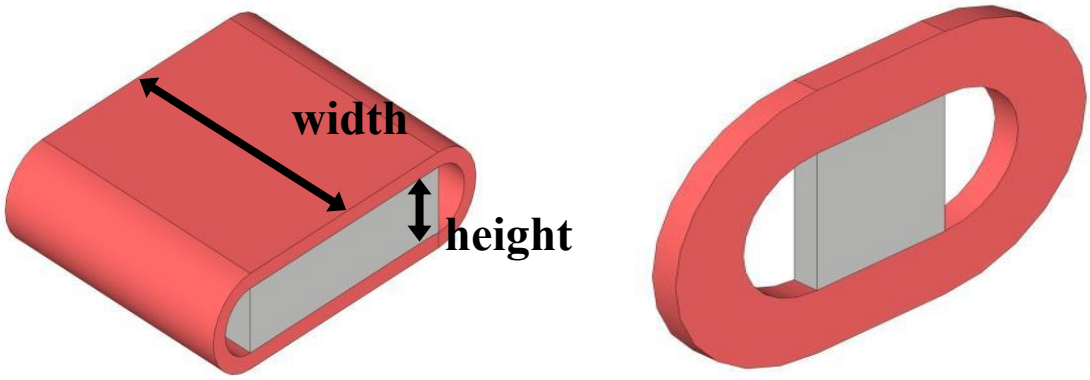

Figure 2.18 Poles with different aspect ratio.

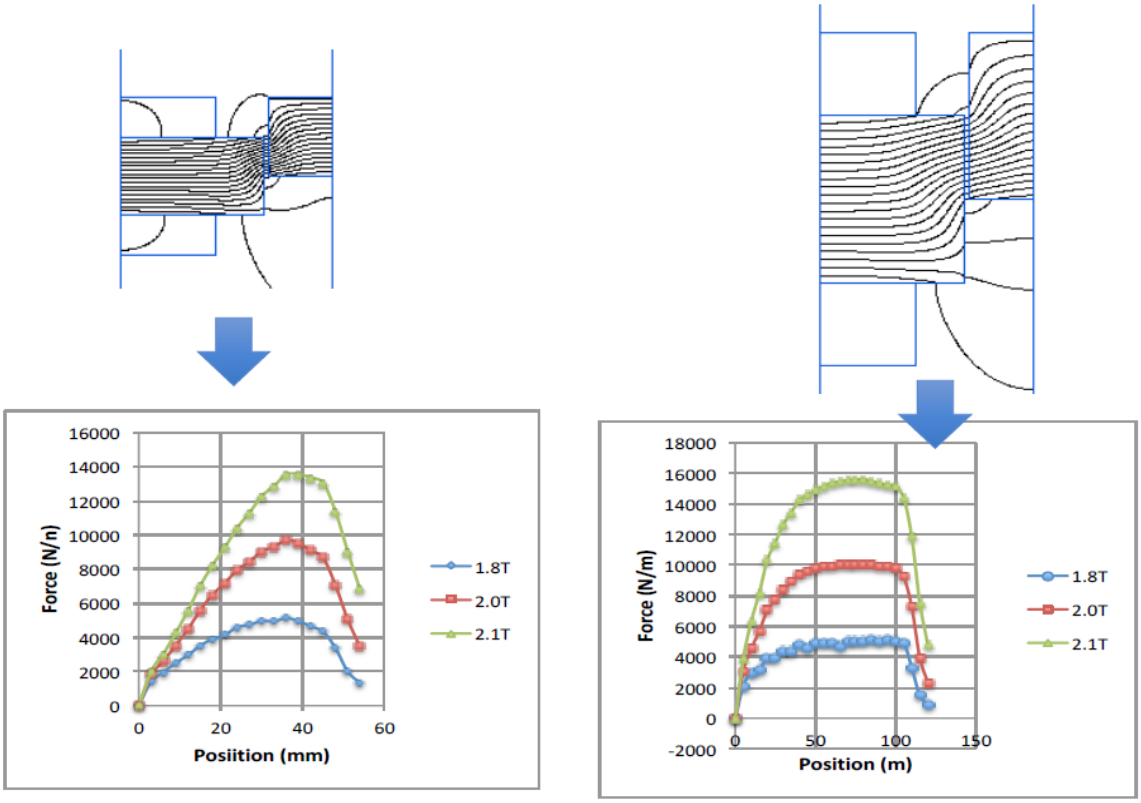

Lower height/width ratio Higher height/width ratio

Figure 2.19 Effect of the pole height/width ratio on the force peak value as a function of the stator/translator relative position.

2.3.3 OTHER MANUFACTURING ISSUES

Other mechanical issues, beyond the scope of this thesis, concern:

- the main frame, namely the external carter which enclosures the whole PTO. It must be solid but easy to get transported and deployed, and robust against external stresses due to the dangerous marine environment;
- bearings and rolling guides, which are important mechanical parts in this design, since they are responsible not only for the friction reduction but also for the mechanical guidance and balance of the machine. Also, they are subjected to severe stresses;
- cabling, with a particular attention to their flexibility because they interface stationary and moving active parts. They may need a support and, also, the bending radius must be kept within safety margins.

2.4 Control

The PTO solution presented in SEA TITAN is a Direct Drive type, which offers many advantages as stated in the previous chapters.

An important aspect is the simplification of the control strategy, since neither an inertial nor a low-reliability stage is between the wave mechanical movement and the electrical conversion.

The control system must take care of the movement of the linear electric generator, which is high in force values due to low velocities involved.

The mathematical model of the AMSRM consists of a differential equation for each machine phase [17]:

$$\frac{di}{dt} = \frac{V_{dc} - R \cdot i - \frac{\partial \lambda}{\partial x} \cdot v}{\frac{\partial \lambda}{\partial i}} \tag{2.1}$$

where λ is the magnetic flux, R is the phase resistance, V_{DC} is the DC-link voltage, i is the phase current, and v is the linear speed. Magnetic flux λ and force depend on the phase current i and on the relative position x between the active and passive parts. The values of the parameters are calculated by means of a 3D FEM analysis.

The current reference is imposed via a hysteresis soft switching strategy, explained in following paragraphs.

2.4.1 *Resonance condition*

When referred to a heaving buoy in an ocean, the resonance condition corresponds to the matching between the natural frequency of the buoy and the frequency of incident wave.

The natural frequency of the buoy is the frequency of oscillation of the buoy in condition of still water and it is

$$\omega_N = \sqrt{\frac{\rho g S}{M + m_\infty}} \tag{2.2}$$

where ρ is the density of ocean water, g is the gravity acceleration, S is the surface of the buoy in contact with the water, M is the mass of the buoy and m_∞ is the infinitely added mass, which is a parameter that takes into account the inertia of the buoy caused by the displacement of a certain amount of ocean water [18].

The buoy reaches the maximum velocity when its natural frequency ω_N matches the frequency of the incoming wave, which is usually small.

Typically the resonance condition can be achieved either via proper design of buoy parameters (mass and surface of contact and their variations through mechanical systems and actuators) or via the control system, which can force the buoy to move in phase with the wave by locking the buoy motion at certain times.

2.4.2 *Basic operating principle of a Switched Reluctance Machine)*

Let us focus on the RMSRM, whose control is based on the same principles as the AMSRM. Figure 2.20 shows the flux path in the machine.

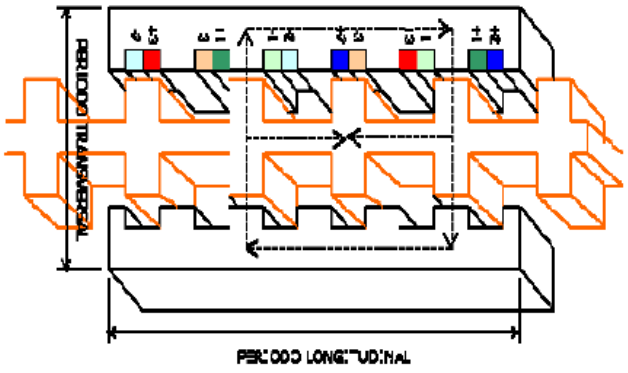

Figure 2.20 Magnetic flux path on the RMSRM machine.

In order to better understand the control principle with respect to magnetic flux and reluctance issues, Figure 2.21 shows the activation/deactivation sequence of the phases, depending on the position of the translator.

In Figure 2.21, the yellow part represents the translator, while the gray one is the stator. The air gap is deliberately exaggerated. As visible, in configuration (a) the energized phase is phase 1 and the translator is in a certain position. In order to make it move in the direction represented by the blue arrow, it is necessary to energize phase 2, since the tendency to reach the minimal value of reluctance for a certain magnetic configuration makes the translator move one step in the desired direction (b). If phase 3 had been energized instead of phase 2, the translator would have moved in the opposite direction from configuration (a).

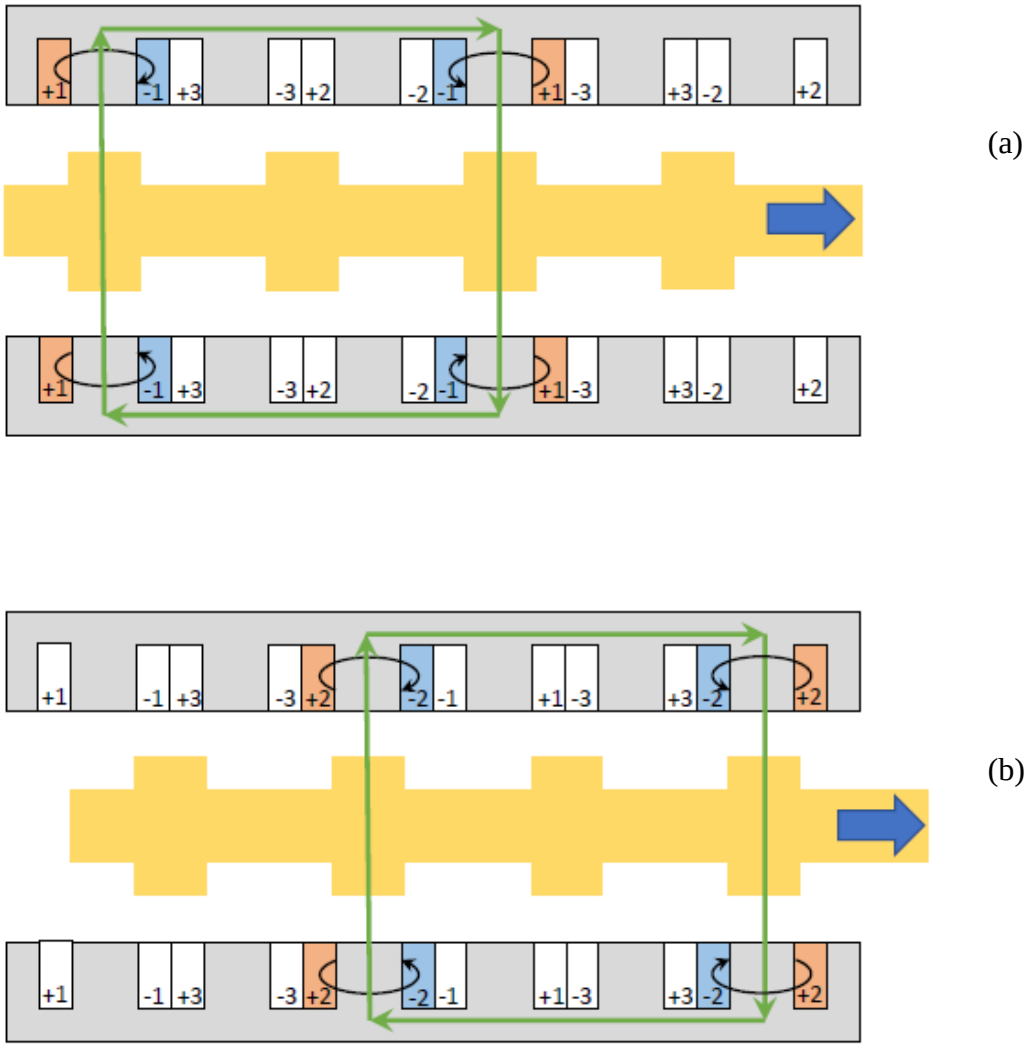

Figure 2.21 Basic principle of the reluctance machine.

2.4.3 *ACTIVATION/DEACTIVATION POSITIONS*

The right activation/deactivation positions are crucial to implement a good control system.

First, simulations at constant current and velocity have been analysed in order to find out the proper activation/deactivation position for each phase.

The knowledge of activation/deactivation positions is necessary to implement the switching strategy, so these positions have been calculated by means of a differential evolution stochastic algorithm for each couple of values of velocity and current (which are the inputs).

The algorithm basically applies survival rules to a certain initial population, thereby resulting in choosing the best solution possible (in a similar way to the evolution theory by Charles Darwin).

The mutation of each family of solutions is based on the distribution of the solutions in the current population, while the objective function is, in this case, the electrical or mechanical power, depending on whether the machine works as generator or motor.

A constraint in the DC-link current has been set in order to avoid the overload of the DC-link and to oversize its dimensions.

The optimum positions have been calculated referring to the corresponding switching angles of an equivalent rotational machine where the angular references can be easily converted into linear positions, standing the correspondence between a full rotation of 360° and the total length of the linear machine.

The results of the analysis for the rated current and force are shown in Figure 2.22.

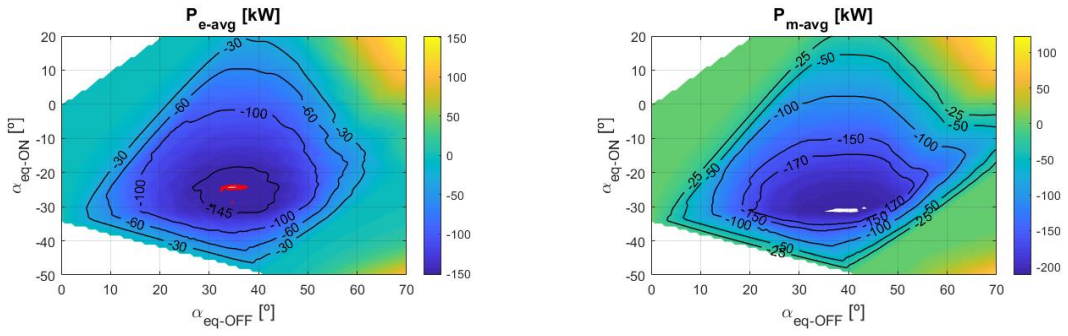

(a) (b)

Figure 2.22 Complete maps of electrical power generated (a) and mechanical power (b) as functions of equivalent switching angles for a rated operational point.

For each velocity/current operational point, the results have been obtained (Figure 2.23).

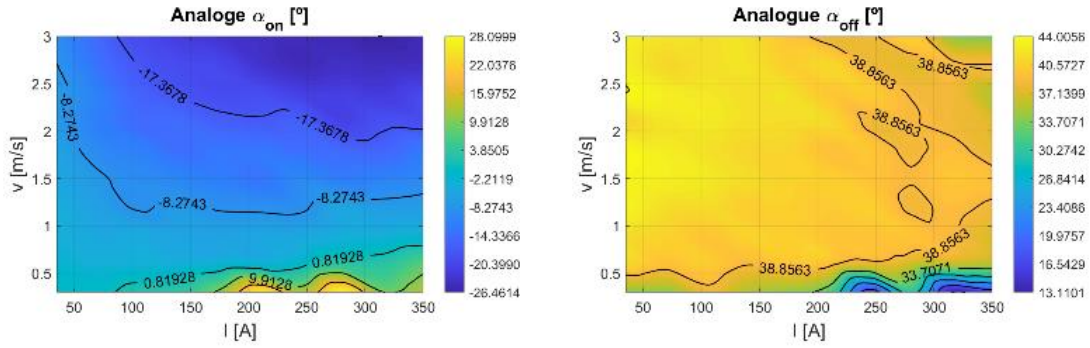

(a) (b)

Figure 2.23 Complete maps of activation (a) and deactivation (b) angle as function of velocity and current.

From the simulations, the correct activation/deactivation positions have been estimated for each phase.

When the machine works as a generator, the optimum activation positions of the phases are those where the electrical power output is the greatest.

When the machine works as a motor, the optimum activation position of the phases are those where a trade-off between efficiency and greatest mechanical power output is obtained [19].

2.4.4 BASIC CONTROL PRINCIPLE

In order to analyse the control strategy, it is better to illustrate the typical four operation modes of a WEC.

- In mode I, the system is at rest, until a certain amount of energy carried out by wave (usually connected with wave height) reaches the WEC.
- In mode II, the wave power is below the rated power of the WEC and a proper control strategy can be applied to extract the available power of the wave.
- In mode III, the output power is limited by the control system, when the wave power is greater than the rated power of the WEC.
- Finally, in mode IV, the operation stops due to the intervention of a safety device to protect the whole system.

In Figure 2.24 the four operation modes are presented in a chart where the output power is a function of the height (H) and the period (T) of the wave [17].

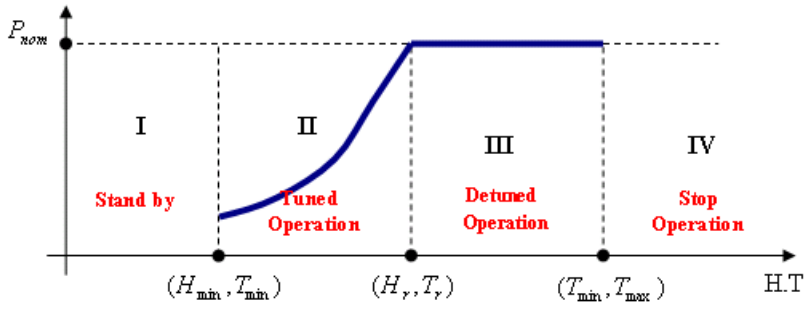

Figure 2.24 Typically four-stage WEC operation.

To absorb energy from a wave by means of a floating oscillating body, the body must create a wave that partly cancel the incident ocean wave. The WEC indeed must work in resonance with the incident wave to extract the maximum energy. It means that the velocity profile of the incident wave and of the wave that is generated by the WEC movement must be opposite and coincident so that the swinging body absorb energy by removing it from incident waves.

In this way, if the velocity profile of the WEC follows the velocity profile of incident wave, the extracted power is maximized with a certain applied thrust.

The control system requires the knowledge of the WEC hydrodynamic parameters, which can be obtained from finite-element analysis and experimental measurements. The chosen control strategy is based on the use of a reversible PTO (which can work as a generator and as a motor) since the double behavior is useful when working close to resonance.

The whole WEC is designed to work in certain rated conditions that are the most likely to occur, but the control system can significantly affect the performance.

The control system is implemented via two regulation loops (see Figure 2.25):

- one external, in charge of managing mechanical measurements from the PTO and from the excitation system (ocean waves), calculating the thrust reference and the necessity of the intervention of the safety systems also with prediction algorithms for the sea-wave behavior;
- the other internal, which calculates the proper switching strategy according to mechanical measurements (position), force values requested by previous control loop and electrical parameters measured from the machine.

The dependence of the current on the thrust values is regulated by the minimum mean square error method, since the relationship is quite complicated and it involves also the characteristics of the machine as well as the speed value.

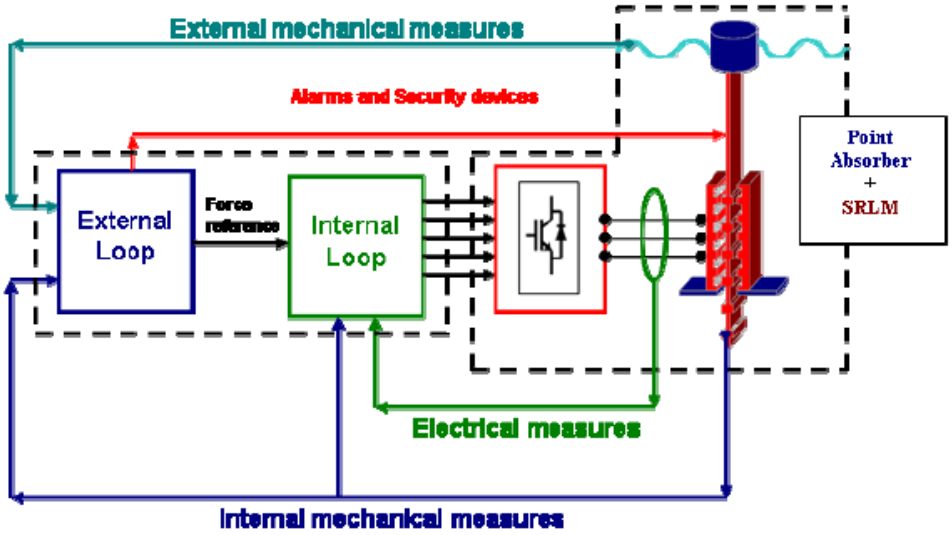

Figure 2.25 Control system architecture for SEA TITAN project.

2.4.5 CONTROL LOOPS

The control loops are briefly described in this section.

The external loop is in charge of the calculation of the thrust reference standing the initial data (actual force, actual velocity, incoming wave). It must communicate with measuring instruments and it can be equipped with predictive systems of waves in order to apply the best energy extraction strategy for a certain wave climate as well as to implement safety measures against severe conditions.

The internal control loop is responsible for the calculation of the power electronics switches commutation commands in order to maximize the power extracted starting from values of current and velocity. The internal loop imposes a certain force value (suggested by external loop) by setting a value of reference current.

The dependence of current on force is affected by the characteristics of the machine, and by values of current and velocity. An approximate function relating current with force was obtained by the method of Minimum Mean Square Error (MMSE).

2.4.6 HYSTERESIS BAND

The current reference is followed by mean of a hysteresis strategy. The GSC must regulate the current in the phases through the application of the bus DC voltage VDC.

At the beginning of an activation period of a phase, the total bus DC voltage VDC is applied to the phase, resulting in an increase in the current.

In order to follow the current reference, the control system establishes a certain switching profile for the power electronics system. The resulting current fits the hysteresis band, without exceeding or failing the value of the reference current over a certain range. To do so, values of 0V and -VDC are applied to the phase so that the current can increase or decrease respectively.

At the end of the period of a phase, -VDC is applied to extinguish the current.

With the counter-electromotive force (EMF) not very high and in low and medium velocity condition, the soft-switching control is applied, meaning that 0V is applied to raise the current to match hysteresis band limits.

When the velocities are low, with low values of EMF, the current cannot be controlled if 0V is applied and the evolution of the current depends on the velocity as shown in (2.1). In particular, the current rises at high velocities and falls at low velocities.

Thus, a certain velocity value defines a certain current behavior. A limit value of velocity cam be chosen depending on the expected current.

Since the swinging movement of waves determines a change in the sign of the velocity in each wave cycle, a multimode soft-switching hysteresis band control has been considered.

This kind of control applies 0V or -VDC to the phase to increase or decrease the current respectively if the velocity is higher than the limit value and it applies +VDC or 0V to the phase to increase or decrease the current respectively if the velocity is lower than the limit value.

Since the estimation of the limit velocity may be unprecise, the external hard-switching hysteresis band is established to manage any possible mistake, thereby ensuring robustness for this kind of control strategy.

This situation can be seen in Figure 2.26: on the left, the soft-switching mode correctly works due to the correct estimation of the limit value of velocity; on the right, the hard-switching mode must be applied to correct the behavior of the current following an incorrect estimation of the limit value of velocity [20].

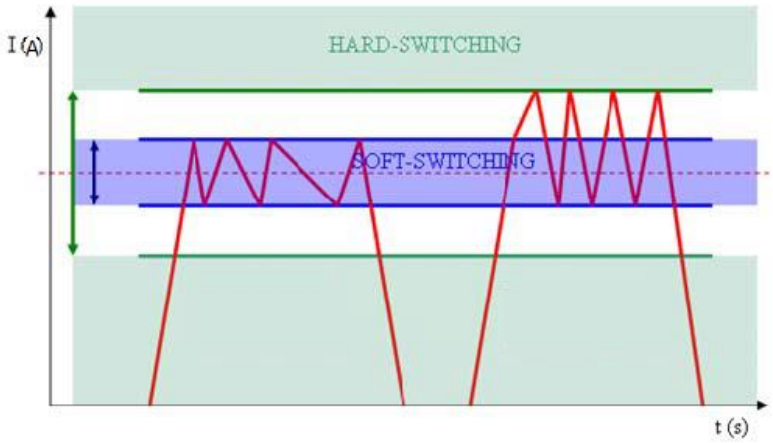

Figure 2.26 Graphical explanation of soft-switching and hard-switching hysteresis control strategy.

2.5 Control electronics

The control electronics architecture has been designed taking into account the concept of modularity of the AMSRM. Each power electronic converter has its own control system unit, but only one master control system supervises all units, as shown in Figure 2.27.

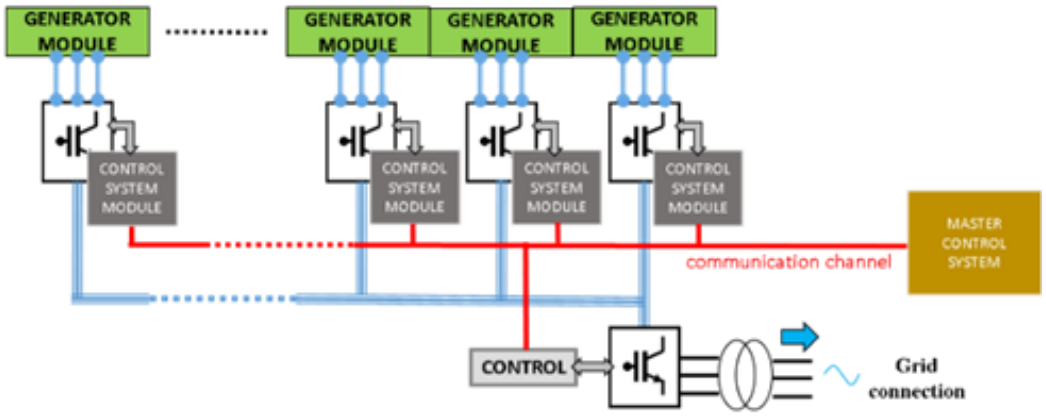

Figure 2.27 Modular control interconnection scheme.

The idea is that each section of the translator is a “module” (“generator module” in Figure 2.27) with its own power electronic converter (described in detail in the following chapters) and control unit (“control system module” in Figure 2.27). Each control unit, then, communicates through a “communication channel” (red line of Figure 2.27, with the “master control system” unit, which also is interfaced with the Active Front End (AFE) converter, i.e., the power electronics converter responsible of the energy exchange with the grid.

Chapter 3 Power electronics simulation and design

During the research activity, the static power electronics conversion system has been developed, designed and tested. The topology has been optimized in accordance to the control system and adapted to the electric grid interface to maximize the energy extraction.

The present chapter is focused on the design of the power electronics apparatus involved in SEA TITAN project. MATLAB Simulink simulations have been used to validate the initial choices and refine the components design.

Safety margins have been kept.

Also the control adaptation electronics interface has been designed. This board includes the acquisition and conditioning circuits for sensors and actuators. The hardware safety systems have been designed in order not to rely only on software safety logics.

3.1 Topology

The power electronics section of the SEA TITAN project is composed of an Active Front End converter called Grid Tied Converter (GTC), the generator converter named Generator Side Converter (GSC) and the electronic apparatus that adapt the measurements and command signals between the control section and the power electronics section.

A general view of the overall system is provided in Figure 3.1.

The left section of the figure is the GTC, the right one is the GSC, which is the subject of the design procedure.

The schematized DC bus is the result of two DC links in parallel: the GTC DC link, whose level is defined by the supplier of the GTC, and the GSC DC link. For safety reasons, the two DC link are separated via a fuse.

From the scheme of Figure 3.1, it is also possible to note that the GSC is formed by three H bridges (namely single phase converters) with a common DC bus.

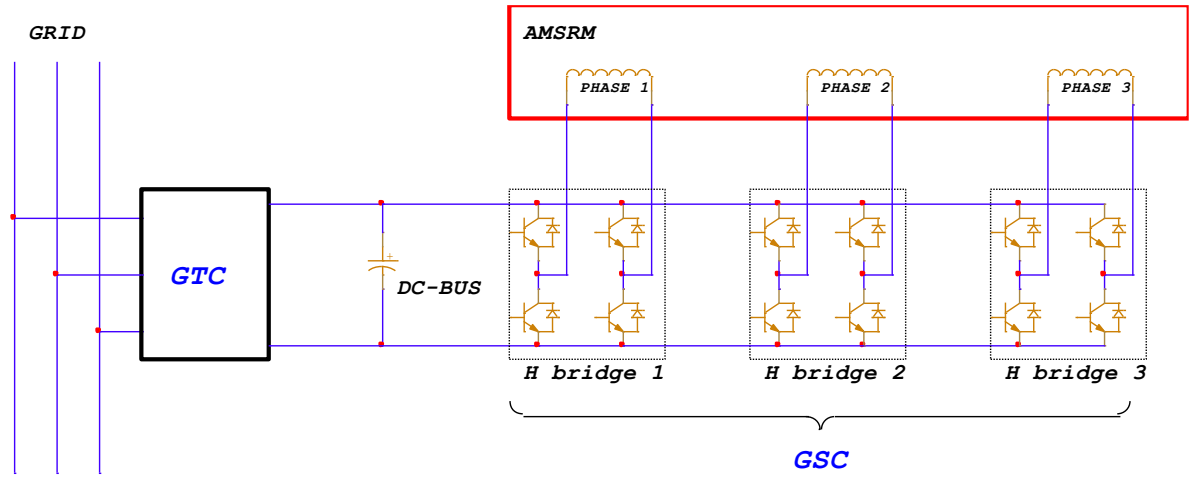

Figure 3.1 Schematic of the whole system.

3.1.1 GTC – GRID TIED CONVERTER

The GTC is composed by a three phase AFE converter, which is dedicated to the energy exchange with the grid.

Since the AFE stands as an electrical interface with the grid, it implements all the logic and algorithms for a grid-connected system.

The main design efforts have been focused on the GSC, due to the innovative and challenging purpose, which involves a new kind of electrical machine. Thus, the GTC has been purchased as a turn-key system, which satisfy the requirements shown in Table 3.1.

Table 3.1 GTC specifications.

Rated Data		
Symbol	**Description**	**Value**
Pdmax	Peak DC power that shall be delivered to grid	120 kW
dPmax	Maximum power derivative	130 kW/s
Tpulse	Duration of the power pulse that shall be delivered to grid	3 - 9 s
Vdc	DC voltage	900 V
Vac RMS	Line Voltage	400 V
Fn	Line frequency	47..53 Hz
λ	Power factor	0.98
THDi	AC current distortion	5%
T amb.	Ambient temperature range	-20 ... +40°C
RH% max	Maximum relative humidity (not condensing)	95%

Basically, the AFE corresponds to the grid-connected converter of an ordinary back to back configuration where the energy can flow in both direction (drawned or given) with respect to the grid.

A picture of the commercially available GTC supplied by EEI is given in Figure 3.2.

Figure 3.2 Commercially available AFE used in SEA TITAN project (GTC).

3.1.2 GSC – GENERATOR SIDE CONVERTER

The GSC is composed of three single-phase H bridge inverters, tied to a common DC bus, each one dedicated to one of the three phases of the generator. The system has been designed in this way to perform a proper control of each phase independently of the other, in order to avoid problems of homopolar currents and to allow higher voltages per phase.

Each H bridge is composed by two IGBT modules in parallel.

Since the current is unidirectional in each phase, a half-bridge power electronics converter has been considered. The control commands concern only the IGBT and diode of the main diagonal of the H-bridge, while the others have been kept off in the simulation as well as in the real application. The complete H-bridge module have been chosen for both availability and thermal stress withstanding.

Further considerations on the GSC system have been explained along the present chapter.

3.1.3 CONTROL ELECTRONICS APPARATUS

The generator power converter control card is supplied by CIEMAT, and OCEM has designed, built and tested a proper adaptation board, which works as an interface between the power electronics part and the control electronics part.

The functionalities of the adaptation board range from signal acquisition of the sensors, input command to the actuators, signals transformation and conditioning and hardware safety mechanisms, which have not to rely on software

3.2 Simulation structure

The overall simulation model used to identify the proper size of the power components has been performed using the AMSRM model and the control system model provided by CIEMAT. The model has been implemented as MATLAB scripts and Simulink block diagrams, where the power converter model, developed with PLECS to get better control on electrical and thermal behavior of the components, has been integrated by OCEM.

The resulting simulation system allows running the real power electronic control code, driving the IGBT of the GSC that feeds the AMSRM model. In the simulation, all the signal and variables reflect their real behavior in the project.

The simulation general block schematic is reported in Figure 3.3.

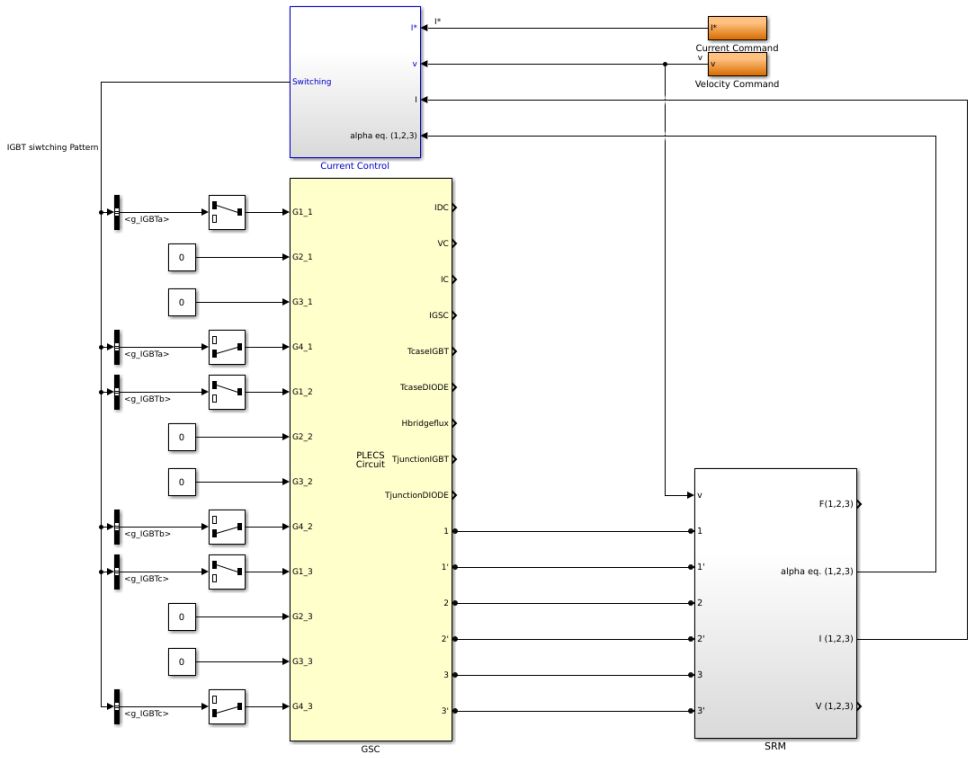

Figure 3.3 General simulation block schematics.

The next sections illustrate the block schematic of Figure 3.3 taking into consideration each part, explaining its function and working principle.

3.2.1 EXTERNAL INPUTS

Two external inputs ("Velocity Command" and "Current Command") can be set by the user in order to view the behavior of the system in different conditions.

On the top right the "Current Command" block provides the current reference "I*" which must be followed by the machine output phases. The reference of the external current stands as a thrust reference (the force is, indeed, directly connected with the current flowing on the machine). In a real system, it would have been provided by measurement systems able also to predict the conditions of the incoming waves.

During the simulation, in order to implement an analysis as general as possible, a sinusoidal wave profile of 350 A peak value and 10 s period value has been used.

The second external input introduced in the model is the "Velocity Command" (the orange block under "Current Command"). The velocity command is a sinusoidal wave profile with a peak value of 3 m/s and a period of 10 s. It simulates the incoming wave speed, detected by external measurement sensor in a real application.

The 10 s period corresponds to the most likely wave period in the chosen location for SEA TITAN, i.e., PLOCAN in Gran Canaria, the same location for W1 prototype) [19].

The "Current Command" signal goes as an input into the control system. Similarly, the "Velocity Command" goes also inside the machine model.

3.2.2 SRM ELECTRICAL GENERATOR MODEL

The block called "SRM" at the bottom on the right of Figure 3.3 represents the model of the electric generator. The block receives the voltage and current of the phases from the "GSC" block and the speed measured from sensors in a real system.

Inside the "SRM" block (see Figure 3.4, two different operations can be seen).

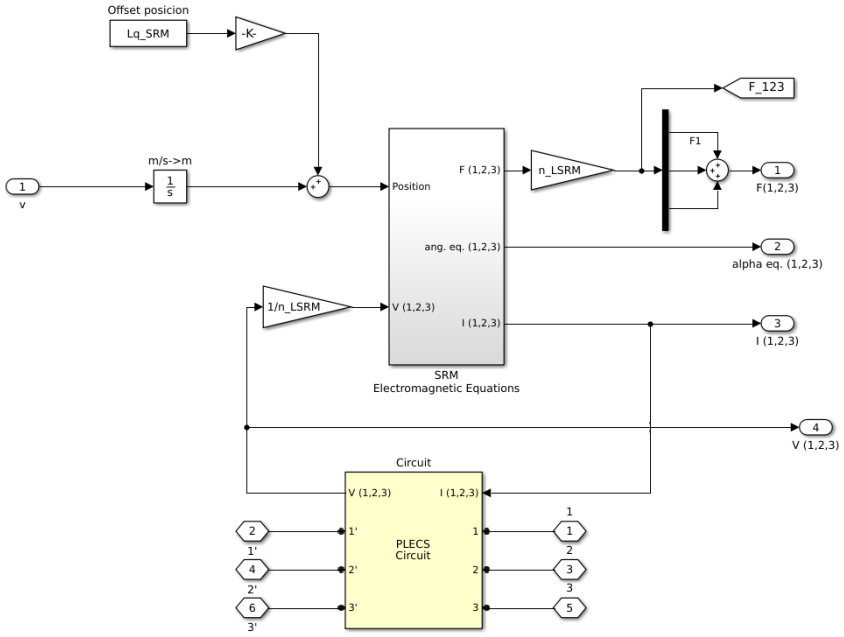

Figure 3.4 "SRM" block inside view.

The first operation involves the PLECS block (yellow “Circuit” block) at the bottom in Figure 3.4. Inside the block, voltages “V (1,2,3)” of the three phases of the machine are measured and the current “I (1,2,3)” are injected into the phases. The currents are calculated by the machine simulation block to follow the reference current, i.e., to exert a certain thrust for the incoming wave.

The calculation of the current is the second operation inside the “SRM” block. As visible in Figure 3.4, the block “SRM Electromagnetic Equations” calculates the values of

- the force in each phase “F (1,2,3)”;
- the equivalent angle “ang. Eq. (1,2,3)”, which corresponds to the equivalent positions of the translator reflected in a round equivalent machine where the total linear length has been compared to a full turn of 360°;
- the phase currents “I (1,2,3)”.

The implementation of the machine electromagnetic equations takes, as inputs, the voltage measured in the PLECS block and the position of the translator, obtained with the integration of the velocity added to an offset position.

Inside the “SRM Electromagnetic Equations” block, the derivative of the current is calculated according to (2.1).

By means of externally defined look-up tables the differential equation is solved and the currents as well as the forces are calculated.

3.2.3 *CONTROL SYSTEM*

The “Current Control” block at the top of Figure 3.3 contains the block schematic of the control system acting to produce the command gate signals for the IGBTs of the power electronics apparatus. The block takes, as inputs, the external references of current and velocity (explained in chapter 3.2.A) and the actual current as well, calculated by the “SRM” block as previously analyzed. Finally, another input is the actual position of the translator (with the equivalence between angular and linear position) calculated in the “SRM” block. A general view of the system is given in Figure 3.5.

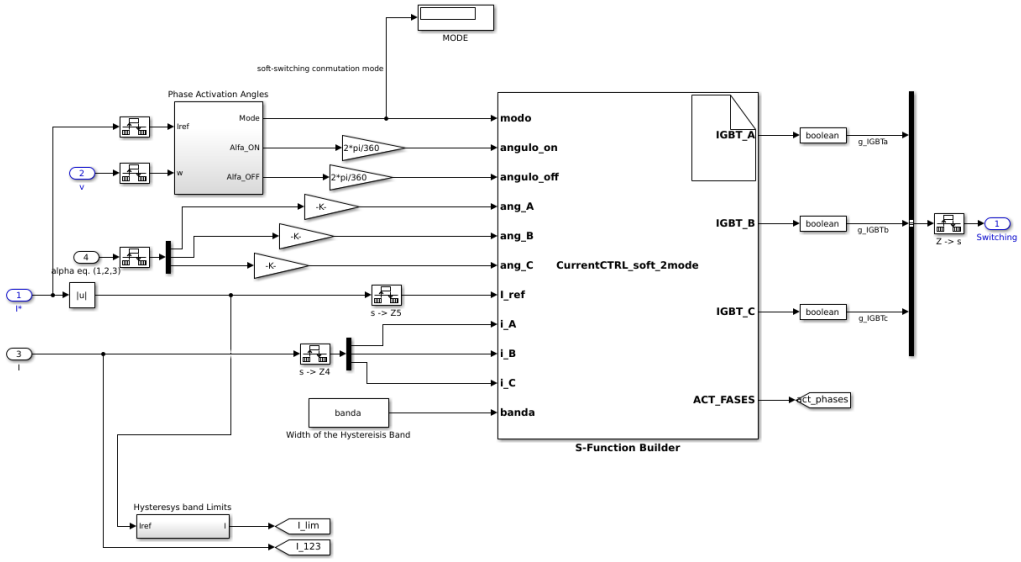

Figure 3.5 Detail of the insight of the "Current Control" block.

As visible, the block “S-Function Builder” is responsible for the calculation of the IGBT gate signals. The overall system takes as inputs the actual current, the reference current and the position of the translator. In the block “Phase Activation Angles”, the phases activation/deactivation positions are computed starting from the incoming wave characteristics (as stated in Chapter 2) as velocity “w” and reference current “Iref”. The overall system is also in charge of taking into account the limits of the hysteresis regulator.

3.2.4 *POWER ELECTRONICS APPARATUS*

As shown in Figure 3.3, the IGBT gate signals coming from the control system go to the PLECS circuit “GSC”, which simulates both the electrical and thermal behavior of the power electronics apparatus.

The circuit inside the “GSC” block is visible in Figure 3.6.

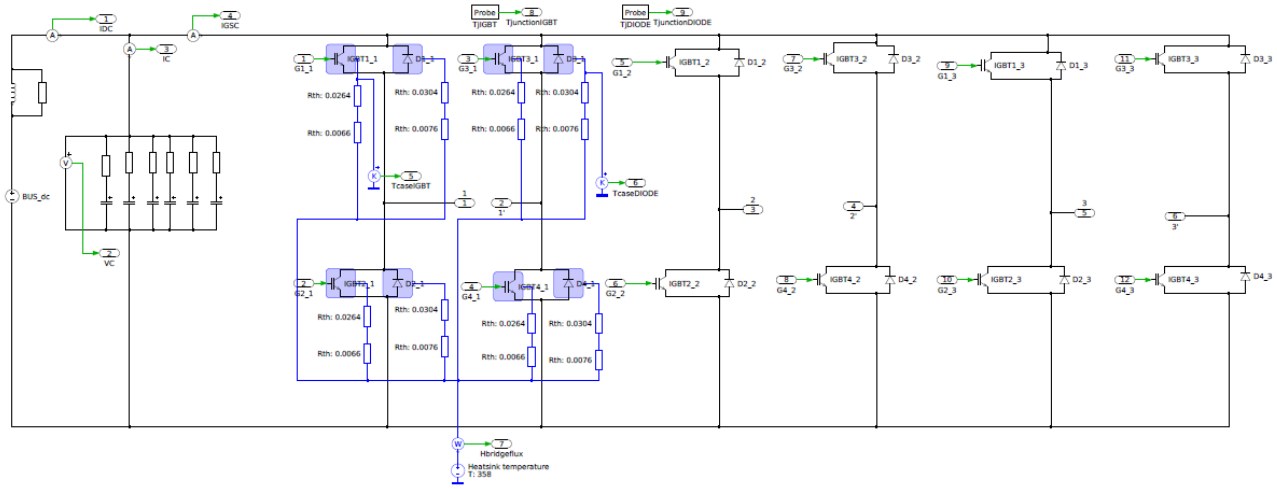

Figure 3.6 "GSC" circuit PLECS schematic.

The schematic of Figure 3.1 can be divided into three parts:

- on the left, the GTC is simulated simply via a DC voltage generator and an ohmic inductive circuit; for the sake of simplicity a 900 V constant voltage source in series with a parallel LR circuit is intended to model the behaviour of the AFE (the resistor value is 200 mΩ, the inductor value is 20 mH and the L/R time constant is 100 ms);
- on the right, the GSC is visible, with a total of six branches (each one composed by two IGBTs with corresponding antiparallel diodes); two by two, the six branches form three H bridges;
- in the center of the figure, the DC bus is composed by six capacitors in parallel with the corresponding equivalent series resistances (ESRs).

The signal input ports receive the IGBT gate commands and distribute them to the IGBT modules, while the electrical output ports are responsible for voltage and current information exchange with the simulation block “SRM” of the electrical machine.

3.2.5 *THERMAL MODEL*

In Figure 3.6 part of the thermal model is also visible.

The thermal modelling procedure is explained in this section. This is an important design method carried out through MATLAB Simulink simulations.

Each component is modelled as a thermal Foster network (see Figure 3.7) starting from the semiconductor junction initial temperature, which is externally defined by the parameter “T_init”. The junction is then modelled as an heat flow generator controlled by the dynamic behavior discussed below. The thermal network of each switch, which terminates with the

component case temperature, is followed by a thermal resistor that represents the case-to-heatsink contact thermal resistance, which is composed of two resistors in Figure 3.6. Finally, a constant temperature source is set, which represent the heatsink temperature. Since the thermal capacity of the heatsink (which is air or liquid cooled) is much larger than that of the power electronics components. Consequently, the heatsink can be modelled as a constant temperature source.

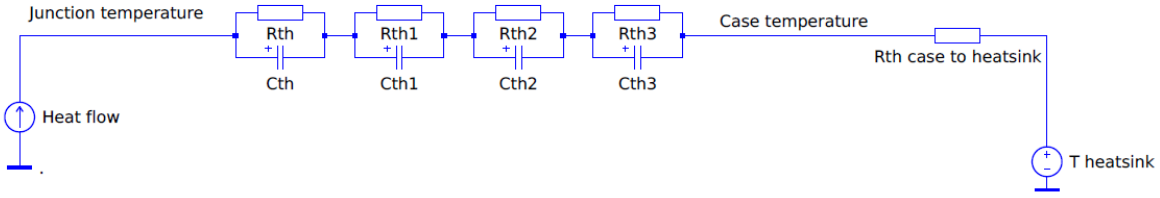

Figure 3.7 IGBT module thermal model.

In the model used for the design of the SEA TITAN power electronics design, four RC thermal impedances have been taken into consideration, as recommended by the datasheet of the switches.

The thermal losses are defined by proper charts for the turn-on losses, turn-off losses and conduction losses. The non-linear behavior is taken into account and the datasheet parameters are used in the model for a description of the components as accurate as possible.

No mutual influence (IGBT and corresponding antiparallel diode) effects have been taken into account since the safety margins kept seem enough conservative.

The thermal models used for the IGBT and antiparallel diode respectively are shown in Figure 3.8, Figure 3.9, Figure 3.10, Figure 3.11.

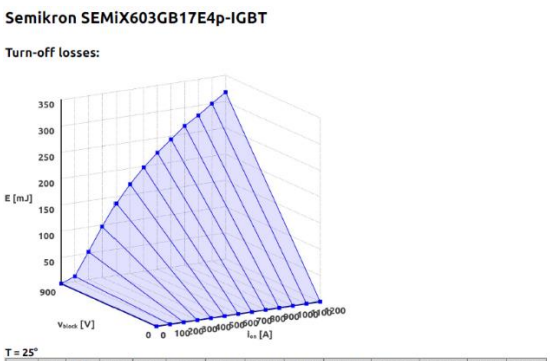

	0 A	100 A	200 A	300 A	400 A	500 A	600 A	700 A	800 A	900 A	1000 A	1100 A	1200 A
0 V	0 mJ	0 mJ	0 mJ	0 mJ	0 mJ	0 mJ	0 mJ	0 mJ	0 mJ	0 mJ	0 mJ	0 mJ	0 mJ
900 V	0 mJ	10 mJ	53 mJ	97 mJ	137 mJ	170 mJ	198 mJ	222 mJ	243.7 mJ	265.3 mJ	281.5 mJ	300 mJ	318 mJ

(a)

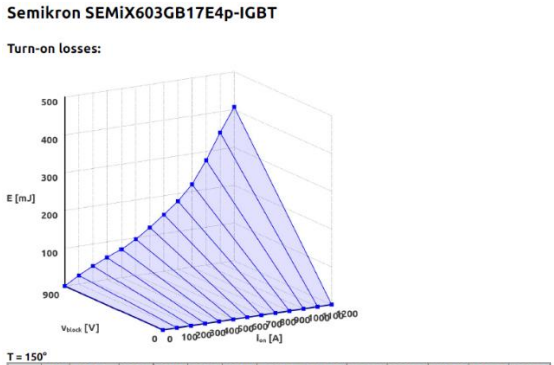

	0 A	100 A	200 A	300 A	400 A	500 A	600 A	700 A	800 A	900 A	1000 A	1100 A	1200 A
0 V	0 mJ	0 mJ	0 mJ	0 mJ	0 mJ	0 mJ	0 mJ	0 mJ	0 mJ	0 mJ	0 mJ	0 mJ	0 mJ
900 V	0 mJ	22.63 mJ	42 mJ	59 mJ	75 mJ	96 mJ	121.5 mJ	150 mJ	180 mJ	219 mJ	277 mJ	345 mJ	407 mJ

(b)

Figure 3.8 Turn-on (a) and Turn-off (b) losses of the IGBT.

Semikron SEMiX603GB17E4p-IGBT

Conduction losses:

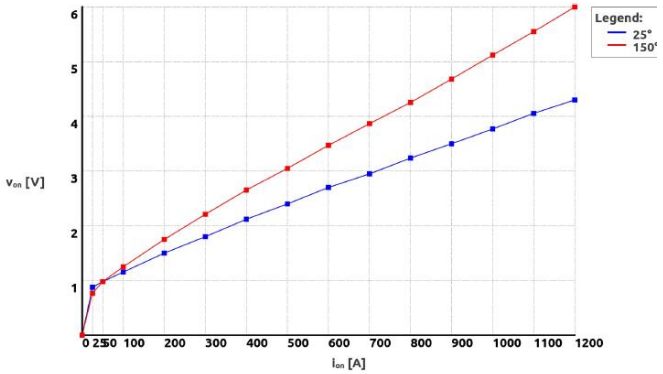

Semikron SEMiX603GB17E4p-IGBT

Thermal impedance (Foster):

	1	2	3	4
R	0.0017 K/W	0.0023 K/W	0.0308 K/W	0.0022 K/W
τ	0.0005 s	0.0032 s	0.0323 s	8.139 s

(a) (b)

Figure 3.9 Conduction losses (a) and Foster thermal network (b) of the IGBT.

Semikron SEMiX603GB17E4p-DIODE

Turn-off losses:

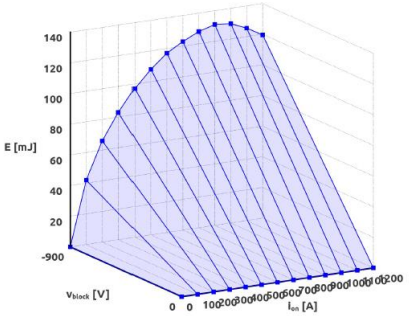

T = 150°

	0 A	100 A	200 A	300 A	400 A	500 A	600 A	700 A	800 A	900 A	1000 A	1100 A	1200 A
-900 V	0 mJ	42 mJ	66 mJ	82.98 mJ	96.97 mJ	108 mJ	117 mJ	123 mJ	128 mJ	131 mJ	130 mJ	125.5 mJ	119.5 mJ
0 V	0 mJ	0 mJ	0 mJ	0 mJ	0 mJ	0 mJ	0 mJ	0 mJ	0 mJ	0 mJ	0 mJ	0 mJ	0 mJ

Figure 3.10 Turn-off losses of the antiparallel diode.

Semikron SEMiX603GB17E4p-DIODE

Conduction losses:

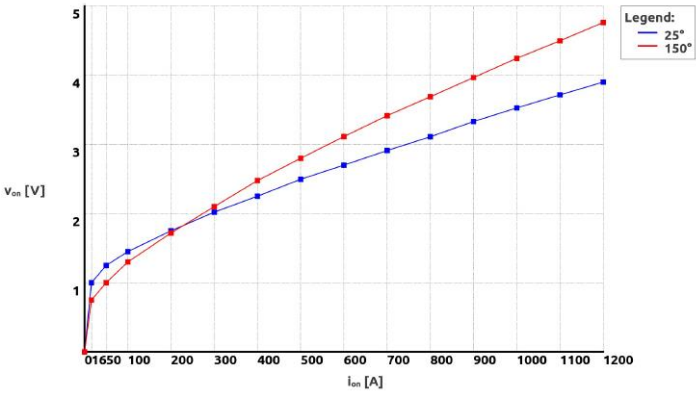

Semikron SEMiX603GB17E4p-DIODE

Thermal impedance (Foster):

	1	2	3	4
R	0.0081 K/W	0.0526 K/W	0.007 K/W	0.0053 K/W
τ	0.0009 s	0.029 s	0.1723 s	5.181 s

(a) (b)

Figure 3.11 Conduction losses (a) and Foster thermal network (b) of the antiparallel diode.

3.3 Simulation results and sizing criteria

Simulations have been performed at the rated steady state conditions, where the AMSRM generator has been excited with a sinusoidal wave profile with 10 s period and a maximum speed value of 3 m/s. The generator reference current for each phase is a sinusoidal waveform with a peak value of 350 A and a period of 10 s.

To evaluate the electrical parameters, some periods of the incoming wave have been considered, while the evaluation of thermal stresses has been done with a simulation of 600 s, which is enough to spot the thermal steady-state condition after the initial transient.

3.3.1 PARAMETERS ACTING AND MONITORING

In order to design the power electronics apparatus, the simulations have been analysed to evaluate the stresses on each component and choose the proper size.

The variables that can be changed are:

- Profile parameters of the incoming wave, such as velocity, thrust (which implies the reference current) and period, in order to simulate different situations.
- GSC power electronics components, with different electrical and thermal behaviour as stated in the datasheet. The starting IGBT module (one H bridge branch) was the Semikron SEMiX603GB17E4p due to the initial design requirements (as explained later).
- DC bus capacitors, with a change in the total capacitance value depending on the DC voltage ripple, the mechanical size and the availability on the market.
- Thermal initial conditions for the GSC system, namely the initial junction temperature of the IGBTs and diodes, and the initial temperature of the heatsink.

To perform the analysis, some parameters have been observed and analysed such as

- The currents flowing in the DC bus, in order to design the capacitor bank and the GTC. Currents in the GSC output phases have been analysed as well, to verify that the current references are properly tracked.
- The voltages across the DC link and across the machine phases.
- IGBT and diode junction temperatures in order to be sure they do not overcome the datasheet specifications. The total heatflux has been monitored too in order to design the heatsink and the cooling method.

3.3.2 *ELECTRICAL ANALYSIS*

The measurements taken during the simulations are depicted and commented.

The DC bus voltage has been measured at the ends of the DC link capacitor bank and reported in Figure 3.12.

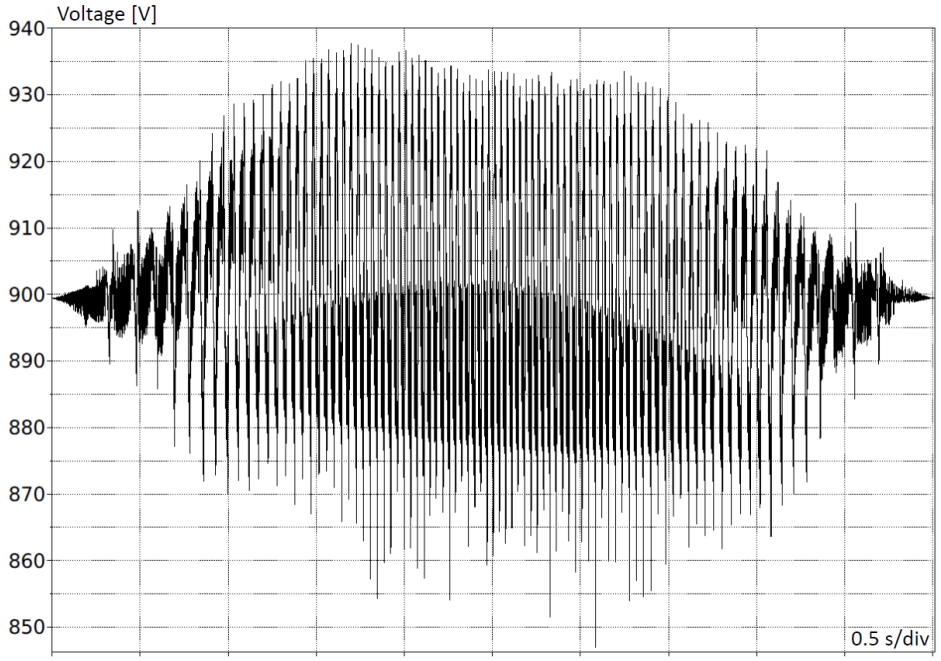

(a)

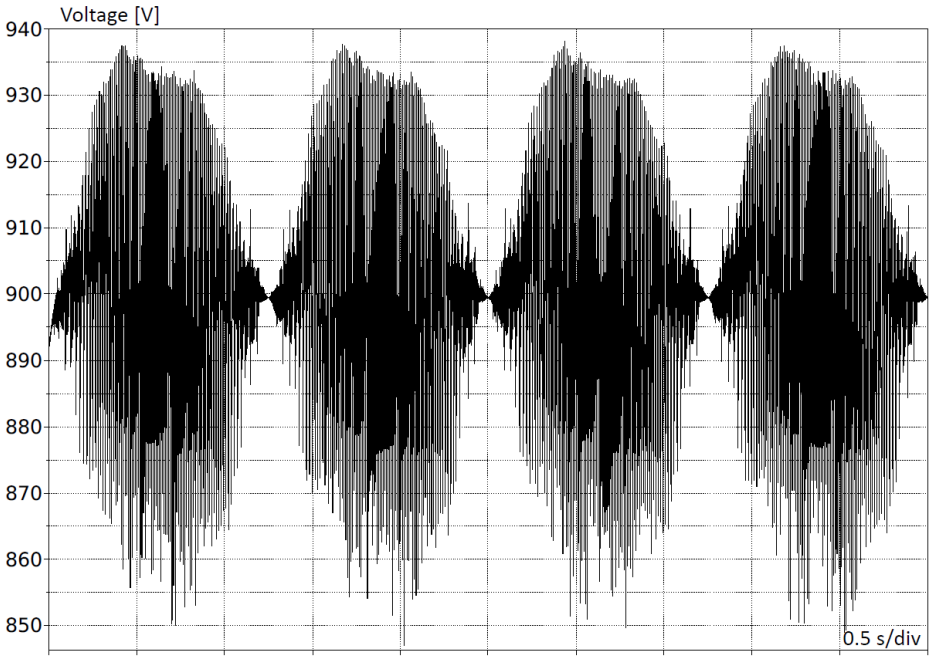

(b)

Figure 3.12 DC bus voltage detail (one period) (a), and general view (b).

As clearly visible, the DC voltage oscillates between 940 V and 850 V with a negligible ripple at different frequencies. The mean value of the DC-link voltage is 900 V (set by the DC generator which simulates the behavior of an ideal AFE).

The ripple of the DC bus voltage is directly connected with dimensioning of the capacitor bank, as reported in section 3.4.

The waveform of the current flowing in the DC bus capacitor bank is reported in Figure 3.13. The mean value is around 0 A, while the RMS value is about 150 A.

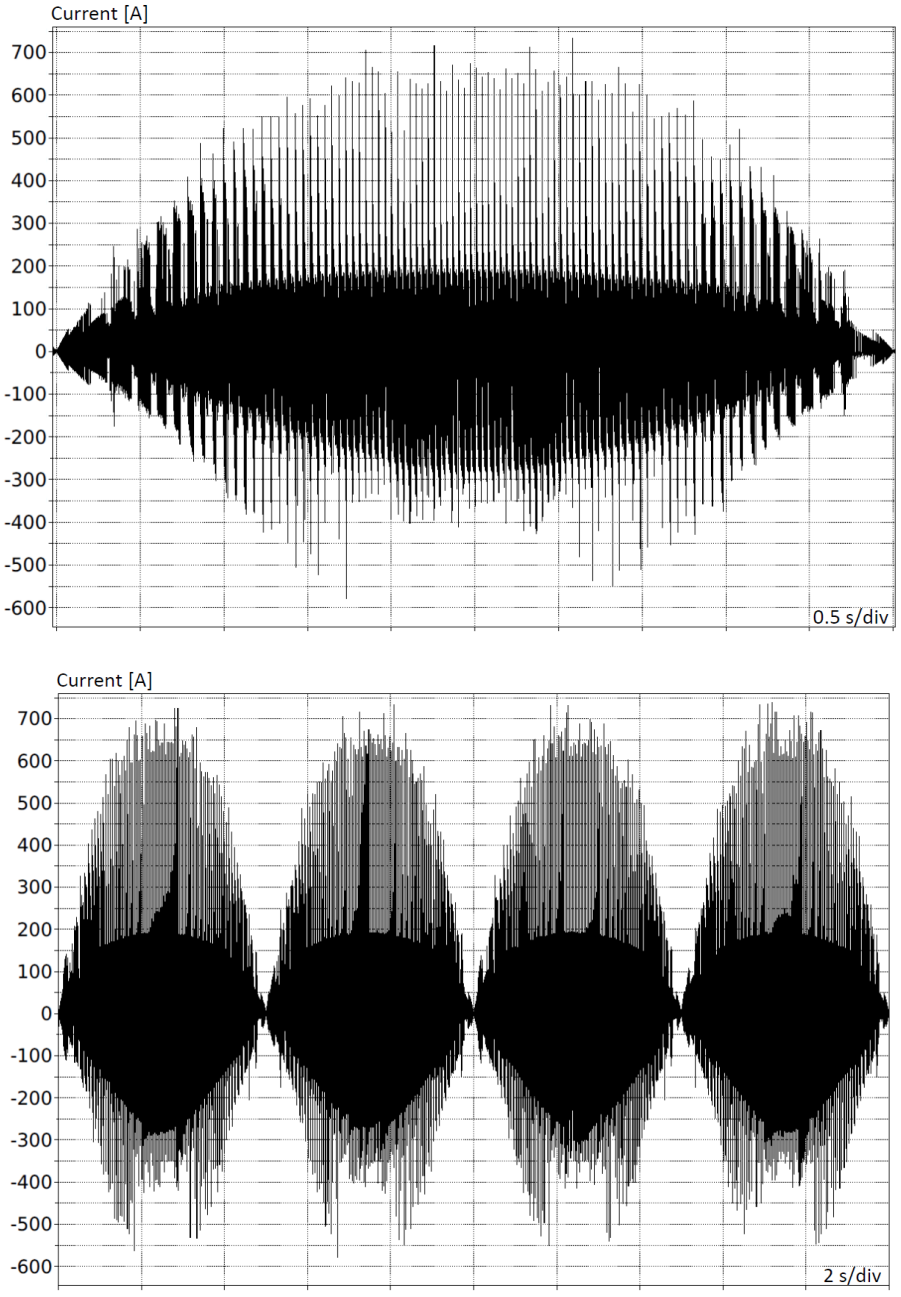

Figure 3.13 DC bus current detail (one period) (a) and general view (b) S.G.K.A..

The value of the DC bus current must be known to calculate the power losses of the capacitors.

The current flowing from the simulated GTC (composed by a DC voltage generator and a ohmic inductive network) to the GSC has been detected too, resulting in Figure 3.14.

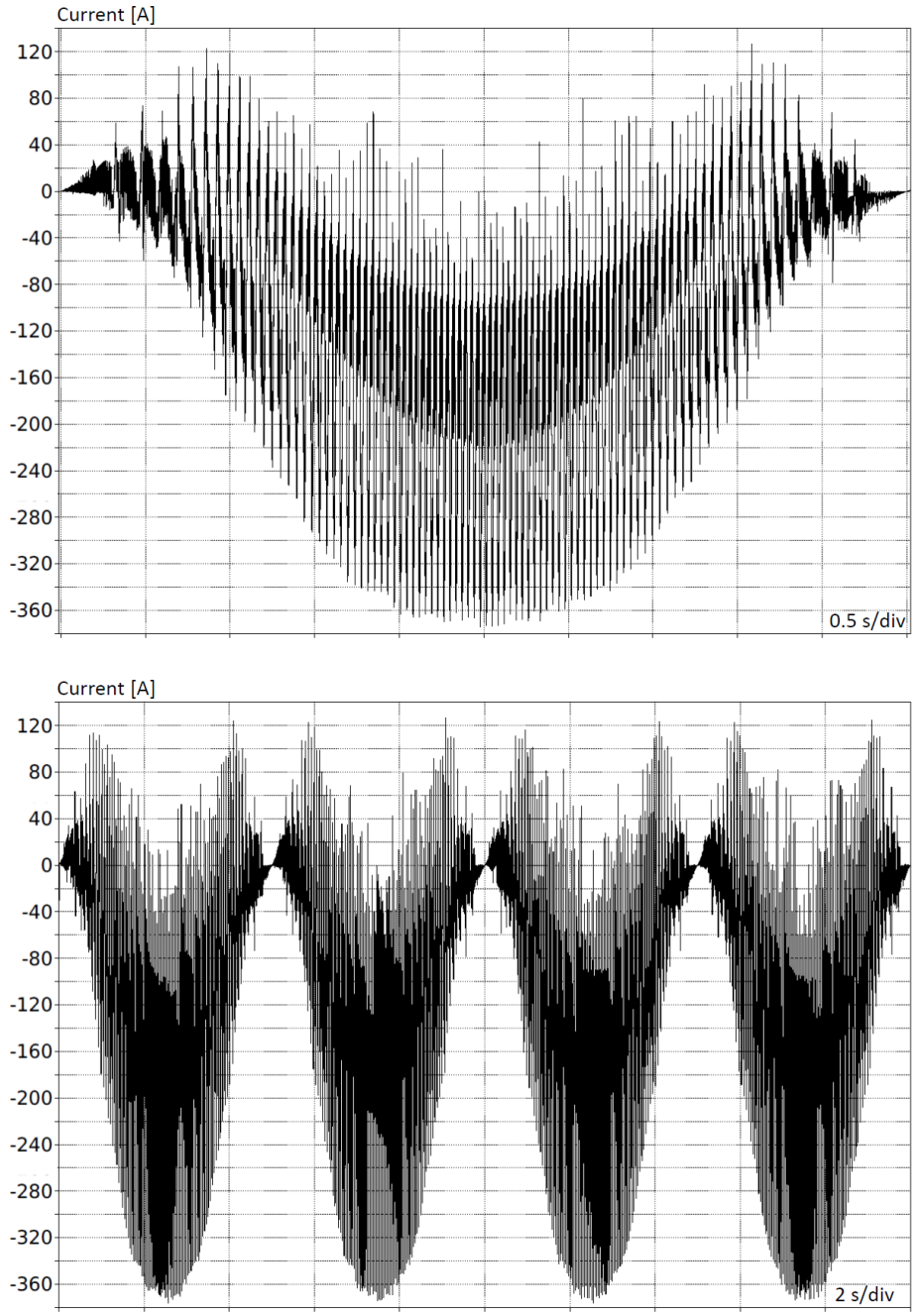

(a)

(b)

Figure 3.14 GTC output current detail (one period) (a) and general view (b).

The GTC output current has -98 A mean value (the minus is due to the chosen measurement direction) and a RMS value of 144 A.

The waveform of the GSC output currents and voltages (i.e., voltages and currents in the electrical machine) is then provided.

The phase current is visible Figure 3.15.

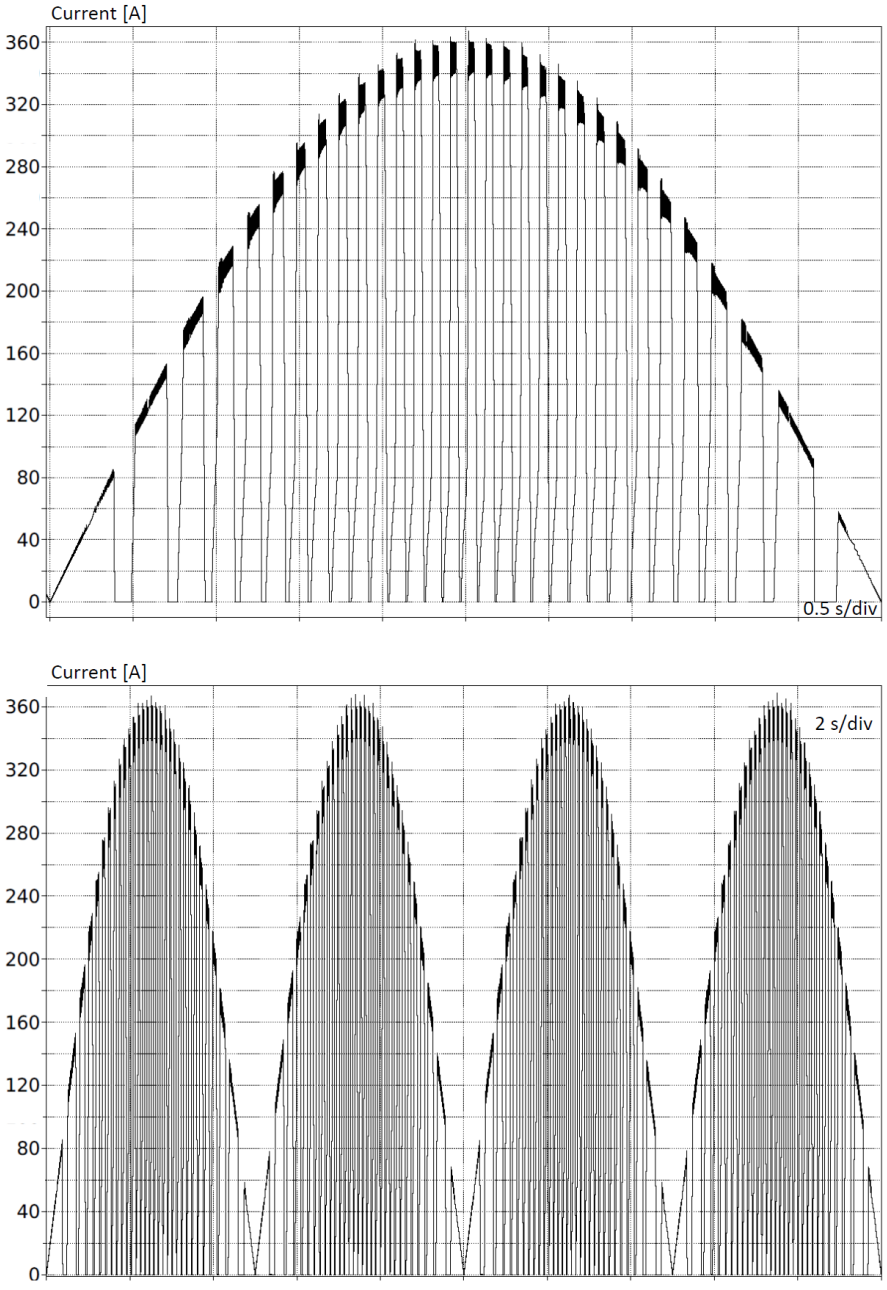

(a)

(b)

Figure 3.15 GSC phase current detail (one period) (a) and general view (b).

A period of 5 s is clearly visible in the phase current. The mean value is about 125 A and the RMS value is about 170 A.

As visible, the envelope of the various pulses of current forms a sinusoidal waveform.

To understand the waveform of the current, a zoomed image is provided (Figure 3.16).

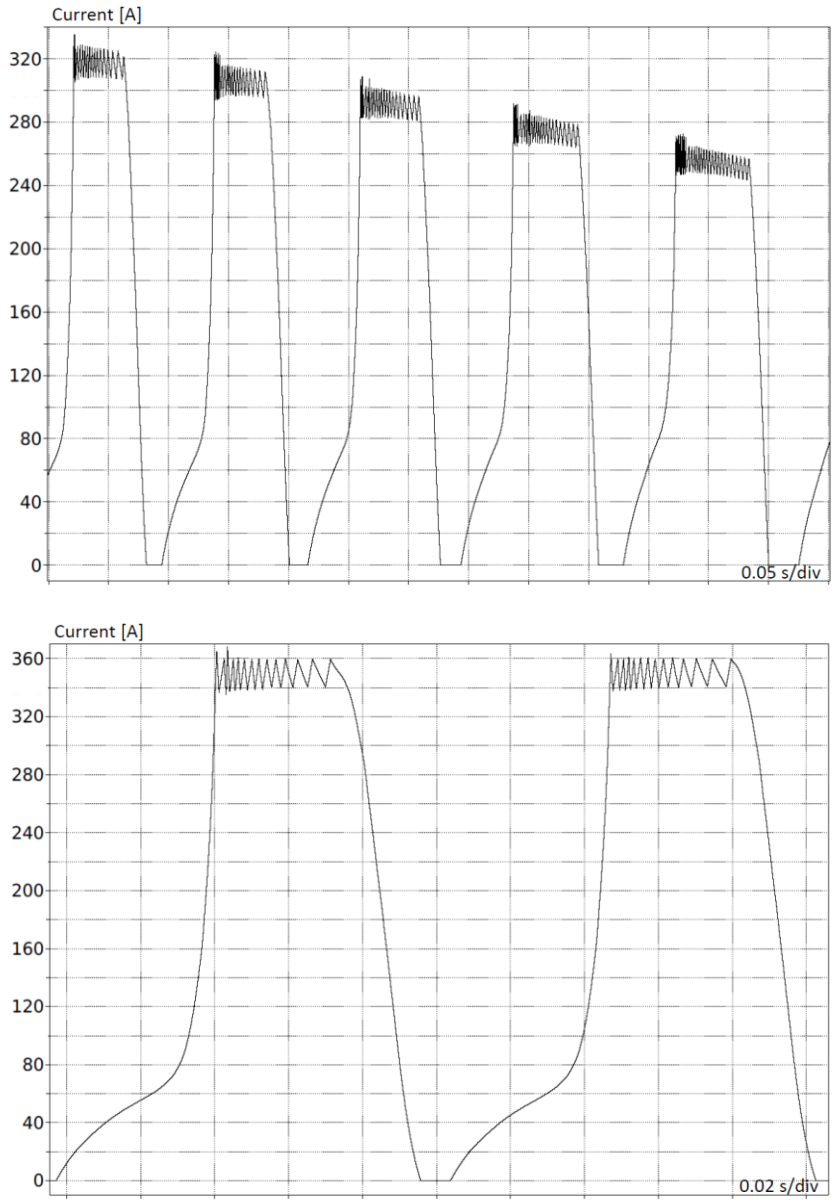

Figure 3.16 GSC phase current trend detail (a) and zoom (b).

The current peak changes shape while approaching to the center of the period and leaving toward lower values.

The Fourier analysis of the phase current is presented in Figure 3.17.

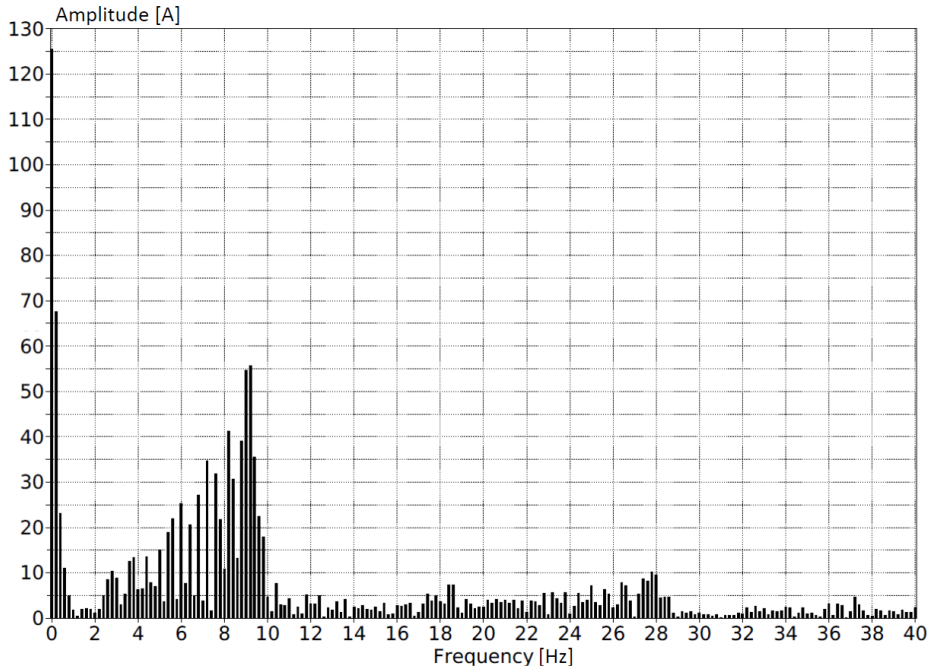

Figure 3.17 GSC phase current Fourier analysis.

The main harmonics are present up to 10 Hz frequency (which correspond roughly to the current ripples shown in Figure 3.16).

A general view of three phase currents is given in Figure 3.18.

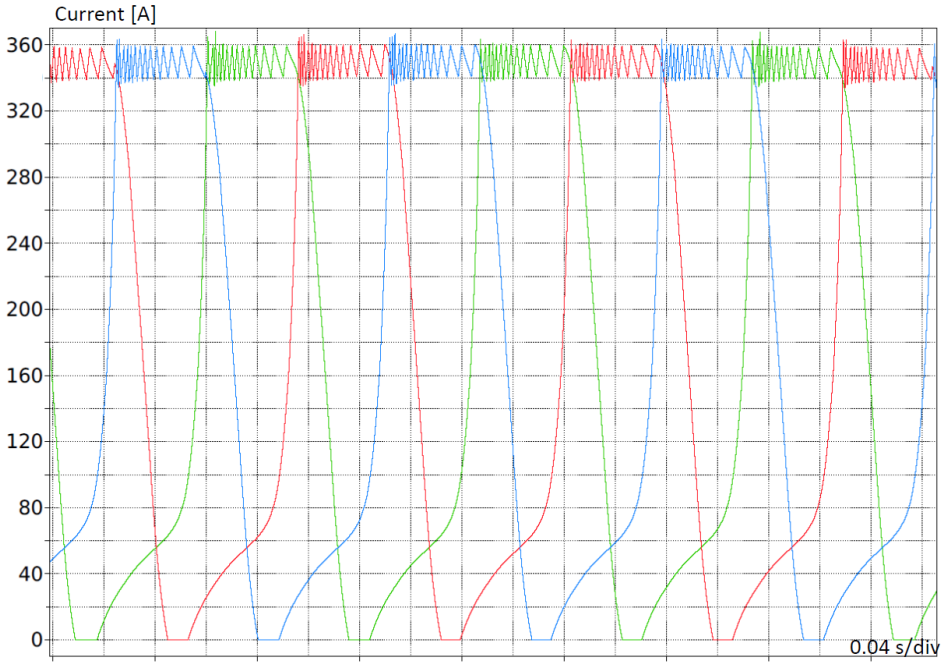

Figure 3.18 Trend of the three phases currents.

The phase voltage is reported in Figure 3.19. As visible, the function is periodic with a period of 5 s as expected.

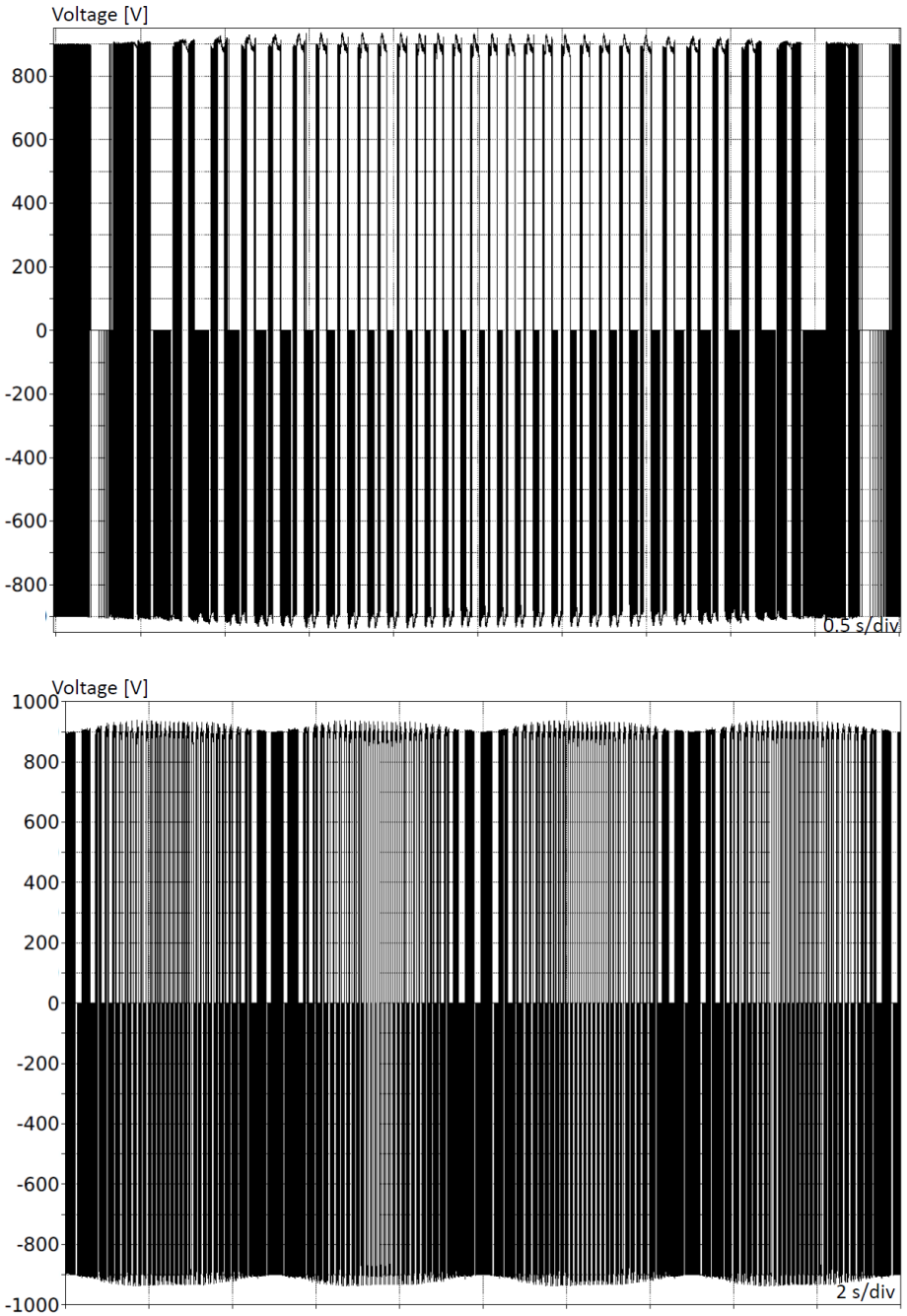

Figure 3.19 GSC phase voltage detail (one period) (a) and general view (b).

The GSC phase voltage has a mean value of about 20 V and an RMS value of about 770 V.

The shape of the GSC phase voltage is quite complicated. Its Fourier spectrum is shown in Figure 3.20.

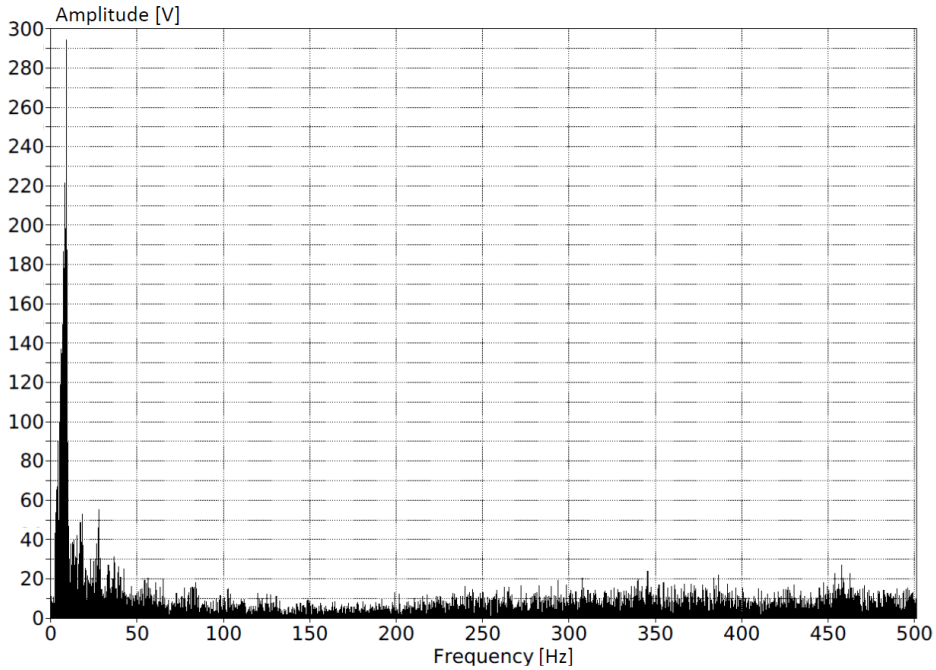

Figure 3.20 GSC phase voltage Fourier analysis.

As visible, some ripple is present also at higher frequencies but main harmonics are within 50 Hz.

3.3.3 THERMAL ANALYSIS

The thermal analysis has been conducted through 600 s of simulation in order to spot the thermal steady-state condition after the initial transient.

The importance of the thermal analysis is in the validation of the selected components.

The aim of the thermal evaluation is to understand whether a certain component is suitable for a certain application, specifically whether its junction temperature does not overcome the limits fixed in the datasheet by the manufacturer.

The analysis has been done starting from the worst initial condition. The initial junction temperature of the IGBT and the diode has been 95°C, which is a pretty high value even if it is far enough from the maximum limits. Moreover, the heatsink temperature has been set to a constant value of 85°C to take into account the worst condition of 40°C for the ambient temperature with an overtemperature of 45°C with respect to the external ambient.

In Figure 3.21 the IGBT junction temperature is visible over a period of 600 s.

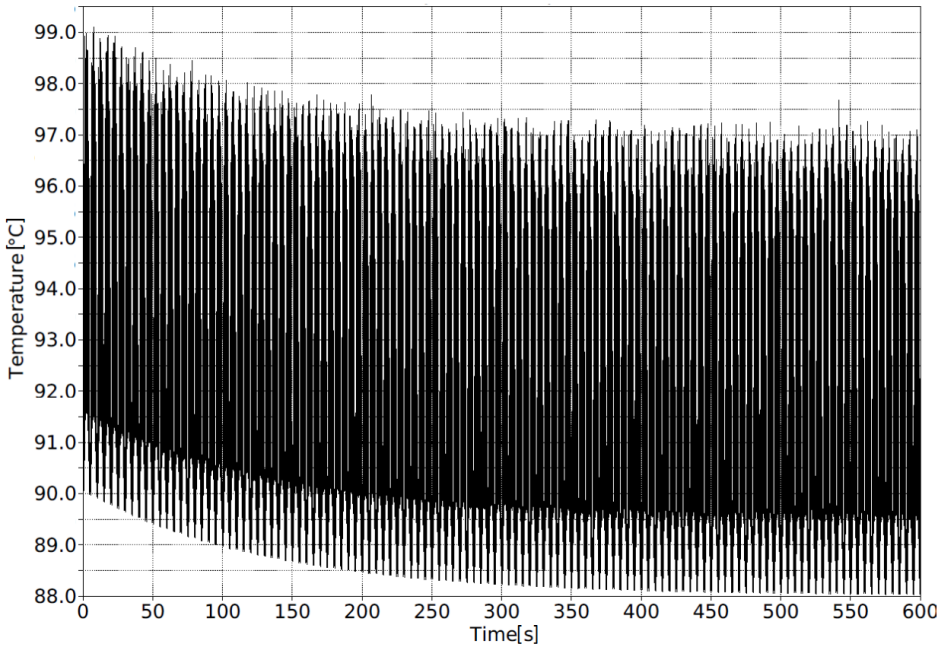

Figure 3.21 IGBT junction temperature over 600 s.

As visible, the steady state value, spotted after the initial transient, is certainly lower than the initial value, since the temperature fluctuates between 88°C and 97°C.

In Figure 3.22 the diode junction temperature is presented.

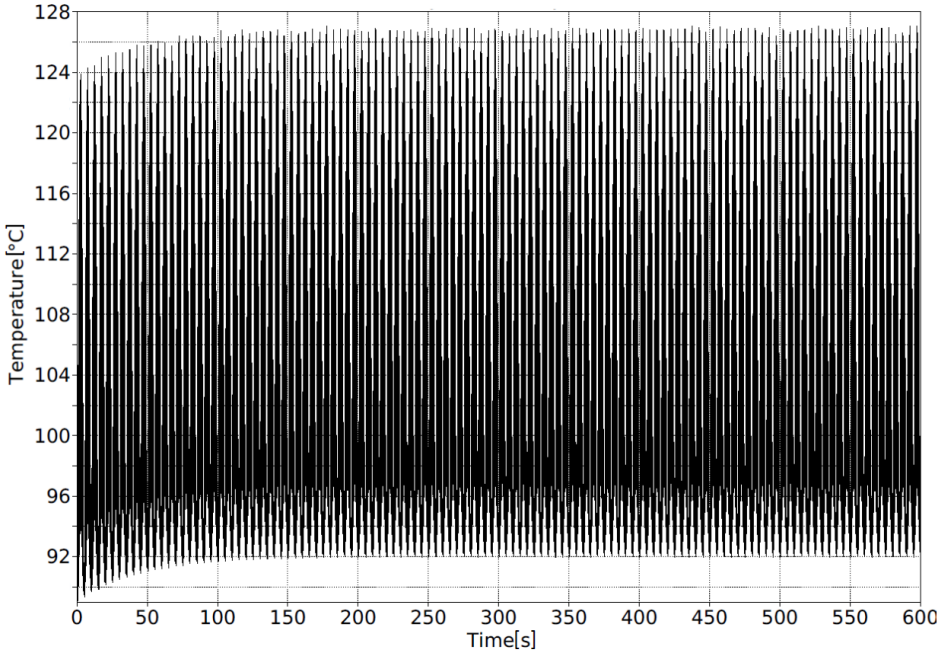

Figure 3.22 Diode junction temperature over 600 s.

Also for the diode case, the final temperature value between 92°C and 126°C brings no problems to the diode, since the limit set by datasheet is higher, i.e., 150°C.

The heatflux produced by a single H bridge (i.e., four IGBTs and the corresponding antiparallel diodes, i.e., two IGBT modules branches) is an important variable in order to estimate the heat to be removed by the heatsink and the cooling system.

Figure 3.23 shows that, after the initial transient, the total H bridge heat flux settles at about 500 W.

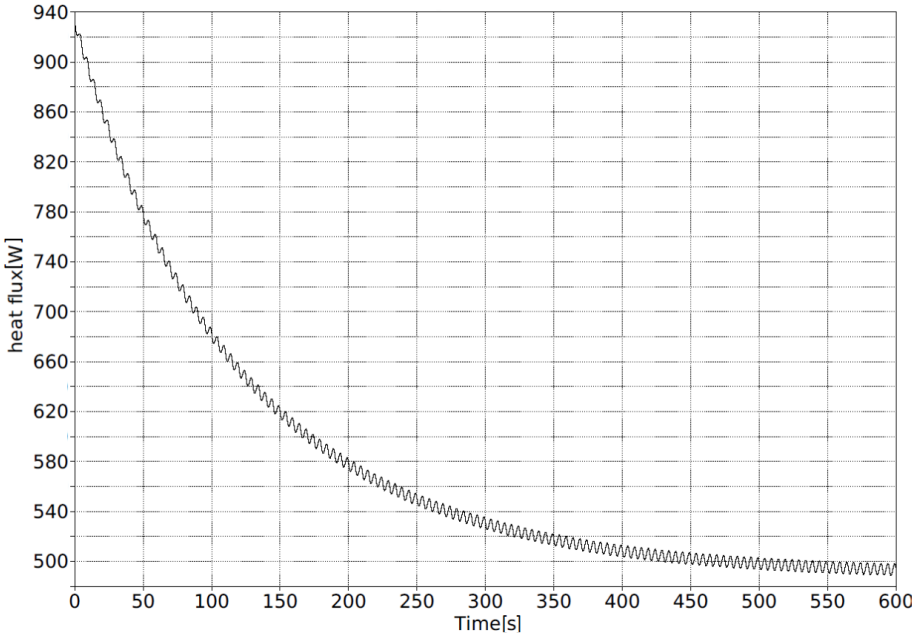

Figure 3.23 Total heat flux per H bridge.

3.4 Choice of the components

The choice of the components has required two different design steps. Some preliminary choices have been useful as a starting point for the initial dimensioning, while the simulations, the measurements and parameters evaluation have allowed refining the choice of the components for the fulfilment of the requirements.

The starting data are as follows:

- the maximum current value for each machine phase is 350 A,
- the rated DC-link voltage is 900 V,
- the maximum average switching frequency in a cycle is 1 kHz.

For these reasons, 1700 V-class IGBT with an adequate rated current has been chosen: in particular, ccommercially available model SEMiX603GB17E4p by Semikron has been selected, keeping the Infineon FF600R17ME4 as a possible substitute, although at the time of dimensioning procedure, the latter IGBT module availability was not good.

As a premise, the whole design has been carried out for a laboratory prototype of the whole system with air cooling and no strict dimensional matters, but the obtained layout is a very compact solution, easily adaptable to the marine application. Many technical advices have been considered in the design: reduced dimensions have been kept, easy maintenance has been guaranteed and water cooling could be achieved in future by simply substitution of the air cooled heatsink and fans with a liquid cooled coldplate.

3.4.1 HEATSINK CHOICE

Standing the previous power calculations, the chosen heatsink is able to drain a heat flow of about 600 W per H bridge (keeping extra safety margin with respect to results of Figure 3.23). Since each H bridge is placed on a single heatsinks, the heat flow of a complete H bridge corresponds to the heat flow of a heatsink.

If the maximum ambient temperature is assumed 40°C in the worst case and the maximum admissible temperature of the heatsink is 85 °C, the thermal resistance of the heatsink needed to dissipate such an heatflow is given by (3.2).

$$R_{TH} = \frac{Delta\ temperature\ [°C]}{Heat\ power\ flux\ [W]} = \frac{45\ °C}{600\ W} = 0.075\ \frac{°C}{W} \tag{3.2}$$

The heatsink used in this application must have a thermal resistance lower than 0.075 K/W in order to drain the desired heat flow maintaining the desired temperature.

For commercial availability reasons, an heatsink model RMRES0020 by Priatherm has been chosen (see profile in Figure 3.24). Starting from the datasheet value of the thermal resistance, with a length of 200 mm, an air flow speed of 2.9 m/s and a temperature difference of 45 °C, the thermal resistance offered by the heatsink per couple of IGBT modules is 0.071 °C/W, slightly lower than the previous calculated value.

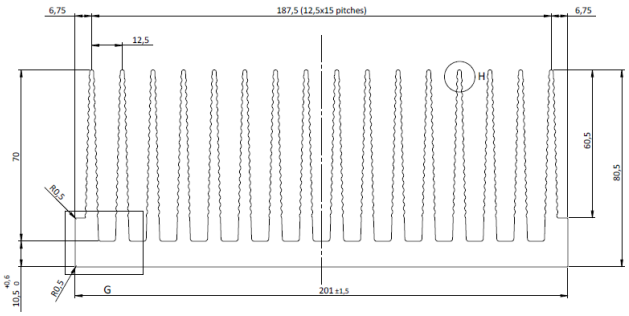

Figure 3.24 Heatsink RMRES0020 profile.

Although the calculated thermal resistance value seems to be slightly lower than the minimum requested, it must be considered that adequate safety margins have been kept during the overall thermal dimensioning.

3.4.2 FAN CHOICE

With the purpose to maintain an air flux speed of 2.9 m/s through the heatsink pins, a set of three fan per heatsink have to be chosen.

Standing a pin height of 70 mm, three fan 70 mm x 70 mm x 25 mm PMD2407PTV1-A GN manufactured by Sunon per heatsink have been chosen.

This choice has been validated by comparing the fan pressure drop VS air flux characteristic (orange curve in Figure 3.25) with the heatsink pressure drop VS air flux characteristic (grey curve in Figure 3.25, with its interpolation curve in black).

Assuming each heatsink cooled by three fans in parallel, the orange curve has been calculated by simply multiplying by three the flow rate of the fan characteristic given by the datasheet by three.

As visible in Figure 3.25, the intersection between the two curves gives a flow rate of about 190 m^3/h. Taking into account a decrease by 10 % due to the mutual interference of the flows, the total flow rate through the heatsink is likely around 170 m^3/h.

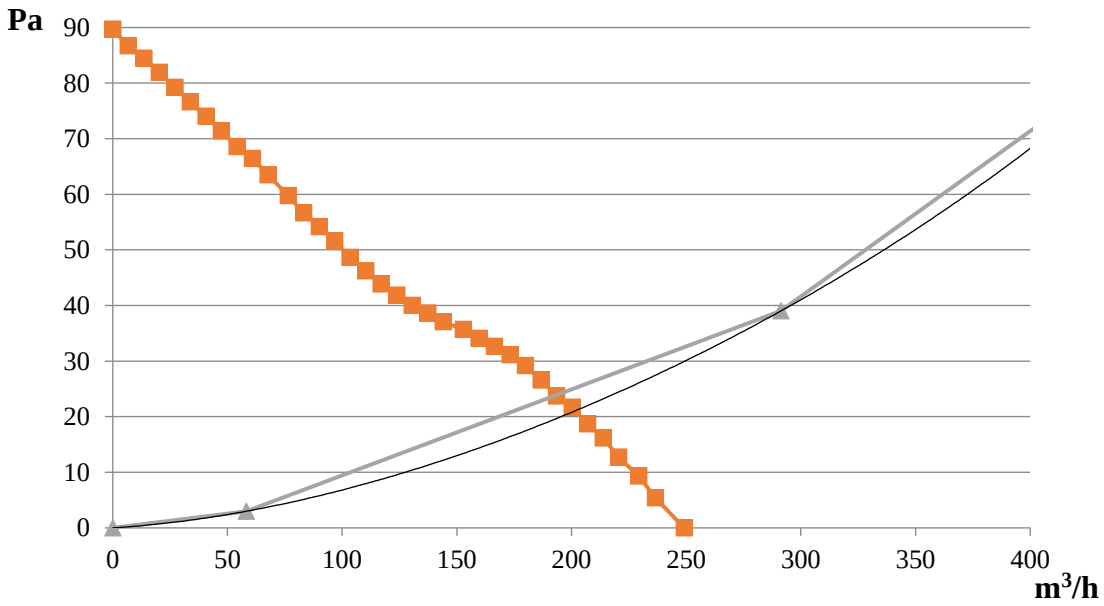

Figure 3.25 Fan cooling system working point.

By knowing the cross section of the heatsink, it is possible to calculate the air speed value from the flowrate, obtaining about 2.9 m/s.

This value is in good agreement with the one previously used for the calculation of the thermal resistance of the heatsink.

The second test on cooling system fans concerns the temperature of the air when leaving the heatsink. Due to the particular layout with the purpose of reducing dimensions as more as possible to comply spatial issues, the air flux exiting from the heatsink could interfere with capacitors bank, which has been placed near the heatsink outlet.

The temperature difference of the air flow between the outlet of the heatsink and the environment can be calculated by dividing the heat flow to be dissipated by the specific heat of the air c_p and the mass flow rate as (3.3) shows.

$$\Delta T = \frac{P\ \left[\frac{J}{s}\right]}{c_p\ \left[\frac{J}{kg\ °C}\right] \dot{m} \left[\frac{kg}{s}\right]} \tag{3.3}$$

With c_p equal to 1007 J/KgK, the air density equal to 1.060 kg/m^3, an air volume flow rate of 170 m^3/h and the power losses to be dissipated equal to 600 W, the temperature difference ΔT is 12 °C. This means that with a maximum ambient temperature of 40°C, the heatsink exhaust temperature is about 52°C. Such a temperature difference is acceptable for this application, as explained in Section 3.4.3 and no further modifications are necessary.

3.4.3 THERMAL SAFETY

The overall design of the system has been conservative despite characteristics of crosscuttingness, adaptability, versatility have been maximized as primary target for the project.

As visible per Figure 3.21, indeed, the temperature reached by the IGBT junction during the simulation time (large enough to clearly see the thermal transients related to the slowest IGBT case thermal constant) is about 90°C on average, which is lower than the maximum limit of 150 °C set by datasheet; thus it is reasonable to think that, having more than 50°C of margin, the IGBT module is safe for this kind of operation.

It can be seen in Figure 3.22 that the antiparallel diode has reached, during simulations, an average temperature value of about 96°C, which is lower than the maximum allowed limit in the datasheet, with a margin of about 60°C.

Moreover, each IGBT module case temperature is acquired and recorded by the control board through the internals NTCs provided by the manufacturer inside the component case.

Thus, temperature de-rating and overtemperature interlock control strategies can be implemented by the control system.

Furthermore, three series-connected 90°C thermal switches are fitted in the three heatsinks and connected to the hardware interlock input of the power converter. This prevents power modules overtemperature damages also in case of control system failures.

3.4.4 DC BUS DIMENSIONING

The DC bus size has been chosen with the purpose to limit the DC voltage oscillations and the IGBT switching ripple current withstanding.

Although in the real application two DC banks in parallel are present (one from the GSC side and the other from the GTC side), only the GSC DC link has been considered as a dimensioning parameter in the simulations in order to keep a safety margin in the design. Lower amplitude oscillations would occur due to the extra GTC capacity bank in the final system.

In order to perform the DC bus dimensioning, the behavior of the system has been simulated with many different capacity values in a commercially available range running from 8000 μF up to 15000 μF. The most suited solution has then been found taking into account the layout of the system as an additional constant. Since the whole GSC has been composed by three identical H bridges, the total number of capacitors has been divided in the three units.

A final choice is the 2030 μF capacitor 416.85V.1720 supplied by Ducati Energia. By using six capacitors, not only the overall symmetry of the whole layout has been preserved, but also a suitable value for the application has been reached, with a 12180 μf capacitor bank, large enough to limit the DC bus voltage oscillations as shown in Figure 3.12.

The oscillations of the DC bus voltage ranges from 850 V to 940 V, with a mean value of 900 V. This means an oscillation of ±5% around the mean value.

The low frequency DC-bus voltage oscillation is in large part due to the dynamic compliance of the AFE voltage control, which is not known in detail, and is modelled with the L/R circuit in Section 3.2.4.

The maximum voltage ripple at the switching frequency shown by the simulations is limited below 100 V peak-peak with enough margin with respect to the maximum value of 150 Vrms reported in the capacitors datasheet.

The current flowing in the DC bus has a RMS value of 150 A and a peak value of 700 A.

The current through each one of the six capacitors is 150 A/6 i.e. 25 A RMS as shown in Figure 3.13. It is lower than the admissible 100 A RMS reported in the component datasheet.

The power dissipated by the capacitor ESR (1.3 mΩ) at 25 A RMS is lower than 1 W. Since the typical hot-spot thermal resistance to ambient is 2.2 K/W (2.2 °C/W), the nominal hot-spot temperature rise with respect to ambient is slightly below 5°C, which means that, standing a maximum ambient temperature of 52°C in the worst-case temperature of the IGBT heatsink exhaust air, the maximum capacitor hot-spot temperature would be below 60°C. A margin of about 25°C in the worst case is ensured with respect to the maximum admissible hot-spot temperature value of 85°C declared in the capacitor datasheet.

3.5 Control electronic layout

Each module control unit controls the currents in each AMSRM module on the basis of the current setpoint determined by the "master control system" (see Figure 2.27). A hysteresis double-band regulator is implemented to control the current.

The "master control system" is a CompactRIO (cRIO) from National Instruments, i.e., a reconfigurable embedded system that contains a processor running on a real-time operating system (RTOS) and a reconfigurable field-programmable gate array (FPGA).

The cRIO is programmed with the real time WEC energy extraction control, which sets the reference force of the AMSRM depending on velocity of the translator. Hence, based on the wave profile, site data, WEC control, and the hydrodynamics characteristics of the WEC, the cRIO sends the current reference for each unit, so the desired power can be extracted. The communication between the power converters and the cRIO is performed via CAN protocol, receiving the cRIO status and alarms information.

Each module control unit is composed of a microcontroller (TMS32F28335 by Texas Instruments for the slave modules) hosted on a control card (Figure 3.26), which is located on an adaptation board (Figure 3.27). This last board is in charge of adapting the signals coming from the sensors / measurements systems, carrying the control signals to the power section, and elaborating hardware safety strategy, which do not rely on software intervention.

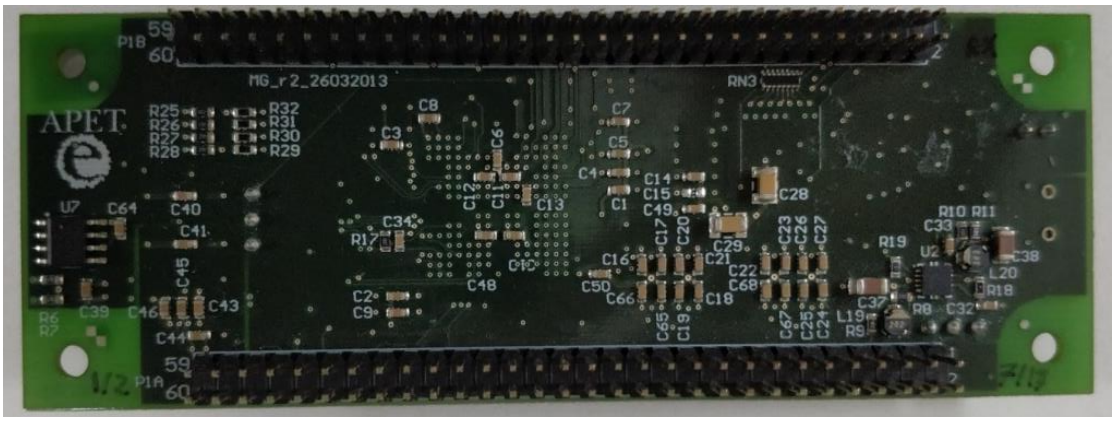

Figure 3.26 Control card hosting the microcontroller for the module control.

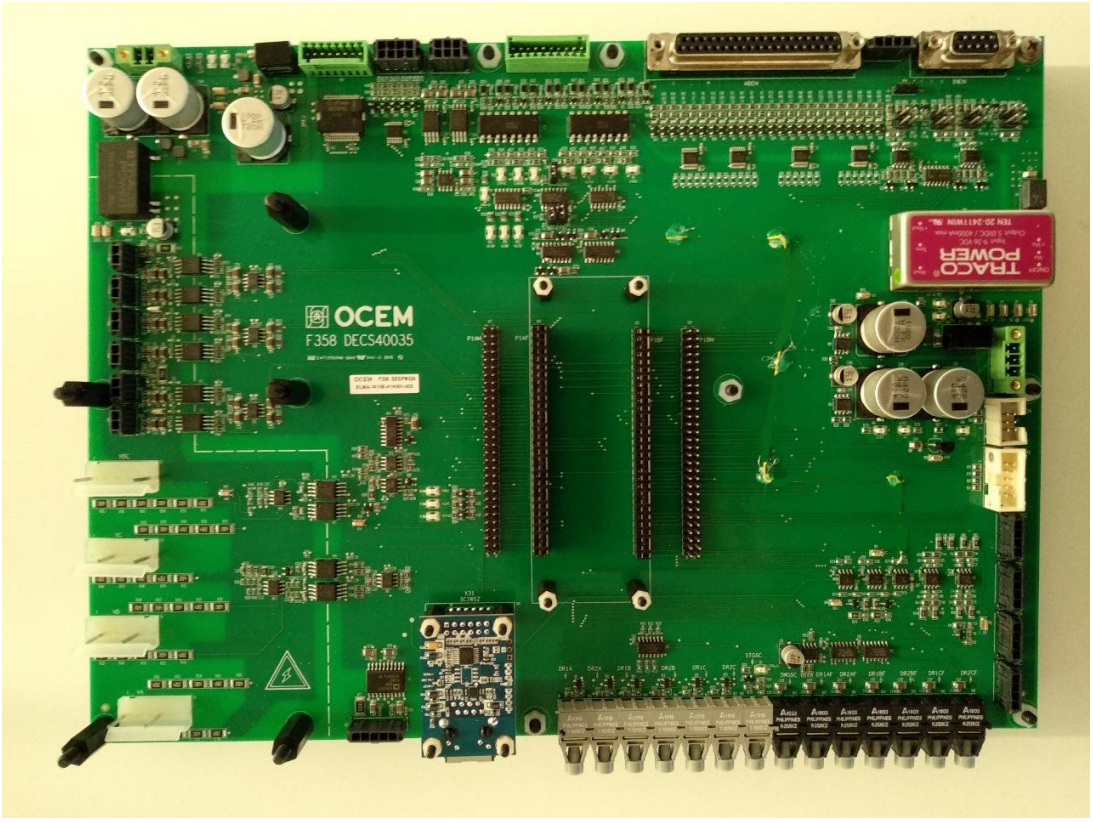

Figure 3.27 Adaptation board of each module to interface control electronics and power electronics.

3.5.1 *ADAPTATION BOARD*

All the sensor and actuators interfaces have been located in another board, named "adaptation board", designed from scratch to host the control card. The adaptation board has to acquire, elaborate and adapt signals and commands from the power electronics world to the control world, thereby providing proper insulation, protection and implementing also some safety and protection logic via hardware components.

The design of the adaptation board has been carried out alongside the power electronic section dimensioning. A conceptual block diagram for each measurement circuit has been developed in order to point out the different kind of input/output signals and the power input and ground connection placement. Starting from this diagrams, detailed signal adaptation and conditioning circuits have been dimensioned with commercially available components. In Figure 3.28, block schematic of the adaptation board is reported, with the highlight of the separated insulation areas realized over the board and the logical connections between every conditioning circuit.

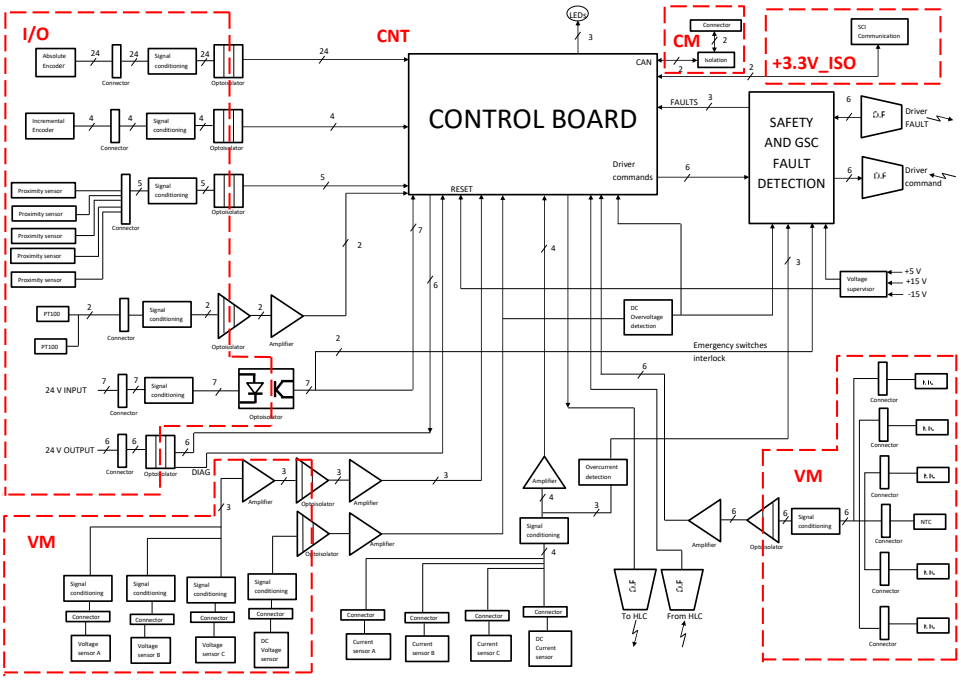

Figure 3.28 Adaptation board conceptual schematic, the control card is clearly visible in the upper center.

As visible, to ensure operational safety and the maximum possible level of EMI immunity, five galvanically insulated areas are provided on the board. The five isolation areas are defined in Table 3.2.

Table 3.2 Classification of the isolated zones on the adaptation board.

Area Name	***Zone description***	***Purpose***
CNT	Main control circuits area including control board	Control and safety signal elaboration
I/O	I/O signals	Input / output wired signals referred to aux. 24 Vdc cabinet supply voltage
CM	CAN-bus communication circuits	CAN bus signals isolated from other control and measurement signals
SCI	Asynchronous Serial Communication circuits	Serial communication signal
VM	Power converter voltage and temperature measurements	DC-Bus and generator related voltage measurements, IGBT temperature measurements

The insulation characteristic has been designed in order to obtain SELV classification for the communications and I/O circuits (areas CM, SCI, I/O), which any operator could come into contact with. The insulation between area VM and the other areas is designed to be reinforced, considering the DC-Bus voltage up to 1000 Vdc. Although the temperature measurement systems on the IGBT (namely NTC components) are isolated inside the IGBT module itself from the high voltage, their acquisition and conditioning circuits have been safely separated from the rest of the board to prevent problems in case of a fault, which could lead NTC circuits to go to high voltage.

The adaptation board has been provided with all the connections required to acquire and drive the following circuits:

- one absolute encoder 24 bit inputs suitable for push-pull driver and 24 Vdc supply;
- one incremental encoder input signals (A, B, Z1, Z2) suitable for push-pull driver with 24 Vdc supply voltage;
- five proximity sensors with PNP output and 24 Vdc supply voltage;
- two PT100 inputs with -6 °C ÷ +150 °C temperature acquisition range;
- seven digital inputs for general interfacing (two safety interlock circuits) suitable for 24 Vdc signal;
- one digital input for the IGBT heatsink thermal switch;
- six digital output with 1 A drive capability each;
- four current measure (external sensor) with three overcurrent comparators interlocks;
- four voltage measurement (internal voltage divider, reinforced insulation) with one DC-bus overvoltage comparator interlock;

- six isolated IGBT temperature measurement (NTC);
- six PWM commands over plastic fiber optic transmitters;
- six IGBT driver faults status over plastic fiber optic receivers;
- safety and interlock logic circuit for reliable and safe power converter management;
- logic and analog supply voltages supervisor for reliable interlock upon out-of-tolerance supply voltages;
- fiber optic transmitter and receiver for HLC controller status interface;
- CAN-bus interface;
- SCI interface with SCI-to-Ethernet module hosted on board.

Two power supply inputs are required for the adaptation board.

The first 24 Vdc power supply has been derived directly from the common auxiliary 24 Vdc power supply used for all the low voltage circuits (relays, switches, fans, etc…) of the whole power electronic section. The 24 Vdc is used to supply all the logic and analog circuits on the board through isolated DC/DC converter fitted on the board and capable to deliver +5V, +3,3V for the CNT area and 5V_ISO (+5V) for the VM area.

The second ±15 Vdc power supply is dedicated for the current sensors (LEM current sensor) supply and for the overcurrent comparators. It is connected with the CNT area.

3.5.2 DRIVER BOARD

Each IGBT is driven by a driver board, namely an electronic board which implements the switching commands by acting on the gate terminal after having received the proper commutation profile from the control card via the optic fibers of the adaptation board. The driver board is also in charge of detecting driver-related faults.

A driver board is used for each one of the six IGBT modules (namely one branch of an H bridge). The board is not only capable to drive a couple of IGBTs in a standard leg (upper, lower), but also to perform the desaturation protection and undervoltage lockout. All the input/output signals are exchanged with the control logic with optic fiber.

Since, for the SEA TITAN application, the generator winding current is uni-directional, only two of the four IGBTs related to each H-bridge are controlled, while the other are kept switched-off by the constant application of a negative gate voltage.

In conclusion, the six IGBT modules of the converter are driven by six driver boards, each one configured with only one fiber optic input.

Finally, the IGBT modules have been equipped with proper boards to bring the internal signals and measurements to the external control system.

3.6 Mechanical layout

Since the key desired features of SEA TITAN are the modularity, adaptability, versatility and compactness of the resulting system, the power electronic apparatus has been designed to be as modular as possible, as well as compact and dimensionally reduced, although in the laboratory application no spatial issues have been arisen.

3.6.1 H-BRIDGE

The starting point for the mechanical layout has been the single H bridge converter, namely the converter associated with one of the tree phases of the generator.

By taking advantage from the three-phase symmetry of the overall system, three equivalent modules have been designed, each one containing one H bridge and two of the six capacitor of the whole DC bus.

The 3D model of the solution adopted is presented in Figure 3.29.

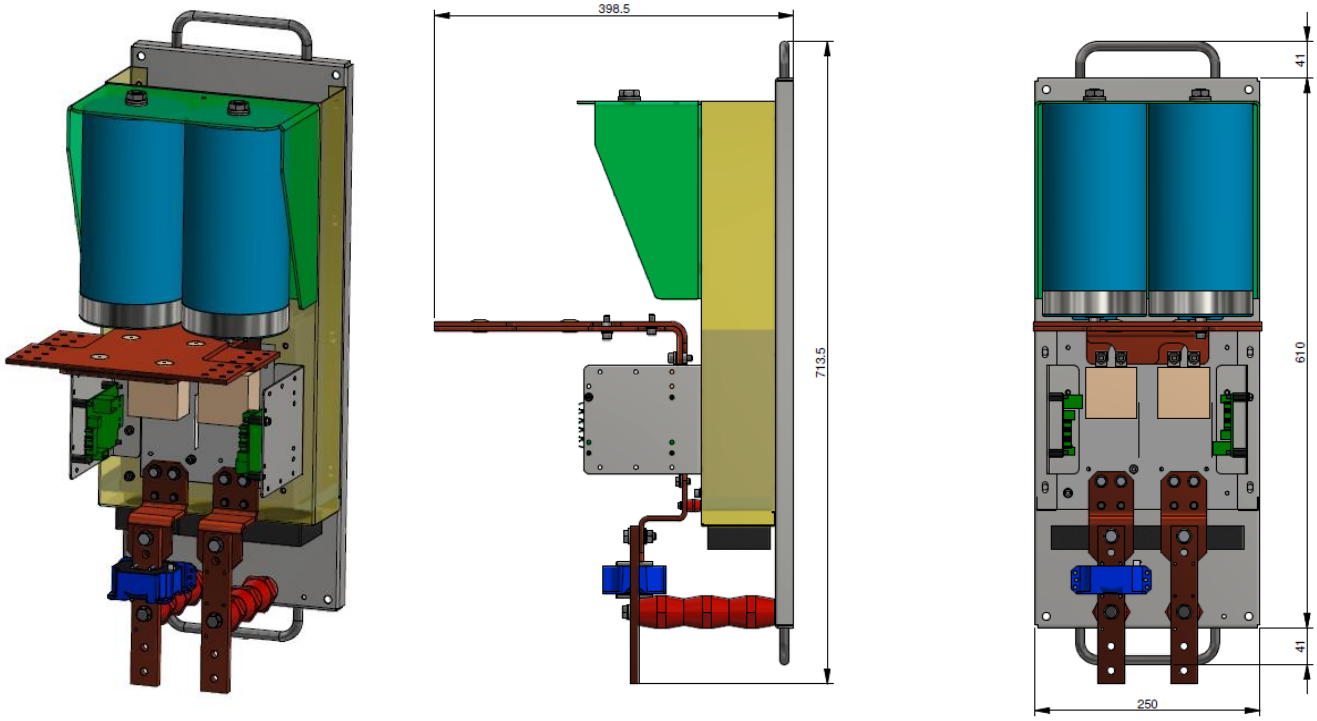

Figure 3.29 3D model of the SEA TITAN single phase H bridge.

A picture of the real assembled H bridge module is given in Figure 3.30.

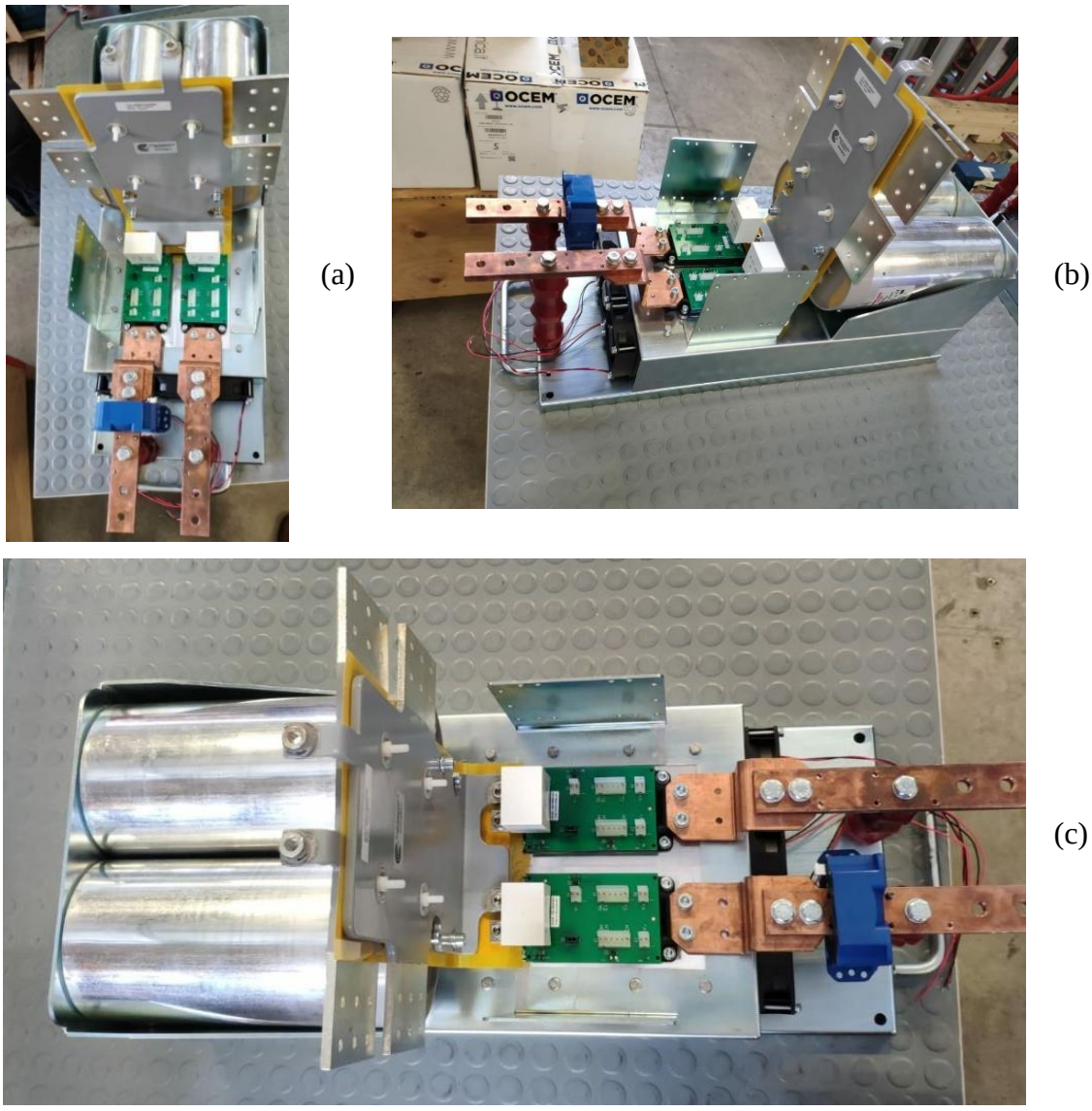

Figure 3.30 Pictures of SEA TITAN H-bridge module.

The GSC power converter mechanical design has been performed following the modular approach. This allows obtaining an easy serviceable and transportable power module, suitable for the future integration in the space-constrained marine environment.

Each one of the three H-bridges that compose the GSC is built over a backbone panel, provided by lifting and transportation handles.

Despite the design suitable for laboratory tests application, this solution can be easily adaptable to liquid cooling by simply replacing the heatsink with a custom coldplate with the same overall dimensions and the same threaded mounting holes.

The DC bus that runs across the copper busbar allows connections on both sides. This allows connecting multiple modules in a row, sharing a common DC-bus, thereby being

suitable also for different architectures. The DC bus connections on both module sides have been simply obtained by copper plates tied together with bolts and nuts.

The output connection toward the generator winding has been realized with copper bars, one of which equipped with the DC current sensor.

The two IGBT driver boards have been fixed over the two lateral metallic support, allowing for an easy connection of the optic fibres and the power supply cables as well as for an easy inspection and checking of the IGBT modules status.

The yellow part in Figure 3.29 is a tunnel under which the IGBT heatsink has been fitted. The three fans are mounted in the lower part of the drawing, and the exhaust hot air is expelled at the top of the module, without interference with other components.

3.6.2 CABINET

The mechanical layout of the overall cabinet has been developed taking into account the implementation of the whole system for a lab test facility. Both the GSC and the GTC have been placed in a unique big cabinet, split by an internal wall.

The overall GTC+GSC cabinet size is 2200x 2200 x 600 mm (HxWxD). The portion of the cabinet that hosts the GSC is 2200 mm high, 1000 mm wide and 600 mm deep, with a dedicated fan to drain out the internal produced heat. The GTC section is 2200 mm high, 1200 mm wide and 600 mm deep and this part as well as its auxiliary system and cooling devices have been commercially purchased.

Regarding the GSC, three H-bridge modules have been hosted inside the GSC cabinet and connected together through their DC bus, as shown in Figure 3.31 and Figure 3.32.Figure 3.32 Pictures of GSC cabinet with three H.bridge modules visible.

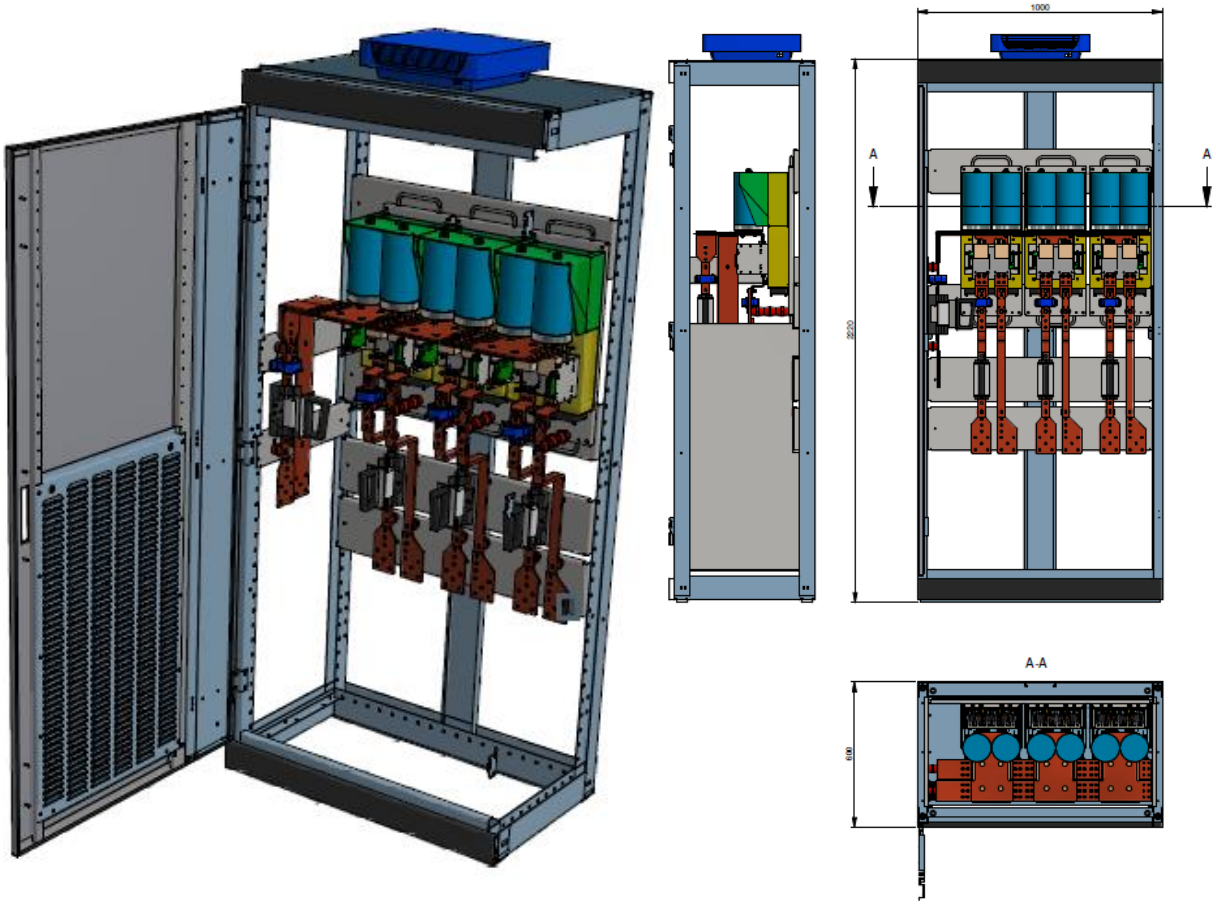

Figure 3.31 GSC cabinet 3D drawing.

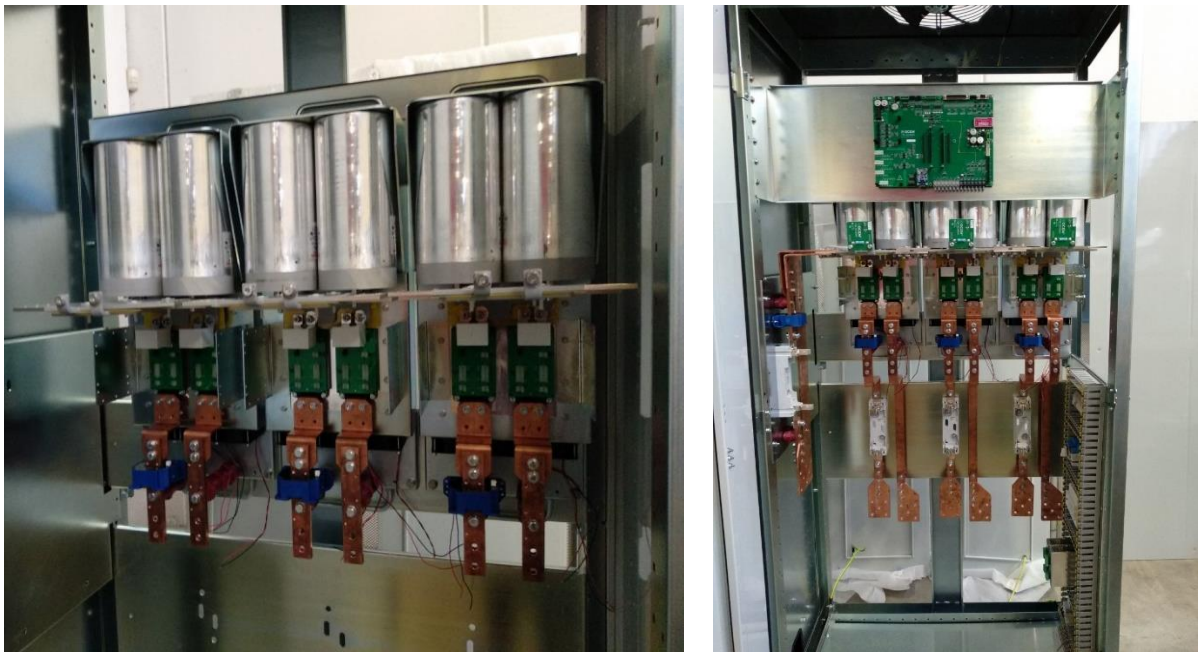

Figure 3.32 Pictures of GSC cabinet with three H.bridge modules visible.

The sizing of the GSC air extraction ceiling fan has been computed with (3.4):

$$\Delta T = \frac{P_{FAN}\ \left[\frac{J}{s}\right]}{c_p\ \left[\frac{J}{kg\ °C}\right] \dot{m}_{FAN}\ \left[\frac{kg}{s}\right]} \tag{3.4}$$

by choosing a maximum temperature difference of the air between the entrance and the exit of the cabinet of 15 °C, standing a total heatflux of 1890 W (i.e., 600 W multiplied by 3 with an increment of 5% for ancillary equipment), a value of c_p of 1007 J/kg°C and an air density of 1.060 kg/m^3, the needed volume air flow is about 426 m^3/h. Therefore, a proper fan has been chosen for the GSC cabinet portion.

Besides thermal safety, the cabinet has been protected also from an electrical point of view by means of fuses, which limit the current in the unlikely case of an IGBT failure.

The chosen DC-bus fuse is gPV NH-2XL DC 1100V with a nominal current of 160 A. It allows a continuous power of 144 kVA over the DC-bus, while it is able to limit the peak short circuit current below 10 kA. The selected output fuses are gPV NH-2XL DC 1100V by Italweber with a nominal current of 200 A. They can withstand the 350 A peak current of the generator for up to 200 s. These fuses ratings are the best trade-off between protection and reliability.

Chapter 4 Power electronics laboratory tests

The formal conclusion of the design activity is the Factory Acceptance Test (FAT) of the power electronics apparatus.

Type tests and functional tests have been carried out in the OCEM facilities first to ensure the proper behaviour of the system in safety conditions and then to test its capability of withstanding the full power.

Tests have been performed using the main grid as power supply and dummy loads replacing the generator phases, with the purpose to obtain the same conditions of both applied voltage and circulating current of the simulations.

The operating trials have also included insulation tests to ensure the correct connections of the whole system. Also temperature measurements have been performed in order to validate the cooling system design.

The SEA TITAN power electronics cabinet is easy to put under test since each part is clearly visible and reachable (even with proper safety system to avoid electrocution).

The GTC has been tested by the supplier and it has not been investigated any longer.

Tests have been separately performed also on the electronic adaptation board which has been used to adapt the control strategy and to exchange measurements and commands with the cabinet. Once fully tested, the adaptation board has been installed in the power electronic cabinet ready for the FAT.

4.1 Topology

The system under test has been the complete one, as described in the previous chapter and presented in Figure 4.1. It is composed of the GTC (Grid Tied Converter) on the left and the GSC (Generator-Side Converter) on the right.

The schematized DC bus in the picture is the result of two DC links in parallel: the GTC DC link, which is defined by the supplier, and the GSC DC link previously designed. For safety reasons, the two DC link are separated via a fuse.

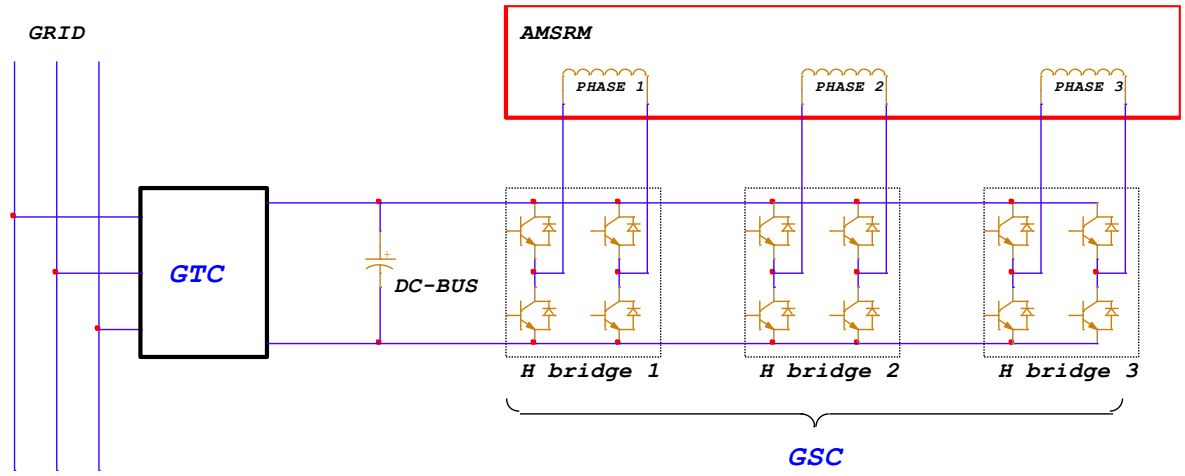

Figure 4.1 Schematic of the whole system.

Auxiliary circuits, including the control electronics, have been powered using a single phase power source derived from the main three phase power supply.

Two different kinds of IGBTs have been used:

- Semikron SEMiX603GB17E4p;
- Infineon FF600R17ME4.

In particular, only the two IGBT modules composing the H bridge of phase 1 have been replaced with FF600R17ME4, while others IGBT modules are SEMiX603GB17E4p.

Due to high lead time of such components, high cost and oscillating availability it has been necessary to find at least two alternative IGBT modules to be used to ensure future applications and developments. Since Semikron SEMiX603GB17E4p and Infineon FF600R17ME4 have the same package and the same behavior according to the datasheet, they have both been used during the FAT, which has confirmed that they have the same performance.

4.2 Instrumentation

The following measurement instruments have been used:

- pulsed generator (to simulate PWM commands sent to the IGBTs driver boards);
- voltage Source (40 V maximum);
- light resistive load 900V, 1A;
- resistive power load 0.25 Ω resistive-inductive;
- 2 x Inductive power load 106 mH 0.2 Ω, 100 A;
- insulated voltage meter;
- insulated current meter;

- thermocouple sensor;
- ground resistance measurement system;
- isolation resistance measurement system;
- multimeter;
- oscilloscope;
- thermal camera.

4.3 *Low voltage commutations tests*

First, low voltage tests have been carried out on the GSC (Generator Side Converter) to ensure the integrity and good wiring of the whole systems and to spot any design or assembly mistake without disruptive consequences.

The GTC (Grid-Tied Converter) has been left disconnected and it has not been taken into consideration during low-voltage test, since full power tests on this equipment have been already been carried out by its supplier.

The system test setup is shown in Figure 4.2, with an external power supply connected to the DC BUS:

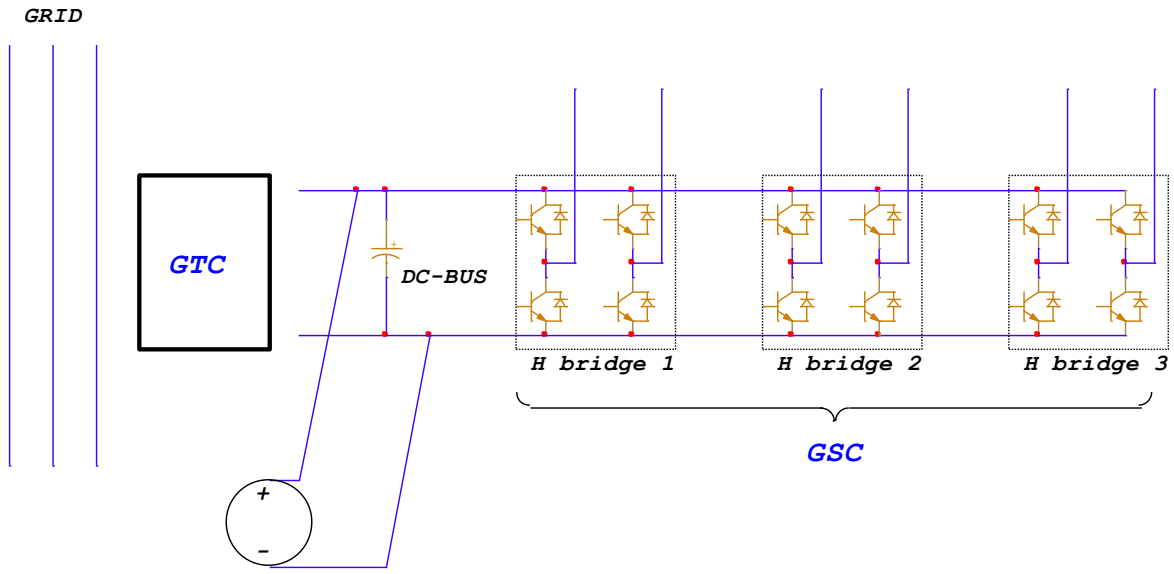

Figure 4.2 Low voltage test setup.

By charging and keeping in charge the DC bus at a constant voltage value (a laboratory test power supply of 40 V has been used), a certain commutation profile (by using a pulse signal generator exciting directly the PWM pin of the adaptation board linked to the driver boards) has been sent to every IGBT branch in order to turn on IGBTs of main diagonal of

each H bridge. The real control card has not been used, but its housing space on the adaptation board provide all the connections to every part of the system.

Some measurements have been done with a 500 Ω load applied to each branch of the H bridges (see Figure 4.3) by measuring the voltage across the resistors. The resistors are necessary to avoid unknown voltages in the branch middle point when both IGBTs of each branch are OFF.

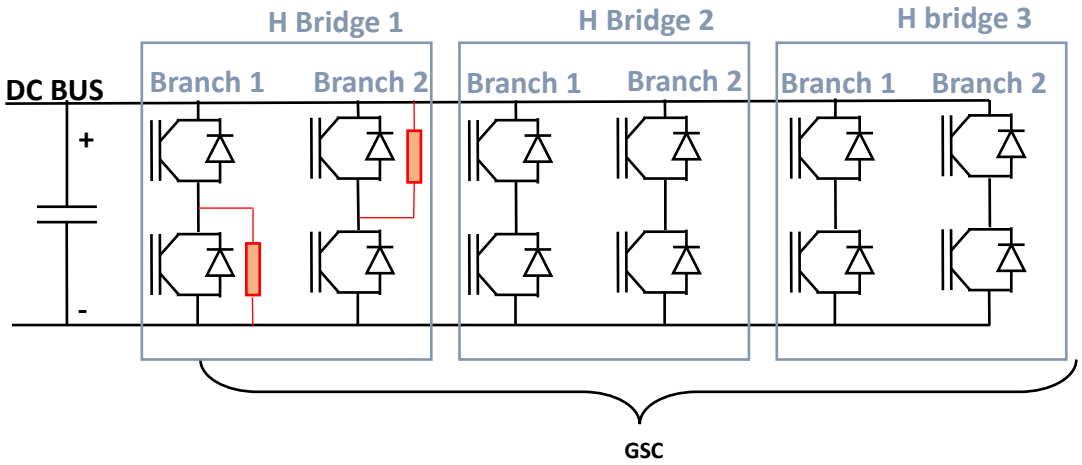

Figure 4.3 Measurement resistor applied to the GSC.

For instance, let us consider the H bridge 1.

- When testing branch 1 of H bridge 1, the upper IGBT is controlled while the lower one is constantly off. To perform proper measurements, a pull-down resistor must be connected between the emitter of the upper IGBT (i.e., the collector of the lower IGBT) and negative supply voltage (i.e., the ground). A orange resistor can be seen in Figure 4.3 in the branch 1 of H bridge 1. In this way, by keeping off the upper IGBT, the branch middle point stands at the ground voltage and does not show an arbitrary voltage.
- When testing branch 2 of H bridge 1, the lower IGBT is controlled while the upper is kept constantly off. To perform the measurements to check the correct behavior of such a system, a pull-up resistor must be connected between the collector of the lower IGBT (i.e., the emitter of the upper IGBT) and the positive supply voltage (i.e. VDC). A red resistor can be seen in Figure 4.3 in the branch 2 of H bridge 1. In the same way as before, when lower IGBT of branch 2 of A bridge is kept off, the branch middle point stands at the DC BUS voltage and does not show arbitrary voltage value.

4.3.1 GTC – MEASURED WAVEFORMS

The commutations for branch 1 of H bridge 2 is shown in Figure 4.4.

The IGBT commutations works at a frequency of 1 kHz, as well as the gate and control commands.

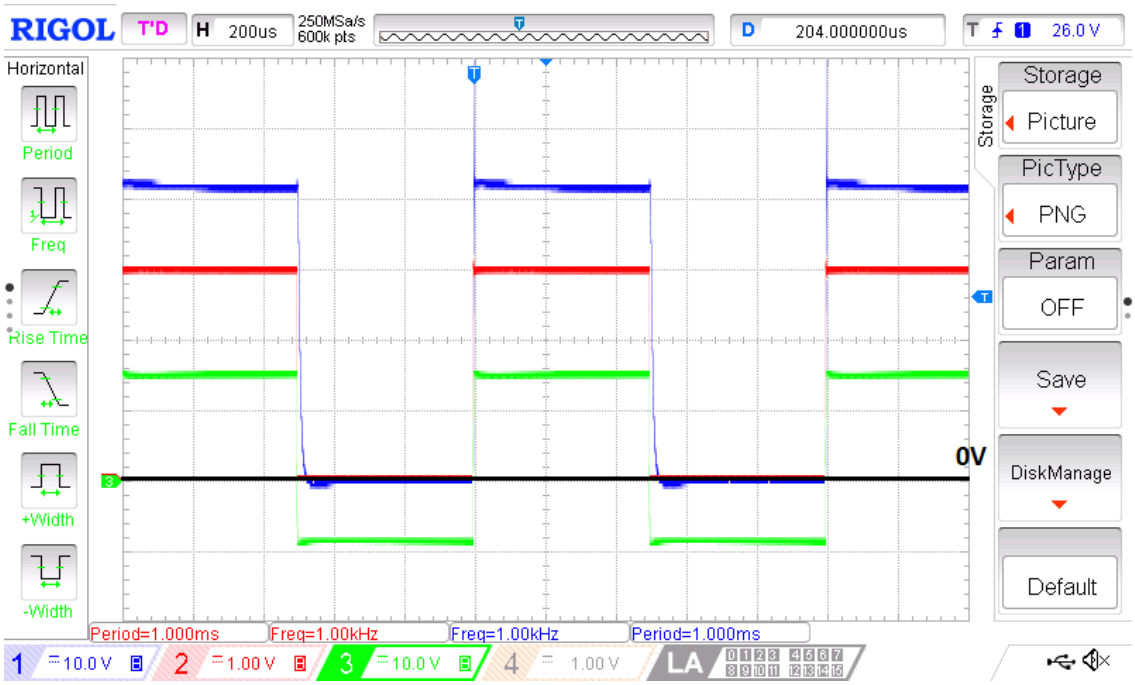

Figure 4.4 Switching behaviour of branch 1 of H bridge 2.

Three traces are visible and the time scale is 200 µs per division:

- The blue trace is the voltage across the pull-down resistor. The scale for the blue trace is 10V per division, so it is easy to spot that the maximum value corresponds to the supplied continuous voltage, which is about 40 V.
- The red trace (the scale is 1V per division) corresponds to the driver command voltage sent from the control board, which is now replaced by a pulse signal generator
- Finally, the green trace is the voltage V_{GE} between the gate and the emitter of the switching IGBT (in this case, the upper IGBT of the branch). The scale is 10V per division. The signal goes from +15 V (IGBT on) to -9 V (IGBT off).

As visible, all the three traces are in phase, as expected.

Out of curiosity, a zoom of the commutation instant is reported in Figure 4.5.

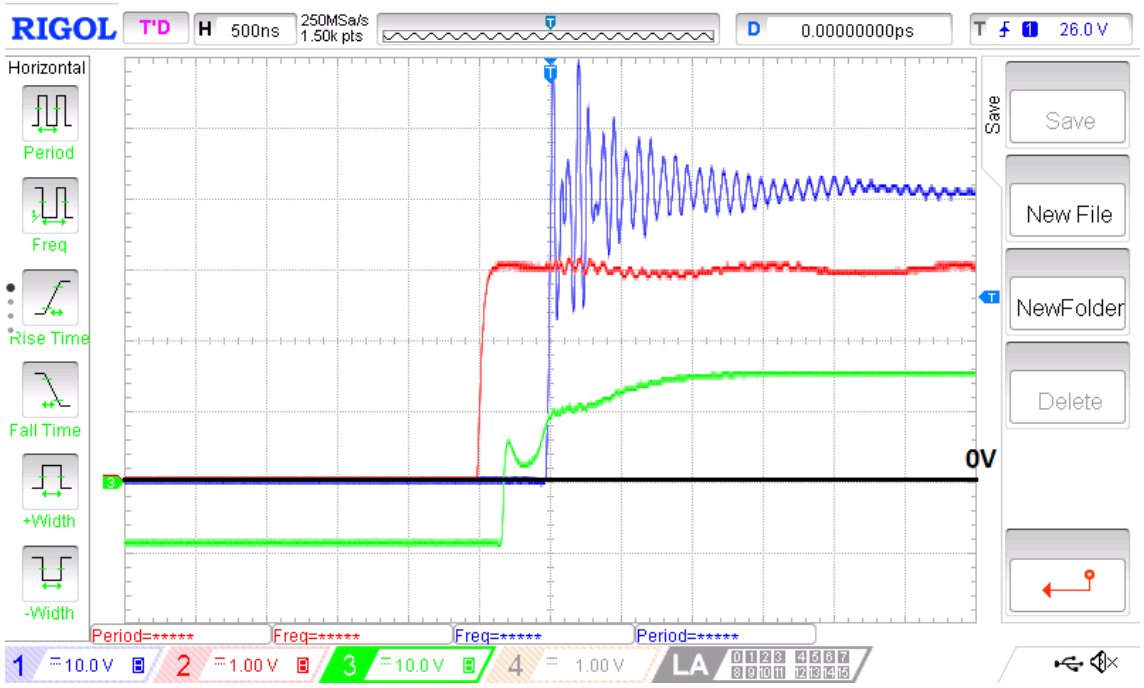

Figure 4.5 Zoom of the commutation instant.

In this figure, the scale is 500 ns per division. Initially, the IGBT is off because the driver signal (red) is low (and the gate-emitter voltage green is at its lower value).

Only after the driver command (red) has gone high, the gate-emitter voltage goes high too (green) and, after that, the voltage across the resistor (blue) goes to the upper VDC value.

The ripple in the blue trace is due to stray inductances and capacitances of the load resistor wires.

Tests equal to the described one have been performed on all the three H bridges and similar good results have been obtained. Thus, it has been verified that IGBT has been correctly driven and its switching behavior is what expected. In Figure 4.5 shows that the commutation delay from the rising edge of the gate-emitter voltage (green) to the rising edge of the load resistor voltage (blue) is about 300 ns, which is compatible with the turn ON delay time value declared in the datasheet of Semikron SEMiX603GB17E4p IGBT module (260 ns typical value).

4.3.2 SAFETY SYSTEMS CHECK

During low voltage tests, safety systems have been tested too. Faulty conditions make the switch commutation stop. When the fault detection system detects that the fault has been cleared, the switch commutation is restored as well. In the real application, the control system shuts off the converter as soon as a fault is detected, without restoring the normal operation unless an external intervention in performed.

Some fault conditions are listed below:

- driver fault;
- overcurrent event;
- DC overvoltage event;
- adaptation board voltage levels instability;
- door switches;
- emergency mushroom button;
- thermal switches;
- IGBT NTC temperature sensors;
- DC fuse fault;
- AC fuse fault;
- cabinet fan status.

The overcurrent detection system test is explained here in details. Since the rated level of the phase current cannot be reached during the low-voltage tests, a proper voltage waveform has been applied to the current detection circuits to simulate an overcurrent event.

For the sake of brevity, only the results for branch 1 of H bridge 1 are reported.

As seen in Figure 4.6, the blue trace is the external sinusoidal voltage waveform used to simulate the acquisition of the current sensor. The red trace is the voltage across the measurement pull-down resistor (as explained above) between the middle point of branch 1 of the H bridge 1 and the ground.

If the current measurement (blue) exceeds either the upper or the lower limit (dotted lines in black), the output voltage (red) goes low for about 0.4 s (because the fault detection system gives a fault pulse of about 0.4 s duration). When the fault pulse has passed, the voltage (red) restores to the previous conditions (in the figure this is visible just for a short amount of time, lower than 0.1 s, then another overcurrent detection occurs. In a real application, the control system would not restore the voltage (red signal) until the fault condition is cleared.

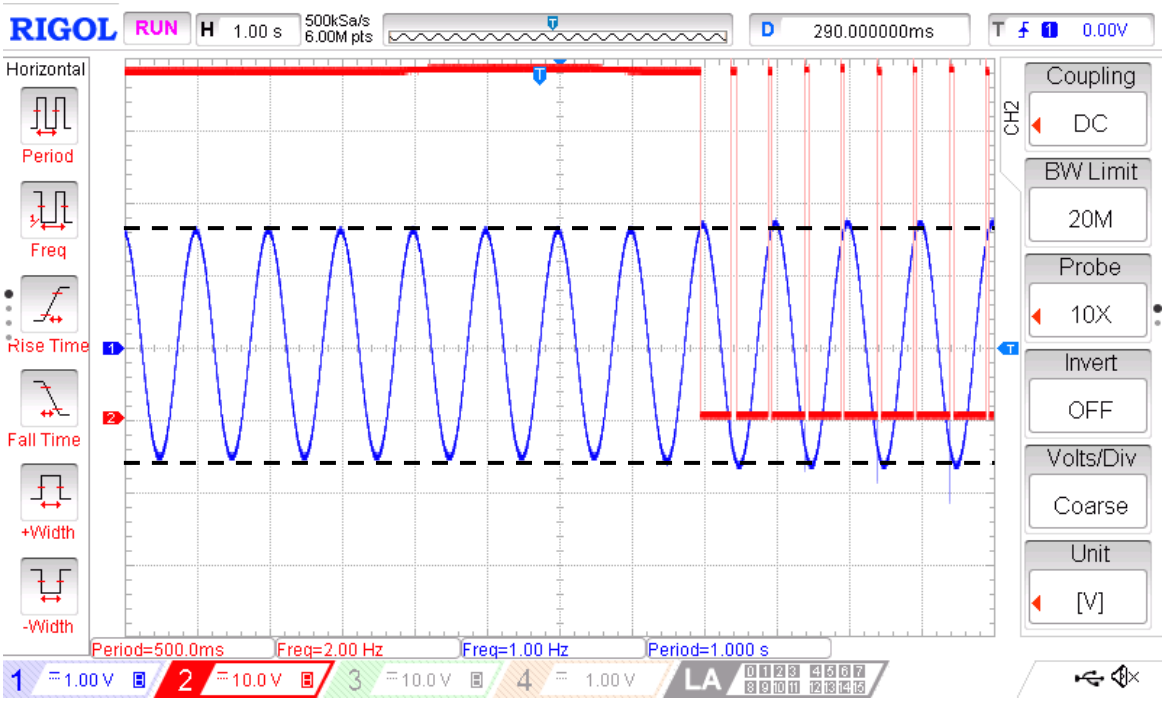

Figure 4.6 Overcurrent protection intervention (time scale is 1s/div).

The DC overvoltage detection acts as the overcurrent detection and generates a pulse signal with a duration of 400 ms managed by the software. Since it is not possible to recreate a real DC overvoltage event, the DC overvoltage protection intervention has been successfully tested by emulating an overvoltage event with a signal generator.

Other interlock conditions have been tested either during the tests of the power electronics cabinet (low voltage conditions) or during the laboratory tests of the adaptation board, in order to perform full voltage and full power trials with safety systems all ready to intervene.

4.4 Insulation tests

According to standard IEC 61439-1 “Low-voltage switchgear and controlgear assemblies – Part 1: General rules” and IEC 61439-2 “Low-voltage switchgear and controlgear assemblies - Part 2: Power switchgear and controlgear assemblies”, insulation tests have been carried out in order to verify the insulation between the power section and the ground system. All the power sections (i.e., all the sections that are at an high voltage compared to the ground, like the phase bars and DC bus bars) have been short-circuited together, as well as, separately, all the ground and negative voltage sections of auxiliary power supplies (see Figure 4.7).

The level of the test voltages has been 1890 Vac for one minute and 2670 Vdc for one minute as reported by the standards for a supply voltage up to 690 Vac.

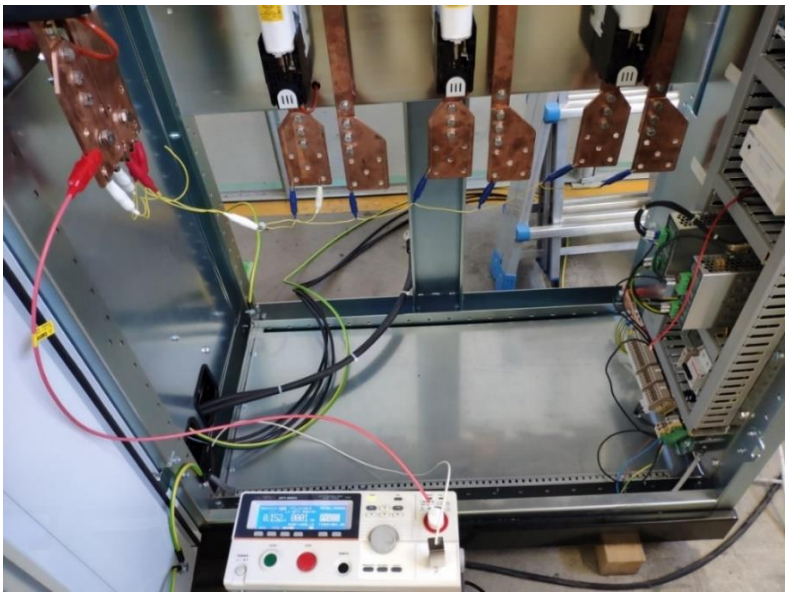

Figure 4.7 Power section short-circuiting and ground and negative auxiliary voltage short-circuiting.

Insulation resistance measurement has given a value of 1 MΩ at 150 V as visible in Figure 4.8. Since, according to standard IEC 61439, the minimum acceptable value of insulation resistance is 230 kΩ, the test has been successfully passed.

Figure 4.8 Insulation resistance at 150 V.

4.4.1 LEAKAGE CURRENT

Keeping the same connection shown in Figure 4.7, a preliminary insulation test has been done using the AC voltage level suggested by the standards (lower than the rated value):

- with a test voltage of 100 V and a rising ramp of 0.1 s, a leakage current of 0.5 mA has been detected;
- with a test voltage of 1000 V and a rising ramp of 0.1 s, a leakage current of 4.85 mA has been detected;

Then, the following tests prescribed by the standard have been performed:

- with a test voltage of 2 kVac (50 Hz) applied for 60 s with a ramp rising time of 5 s, a leakage current of 7.5 mA has been detected, as visible in Figure 4.9 on the left.
- with a test voltage of 2.7 kV DC voltage applied for 1 second with a ramp rising time of 5 s, a leakage current of 0.023 mA has been detected, as visible in Figure 4.9 on the right.

According to Standard IEC 61439, the maximum value of the leakage current is 100 mA (chapters 10.9.2.2 and 10.9.3.4), thus the test has been passed as shown in Figure 4.9.

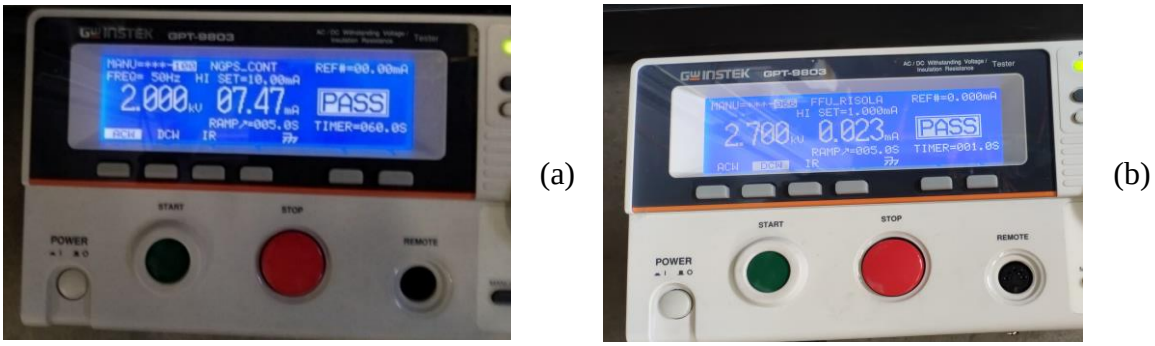

Figure 4.9 Insulation test 2 kV AC (a) and 2.7 kV DC (b).

4.5 Ground resistance tests

The ground resistance in a power electronics apparatus must be low in order to perform a proper ground protection in the event of an insulation fault. The standard requires a ground continuity check performed with an excitation current of 10 A, showing a conductor resistance lower than 0.1 Ω.

Figure 4.10 shows the common coupling point for the ground resistance measurement (the same configuration of Figure 4.7 has been kept).

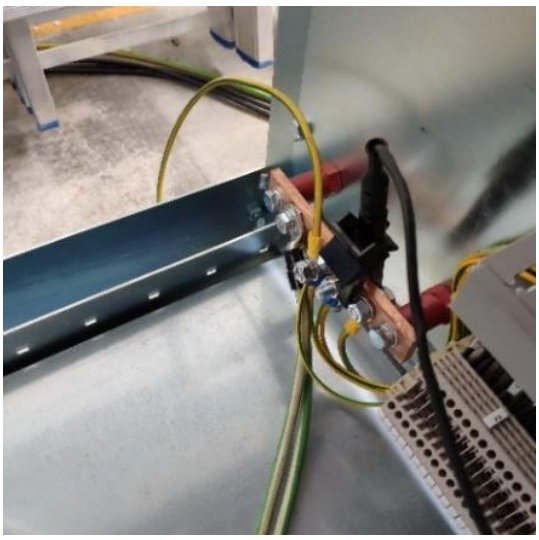

Figure 4.10 Common coupling point of the ground connection with the terminal of the measuring instrument connected.

Following figures show different ground resistance measurement points with corresponding measured value.

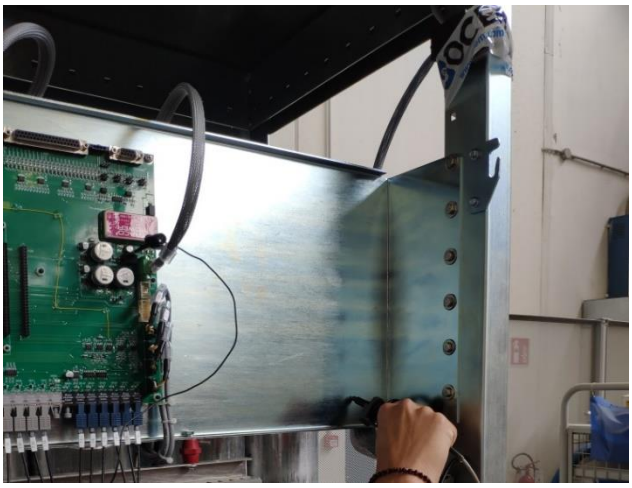

(a)

(b)

Figure 4.11 Ground resistance measurement point (a) and detected value of ground resistance (b).

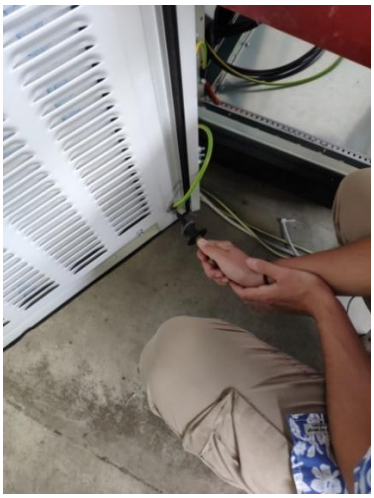

(a)

(b)

Figure 4.12 Ground resistance measurement point (a) and detected value of ground resistance (b).

(a)

(b)

Figure 4.13 Ground resistance measurement point (a) and detected value of ground resistance (b).

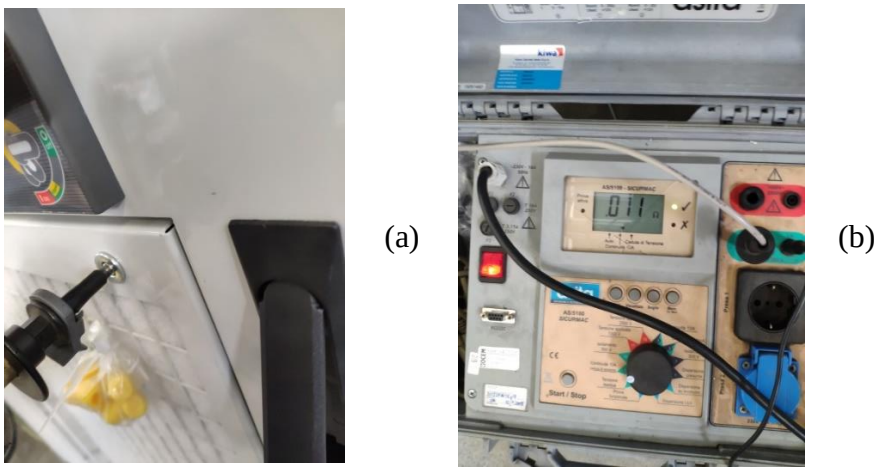

Figure 4.14 Ground resistance measurement point (a) and detected value of ground resistance (b).

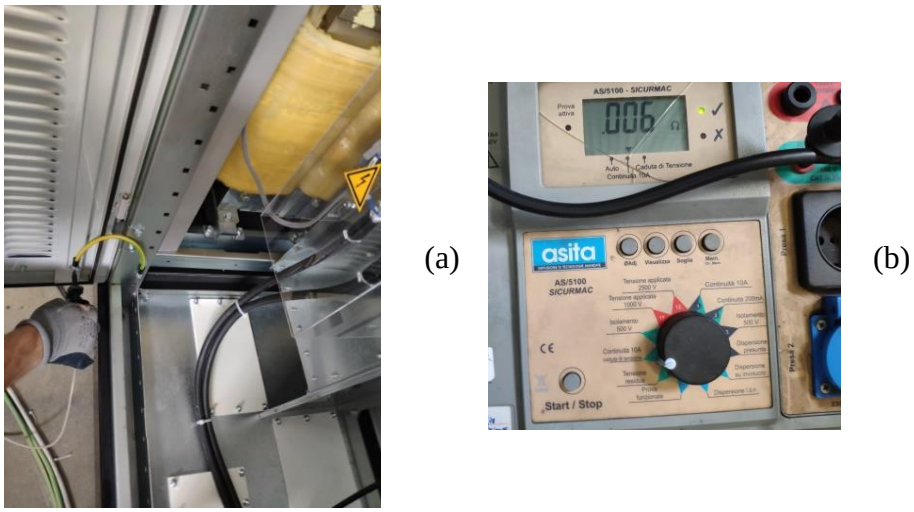

Figure 4.15 Ground resistance measurement point (a) and detected value of ground resistance (b).

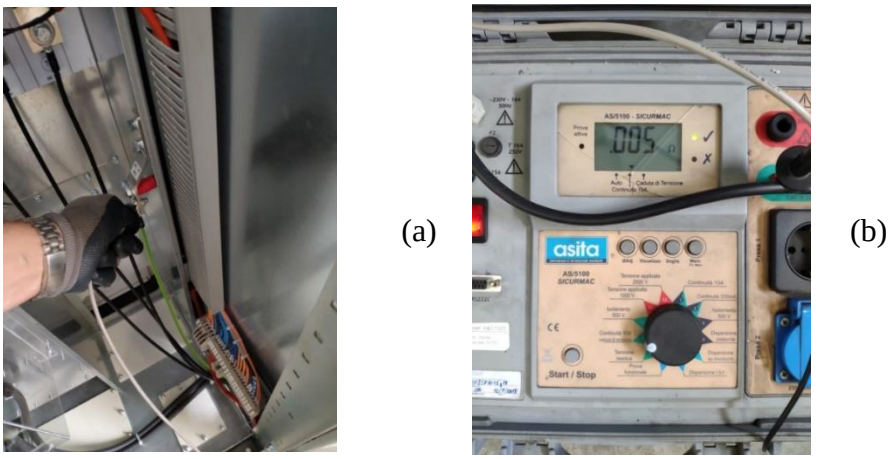

Figure 4.16 Ground resistance measurement point (a) and detected value of ground resistance (b).

The measurements show a maximum resistance of 0.1 Ω, so each analyzed section is well connected to ground according to standards.

4.6 Full voltage commutations test

During the full voltage tests, with the GTC connected to the grid, a DC voltage of 850 V has been applied to the DC bus.

As shown in Figure 4.17, the system is arranged as in a real application. The GTC is connected to the grid and all safety systems have been correctly activated. Since the full current is not required during these tests, a 900 Ω ohmic load (shown in blue in Figure 4.17 and depicted in Figure 4.18) has been used in order to keep the circulating current at about 1 A.

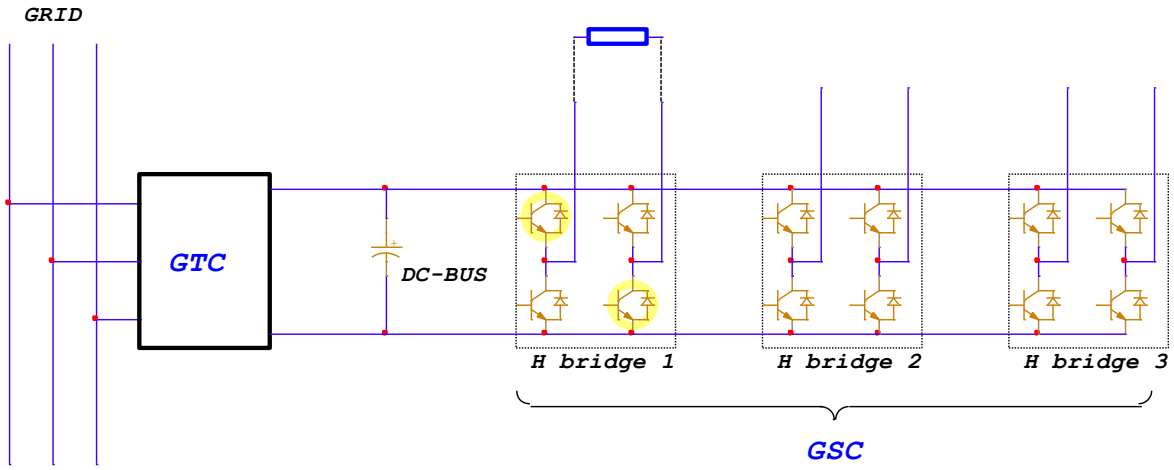

Figure 4.17 System setup configuration for full voltage tests.

Figure 4.18 Load resistor 900 Ω 10 kW.

The voltage across the load resistor has been measured, as well as the load resistor circulating current. Each H bridge (1, 2 and 3) has been tested by moving the load resistor from one phase to the others. Unlike the low-voltage tests, the IGBTs have been now switched on and off in pairs, considering the main diagonal for each H bridge (the two IGBTs of the main diagonal for H bridge 1 are highlighted in yellow in Figure 4.17).

4.6.1 *MEASURED WAVEFORMS*

The operation of the converter has been tested at switching frequency of 1 kHz for different duty cycles.

In Figure 4.19,

- the blue trace, with 2 V per division, is the driver command voltage sent from the pulse signal generator to the adaptation board. It is a square wave with an amplitude of 3 V and a frequency of 1 kHz and corresponds to the user-defined commutation sequence to test the system.
- The green trace, with 500 V per division, is the voltage across the load resistor. It is a square wave with a frequency of 1 kHz whose amplitude corresponds to the DC bus voltage value, i.e., 850 V.
- The orange trace (1 A per division) corresponds to the output current, which is about 1 A, because it corresponds to the current that flows through a 900 Ω resistor (the load resistor) with 850 V applied (the DC bus voltage).

Figure 4.19 and Figure 4.20 show only the waveforms for H bridge 2 since equal results have been obtained for other H bridges.

Figure 4.19 H bridge 2 commutation - duty cycle 20%.

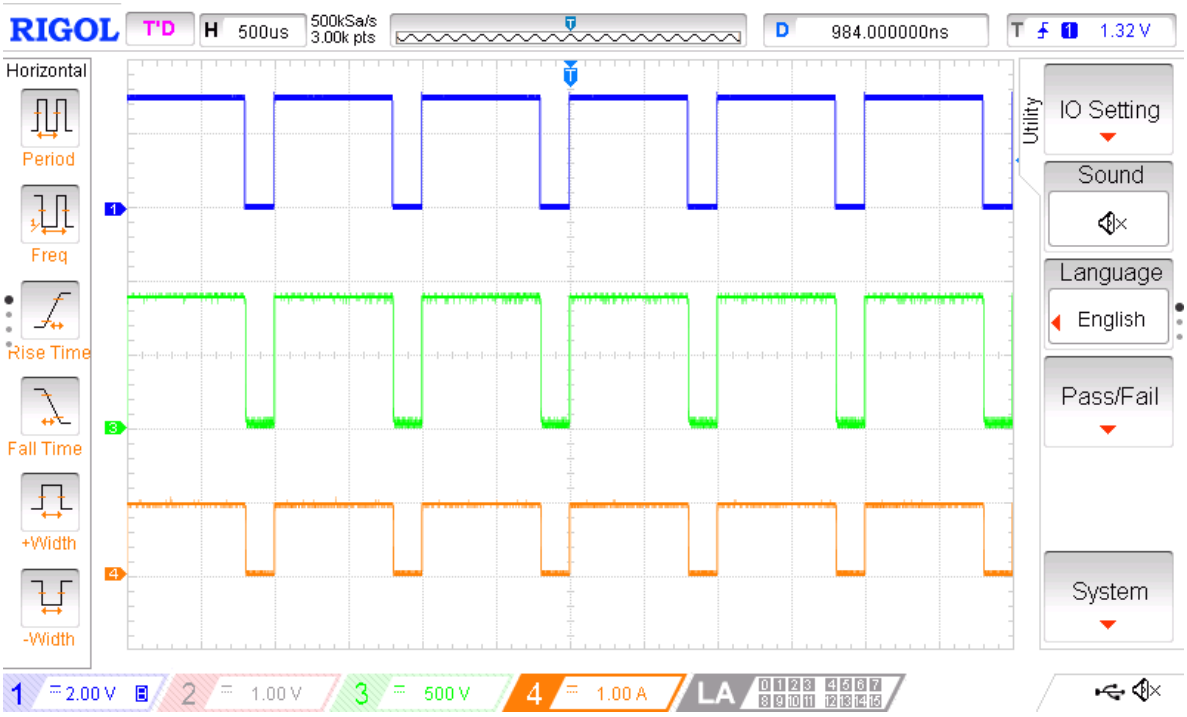

Figure 4.20 H bridge 2 commutation - duty cycle 80%.

Figure 4.21 and Figure 4.22 show in detail the commutation instant.

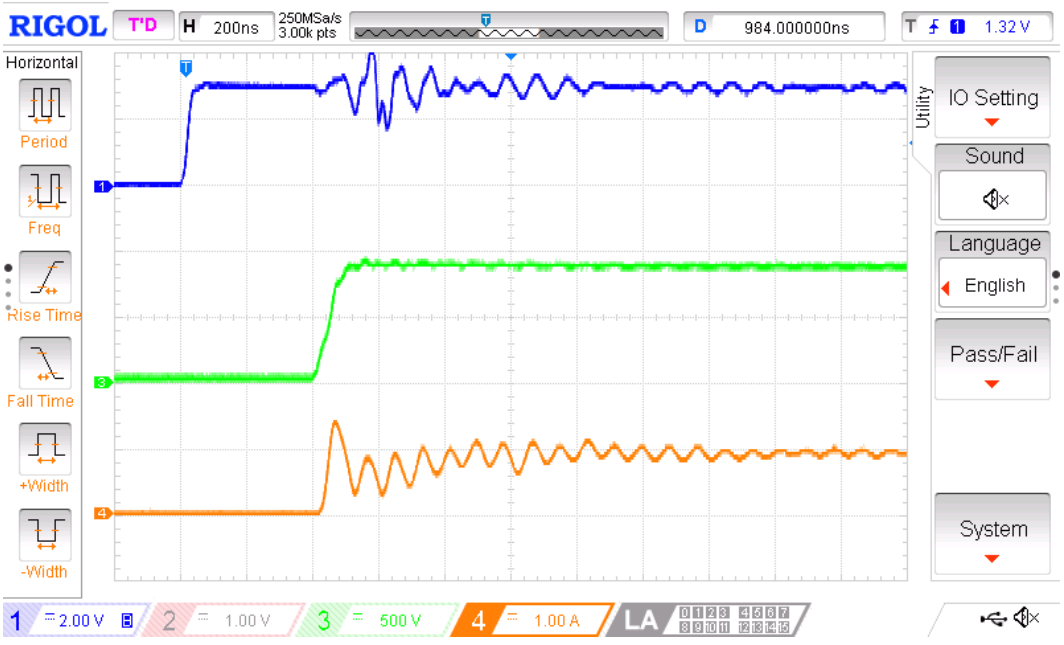

Figure 4.21 H bridge 2 commutation - rising detail.

In Figure 4.21 (with 200 ns per division), after the driver command voltage (blue trace) has risen (up to 3V), the voltage (green trace) start growing across the terminals of the load resistor and it reaches a value of 850 V, causing the current (orange trace) to grow as well, and reach the value of 1 A.

Figure 4.22 H bridge 2 commutation - falling detail.

In Figure 4.22 (with 2 µs per division), after the driver command voltage (blue trace) has fallen (from 3V to 0V), the voltage (green trace) starts decreasing to 0 V with a slow transient (one hundred times slower than the rising process, due to the high value of the resistance used compared to the parasitic capacitances of the power semiconductors). The current (orange trace) has the same behavior.

4.7 Full power commutation tests

Full power tests have been performed with the GTC connected to the grid and a DC bus voltage of 850 V with an ohmic-inductive load properly dimensioned to drain a 200 A continuous current. Although in a real application the current rises up to 350 A, it would not be constant: that is the reason why, by using a continuous 200 A current, reliable results on electrical and thermal stresses are achieved. The value of 200 A comes from the average value of the output current in the foreseen operating conditions.

As visible in Figure 4.23, the power electronics system configuration is the same as the real application (with a dummy load instead of an AMSRM machine). The GTC is connected to the grid (400 V three phase supply) and all safety systems have been correctly activated.

The load (in blue in Figure 4.23) is composed of:

- a resistive part of 0.35 Ω (taking into account both the physical resistors themselves and the resistive value of the inductive load);
- an inductive part of 53 mH obtained with two inductors of 106 mH (100 A rated current each) in parallel.

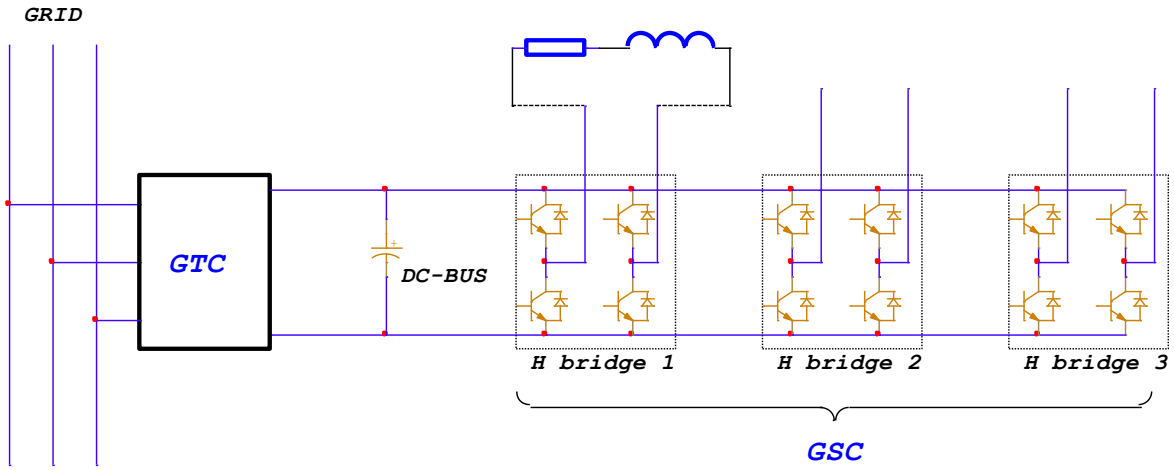

Figure 4.23 System setup configuration for full power tests.

The voltage across the load has been measured, as well as the circulating current. Each H bridge (1, 2 and 3) has been tested moving time by time the load resistor from one phase to the other, as done during full-voltage test. The IGBTs have been switched on and off in pairs, considering the main diagonal for each bridge.

4.7.1 SIMULATIONS DETAILS

Before starting the real tests, some simulations have been performed to predict the behavior of the machine with respect to the ohmic-inductive load.

Simulations have been performed with PLECS by using the circuit visible in Figure 4.24, which is asymmetric and do not include fully bidirectional switches. In practice, the tests are carried out at OCEM by controlling only two switches at a time, while others are disconnected.

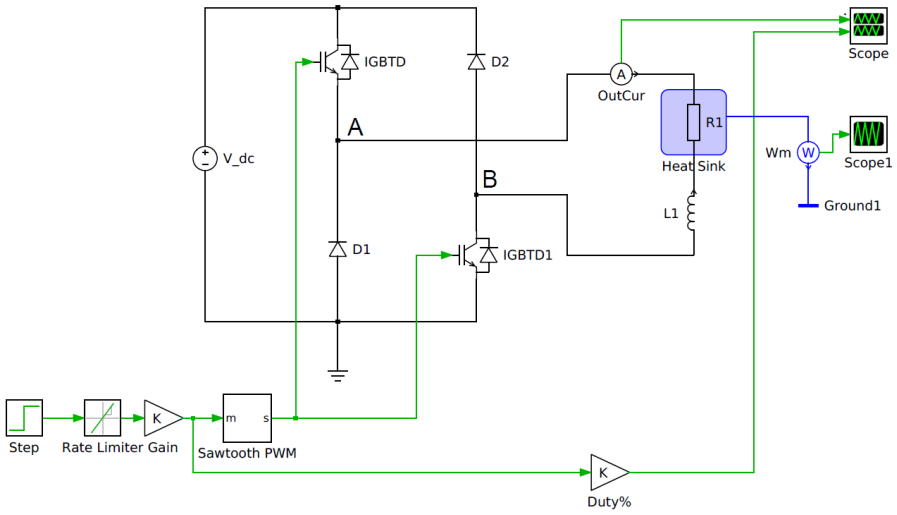

Figure 4.24 Schematic circuit used for full power PLECS simulations.

As visible, only the two IGBTs of the main diagonal of one H bridge have been simulated (the other IGBTs do not matter).

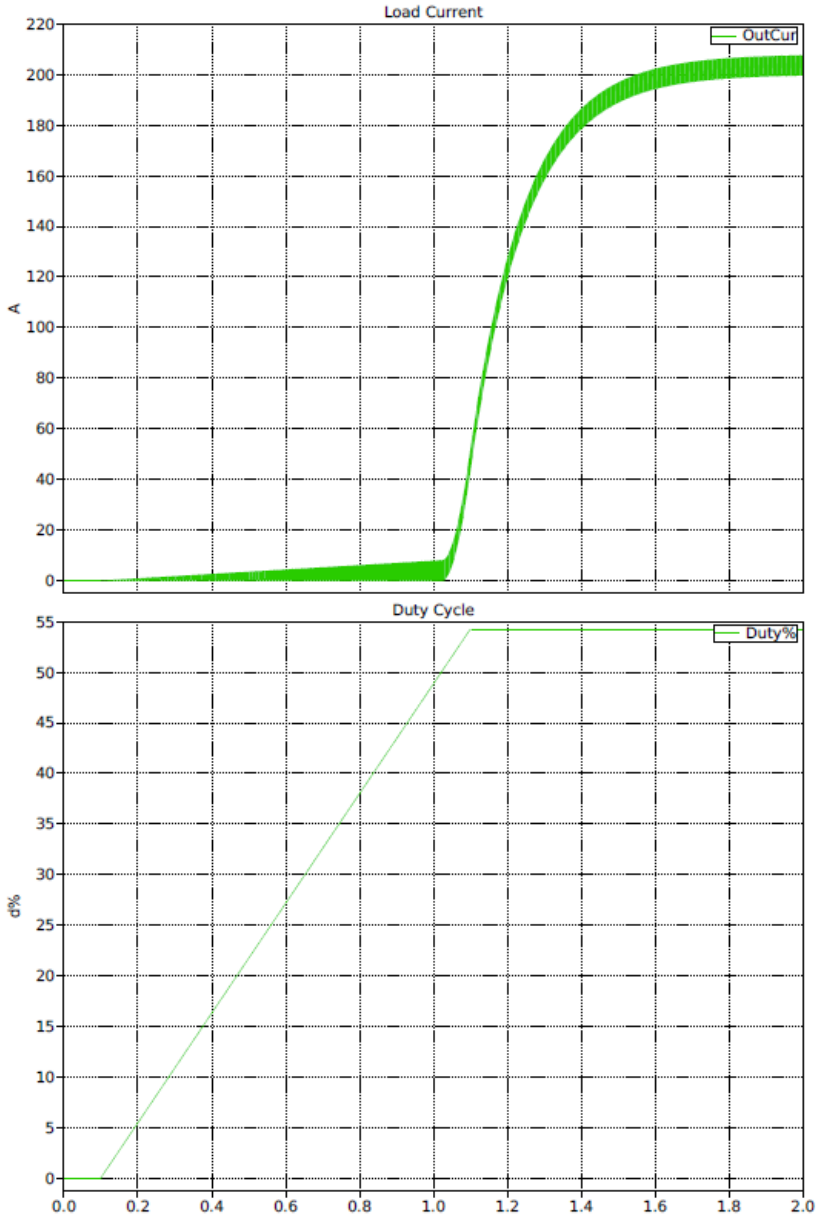

Figure 4.25 Full power test simulation results: current trend (up) VS time (from 0 to 2 s); duty cycle (down) as input to the system with a ramp from 0 to 54%.

As visible in Figure 4.25, until the duty cycle reaches a value of 50%, the current does not increase significantly.

Before showing the experimental results, which are in good agreement with the simulations, an explanation of this phenomenon is given.

The situation for one H bridge is represented in Figure 4.26.

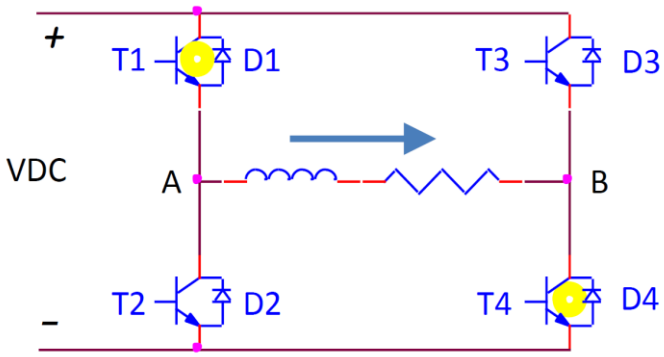

Figure 4.26 Schematic representation of the full current test load behavior.

In the full-voltage tests, the IGBTs that commutate are T1 and T4, highlighted in yellow, while T2 and T3 are kept off. Let us consider a positive load current flow that follows the arrow in Figure 4.26.

Basically, two switching conditions occur within this circuit:

- when the IGBTs are ON, the current follows the positive direction, as shown in Figure 4.27;

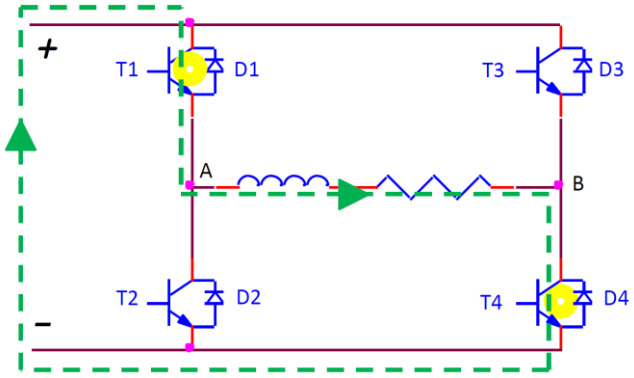

Figure 4.27 Schematic representation of the full current test load behavior when IGBTs are ON.

- When the IGBTs are OFF, the current can either follow the positive direction shown in Figure 4.28, or the current may follow the negative direction, as shown in Figure 4.29.

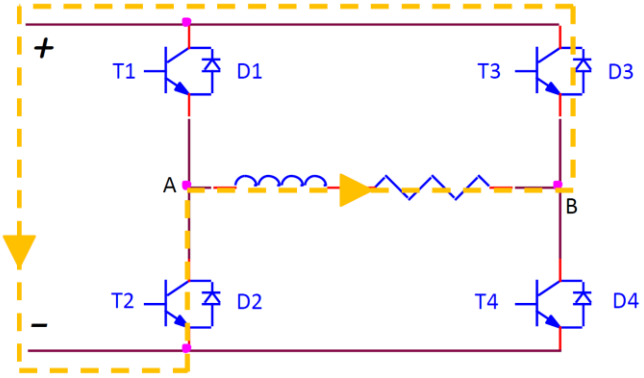

Figure 4.28 Schematic representation of the full current test load behavior when IGBTs are OFF and the current is positive.

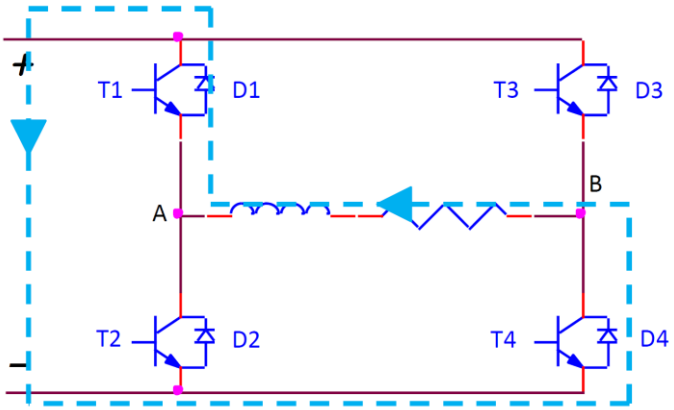

Figure 4.29 Schematic representation of the full current test load behavior when IGBTs are OFF and the current is negative.

Moreover, let us consider the average duty cycle *m* in a switching period. It ranges from 0 to 1: if the duty cycle is 80%, *m* is 0.8. If if the duty cycle is 40%, *m* is 0.4.

- The voltage V_A of point A is as follows,
  - when $m = 1$, i.e., T1 is ON, then $V_A = VDC$;
  - when $m = 0$, i.e., T1 is OFF, so $V_A = 0$ if the current is positive, while $V_A = VDC$ if the current is negative.
- The voltage V_B of point B is as follows:
  - when $m = 1$, i.e., T4 is ON, then $V_B = 0$;
  - when $m = 0$, i.e., T4 is OFF, so $V_B = VDC$ if the current is positive, while $V_B = 0$ if the current is negative.

So, with positive current, it is possible to write:

$$V_A = m * VDC \tag{4.1}$$

$$V_B = (1 - m) * VDC \tag{4.2}$$

and so

$$V_{AB} = 2 * VDC * \left(m - \frac{1}{2}\right) \tag{4.3}$$

With a negative current, it is possible to write:

$$V_A = VDC \tag{4.4}$$

$$V_B = 0 \tag{4.5}$$

and so

$$V_{AB} = VDC \tag{4.6}$$

When *m* is lower than 1/2, i.e., the duty cycle is lower than 50%, (4.3) shows that V_{AB} is negative, so the load current would be forced to become negative. When this happen, (4.6)

must be used instead of (4.3), which results in a positive value of V_{AB} which makes the current become positive and (4.3) must be taken into account. That is the reason why the current oscillates and stays near 0 A before reaching a duty cycle of 50%.

When *m* is higher than 1/2, since the load is ohmic-inductive type, the current is forced to keep always the same direction (because the inductive part acts as a sort of "inertia" for current changes) and equation (4.3) must be used. The resulting load voltage is positive and the current grows.

4.7.2 EXPERIMENTAL RESULTS

Following figures shows the behavior of the system during the full power tests. Each H bridge has been tested separately. Since the inductive load could not sustain a current higher than 200A, the duty cycle has never overcome 54%.

Moreover, test with a current of 200 A is considered adequate because corresponds to the average current of the generator according to the simulations.

Figure 4.30 and Figure 4.31 show the real test setup:

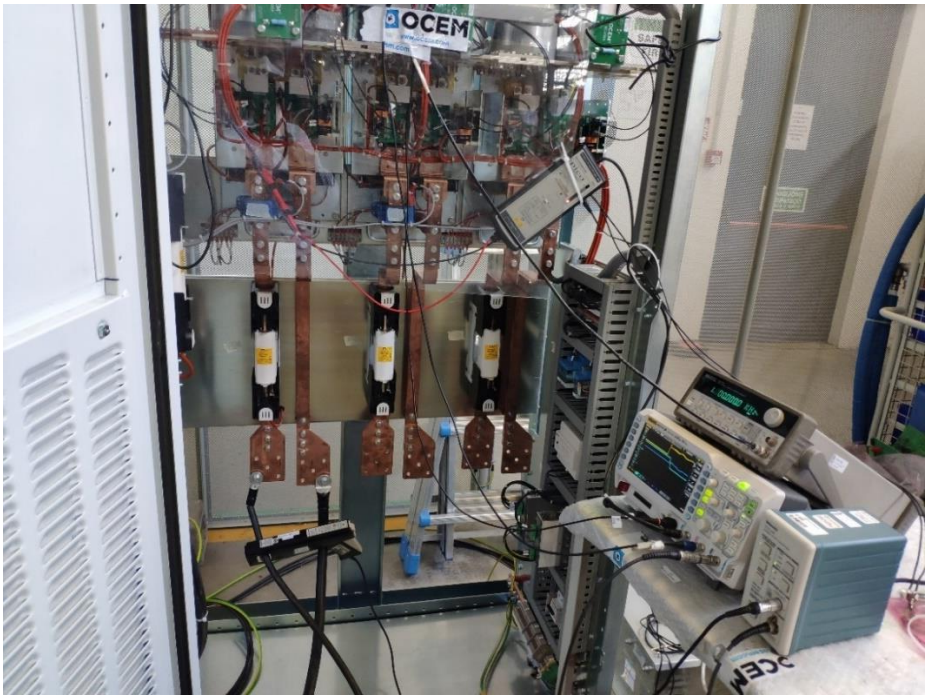

Figure 4.30 Measurement systems connection to the equipment under test during full power tests.

Figure 4.31 Electric load used for full power tests: ohmic part is visible in the foreground and behind, two identical inductors are placed.

Since each chart of measured waveforms has the same color code, they can be explained here for all. The commutation frequency has been set at 1 kHz and different duty cycles have been used.

- The blue trace, with 2 V per division, is the driver command voltage sent from a pulse signal generator to the adaptation board. It is a square wave with an amplitude of 3 V and a frequency of 1 kHz. It corresponds to the user-defined commutation sequence to test the system. Different duty cycles have been tested.
- The red trace, with 500 V per division, is the collector-to-emitter voltage V_{CE} of the switching transistor T1. The trend is the opposite with respect the blue trace (i.e. when the blue trace is high, the red trace is low) and it shows some oscillations until a duty cycle of 50% is reached. Those oscillations are due to resonance between load inductances and the stray capacitances when the H bridge output voltage is not determined due to open state of the IGBTs.
- The green trend, with 0.5 V per division, represents the phase current measured by the internal measurement system installed in the cabinet (LEM LF_510-S/SPA1). It goes from 0 V to +3 V with a current from -400 A to +400 A. When no current is detected, a value of 1.5 V is constantly present due to the topology of the acquisition and conditioning circuit. In the final version of the board, the circuit conversion range has been changed to [0 V, +3 V] → [0 A, +400 A] in order to fully exploit the current range.
- The orange trace (50 A per division) corresponds to the load current measured by an external measurement system.

The following pictures have been taken for H bridge 1.

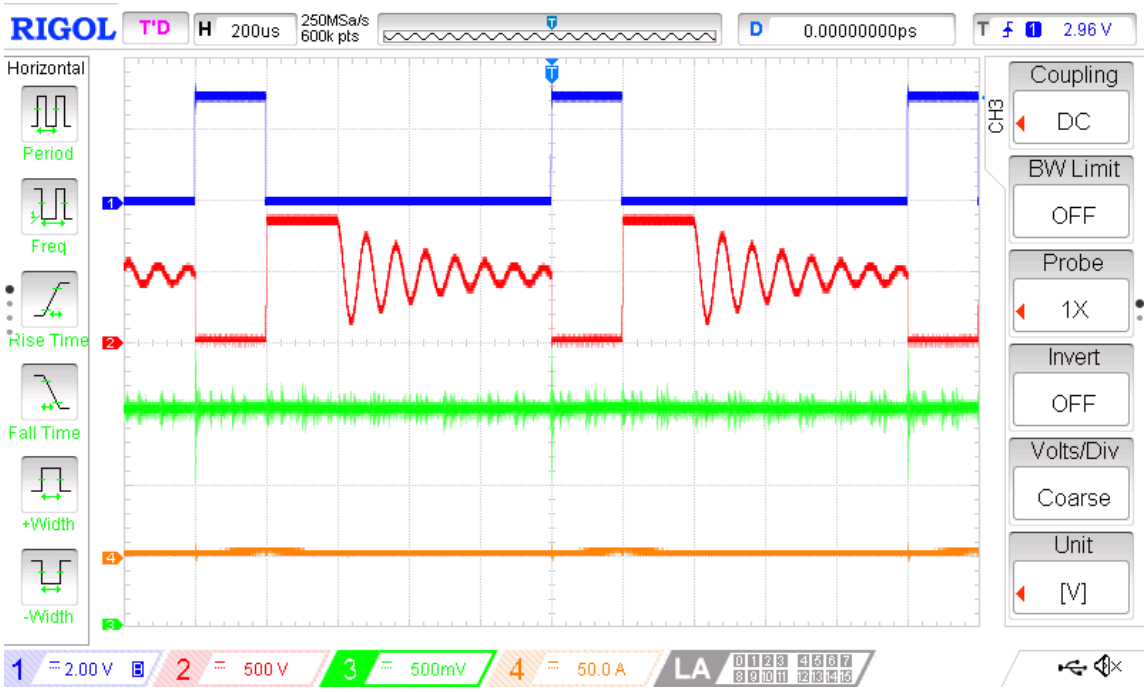

Figure 4.32 H bridge 1 full power test commutation with duty cycle 20%. Blue is the driver command signal, red is the collector-to-emitter voltage, green is the phase current measured by internal system and orange is the phase current measured by external measurement system.

As said, when the duty cycle passes over 50%, the current starts to increase significantly. With a duty cycle of 51% (Figure 4.33) current goes to about 50 A (see orange trace) and the measured current (green trace) goes to about 1.7 V (which correspond to about 50 A).

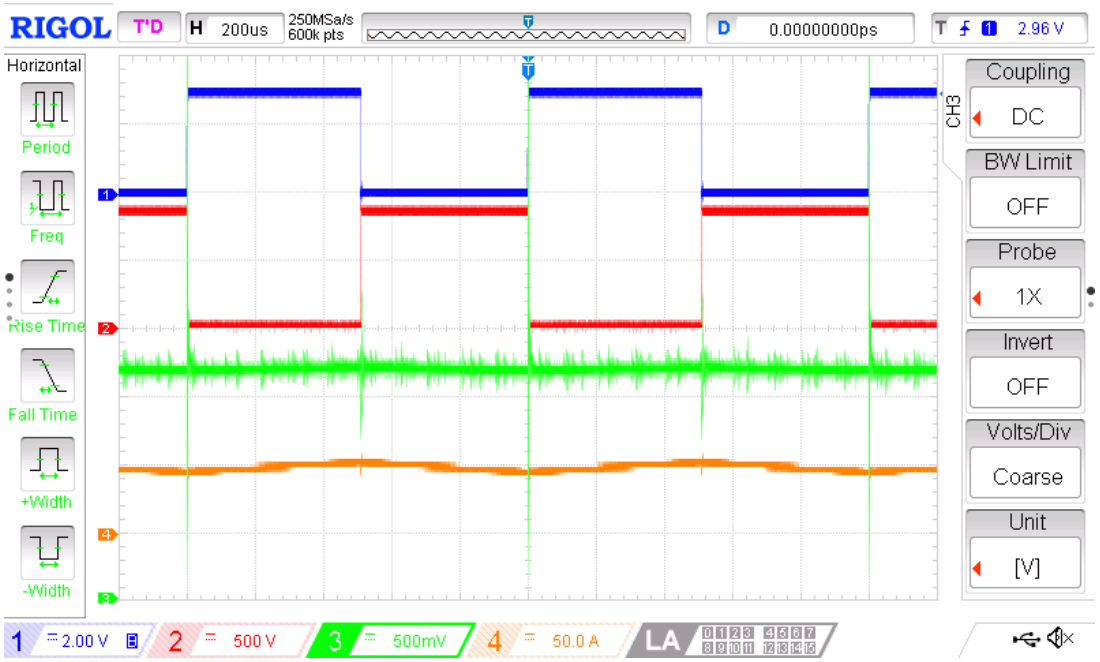

Figure 4.33 H bridge 1 full power test commutation with duty cycle 51%. Blue is the driver command signal, red is the collector-to-emitter voltage, green is the phase current measured by internal system and orange is the phase current measured by external measurement system.

In Figure 4.34, the duty cycle is 52% and the current rises to about 100 A.

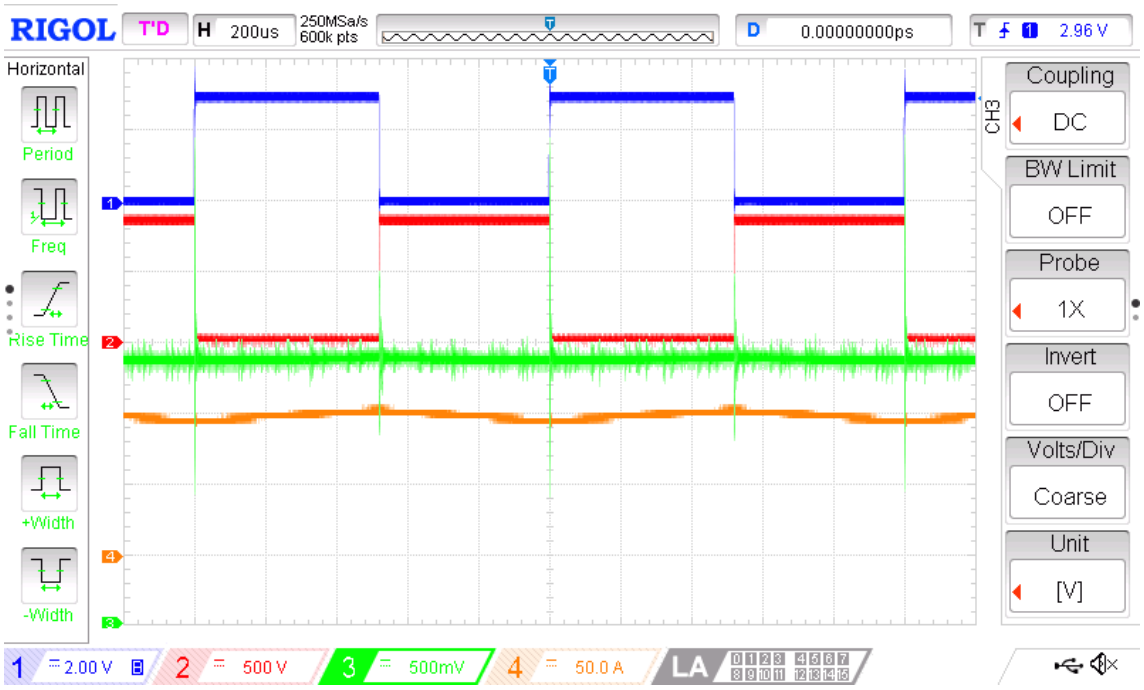

Figure 4.34 H bridge 1 full power test commutation with duty cycle 52%. Blue is the driver command signal, red is the collector-to-emitter voltage, green is the phase current measured by internal system and orange is the phase current measured by external measurement system.

In Figure 4.35 the duty cycle is 53% and the current rises to about 150 A.

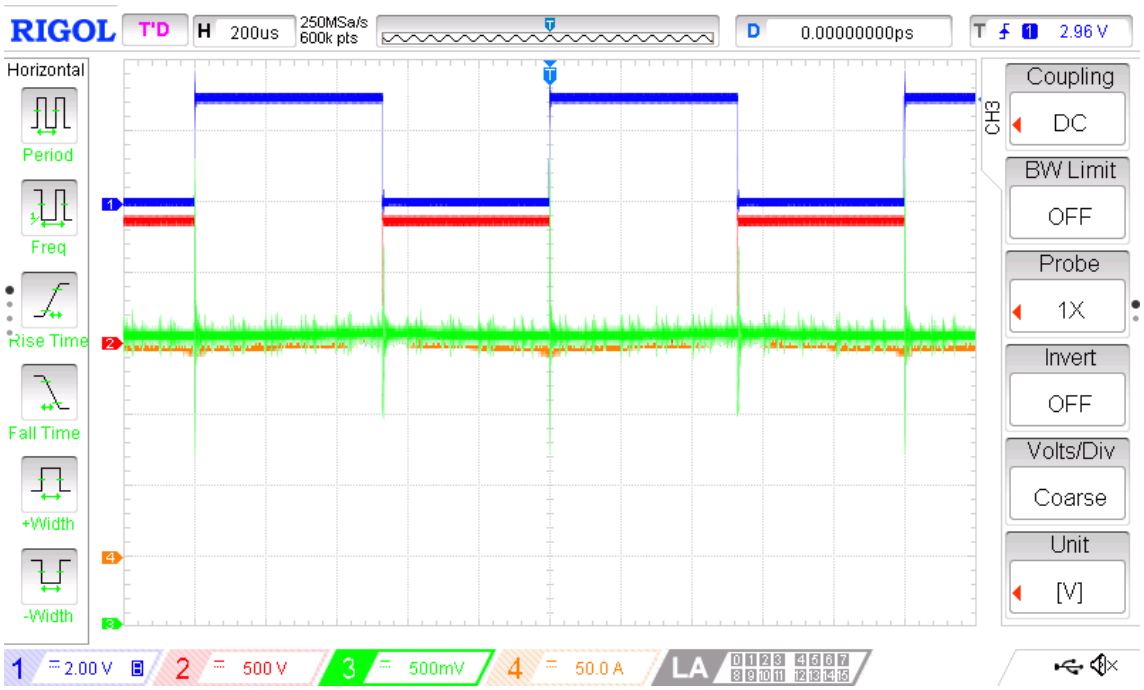

Figure 4.35 H bridge 1 full power test commutation with duty cycle 53%. Blue is the driver command signal, red is the collector-to-emitter voltage, green is the phase current measured by internal system and orange is the phase current measured by external measurement system.

Finally, with a duty cycle of 54% (Figure 4.36), a current of about 200 A has been reached (orange trace) and the measured value (green trace) is a little higher than 2.7 V, which correspond to 200 A.

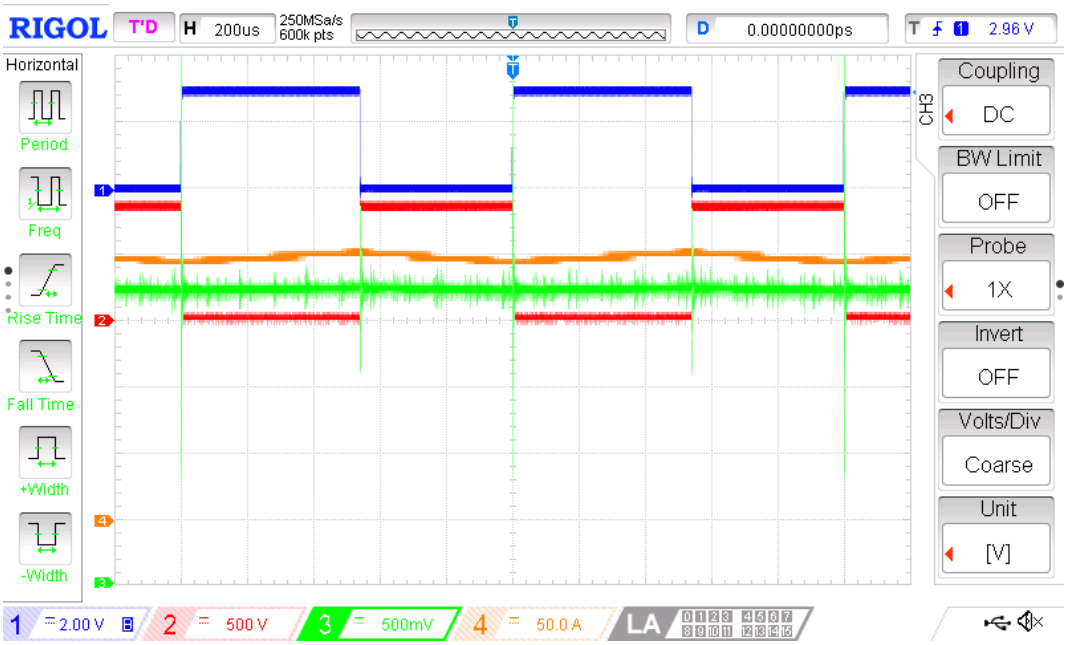

Figure 4.36 H bridge 1 full power test commutation with duty cycle 54%. Blue is the driver command signal, red is the collector-to-emitter voltage, green is the phase current measured by internal system and orange is the phase current measured by external measurement system.

The same tests have been run for H bridge 2 and H bridge 3 (Figure 4.37 and Figure 4.38 show the full power test commutation with duty cycle 54% for H bridge 2 and 3 respectively).

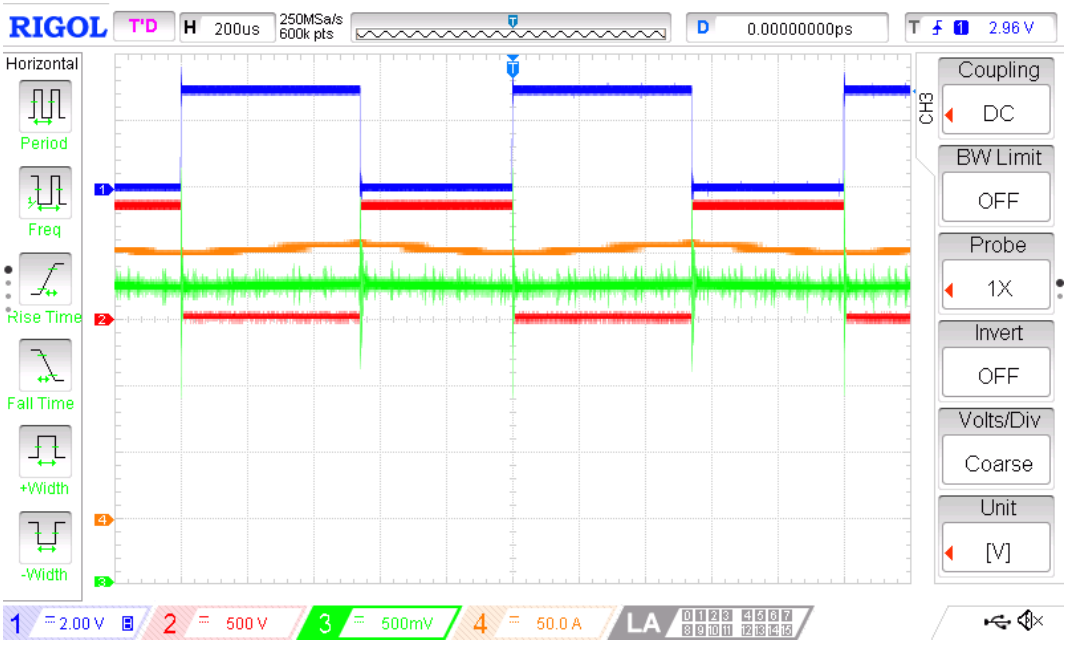

Figure 4.37 H bridge 2 full power test commutation with duty cycle 54%. Blue is the driver command signal, red is the collector-to-emitter voltage, green is the phase current measured by internal system and orange is the phase current measured by external measurement system.

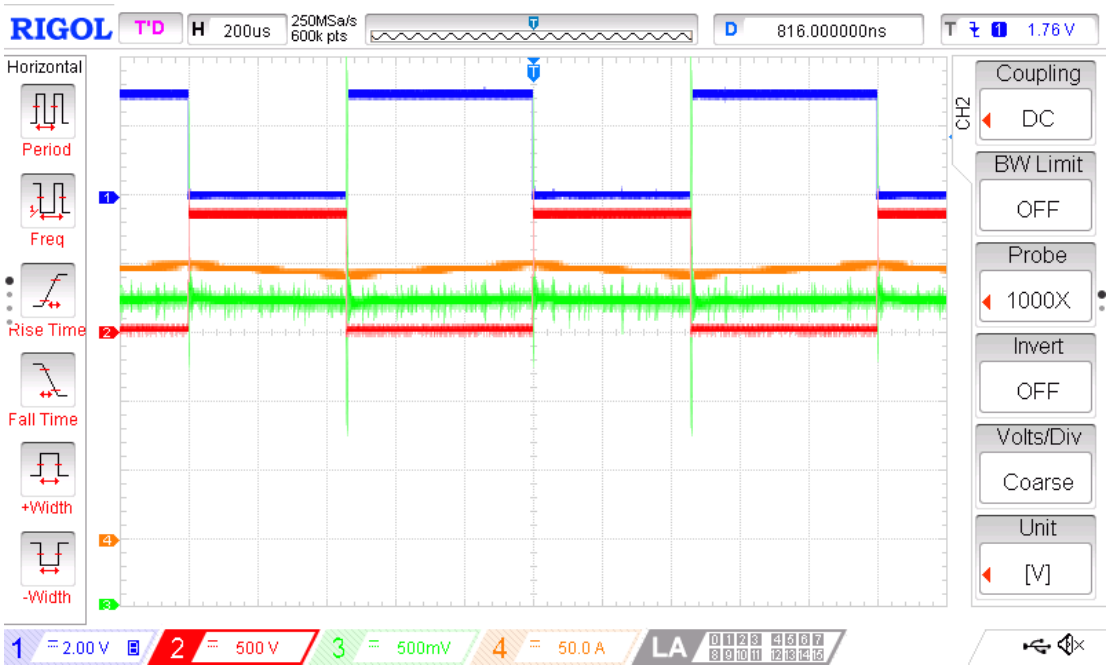

Figure 4.38 H bridge 3 full power test commutation with duty cycle 54%. Blue is the driver command signal, red is the collector-to-emitter voltage, green is the phase current measured by internal system and orange is the phase current measured by external measurement system.

Regarding the internal current acquisition and conditioning circuit (green trace), an unsolicited ripple oscillation is visible immediately after the turn ON (Figure 4.39).

Figure 4.39 H bridge 2 full power test comutation with duty cycle 54% - turning ON current measurement ripple. Blue is the driver command signal, red is the collector-to-emitter voltage, green is the phase current measured by internal system and orange is the phase current measured by external measurement system.

In Figure 4.39 (500 ns per division) a ripple in the green trace is visible, lasting for about 15 µs as shown in Figure 4.40 (2 µs per division).

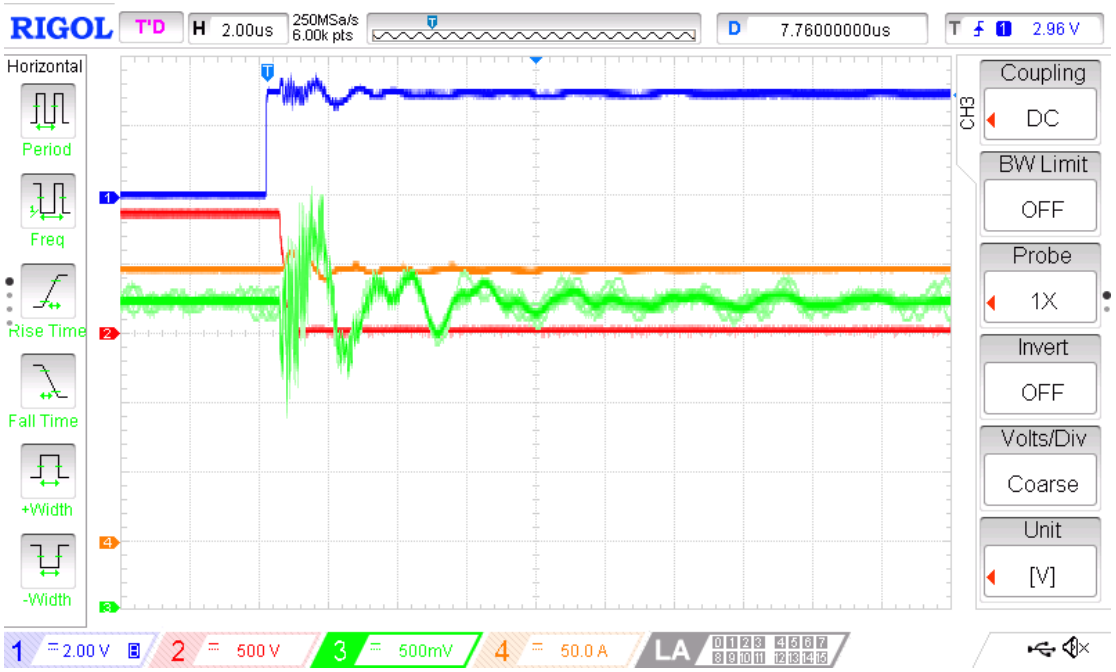

Figure 4.40 H bridge 2 full power test commutation with duty cycle 54% - turning ON current measurement ripple duration. Blue is the driver command signal, red is the collector-to-emitter voltage, green is the phase current measured by internal system and orange is the phase current measured by external measurement system.

The same situation as above occurs during the turn OFF, as shown in Figure 4.41 and Figure 4.42.

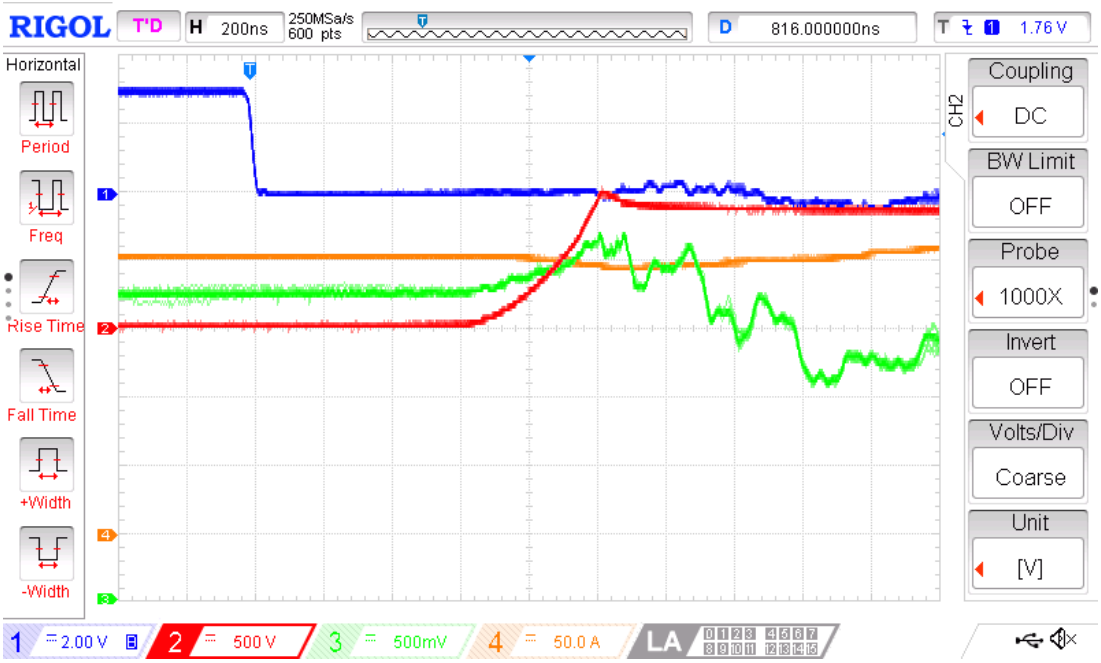

Figure 4.41 H bridge 2 full power test commutation with duty cycle 54% - turning OFF current measurement ripple detail. Blue is the driver command signal, red is the collector-to-emitter voltage, green is the phase current measured by internal system and orange is the phase current measured by external measurement system.

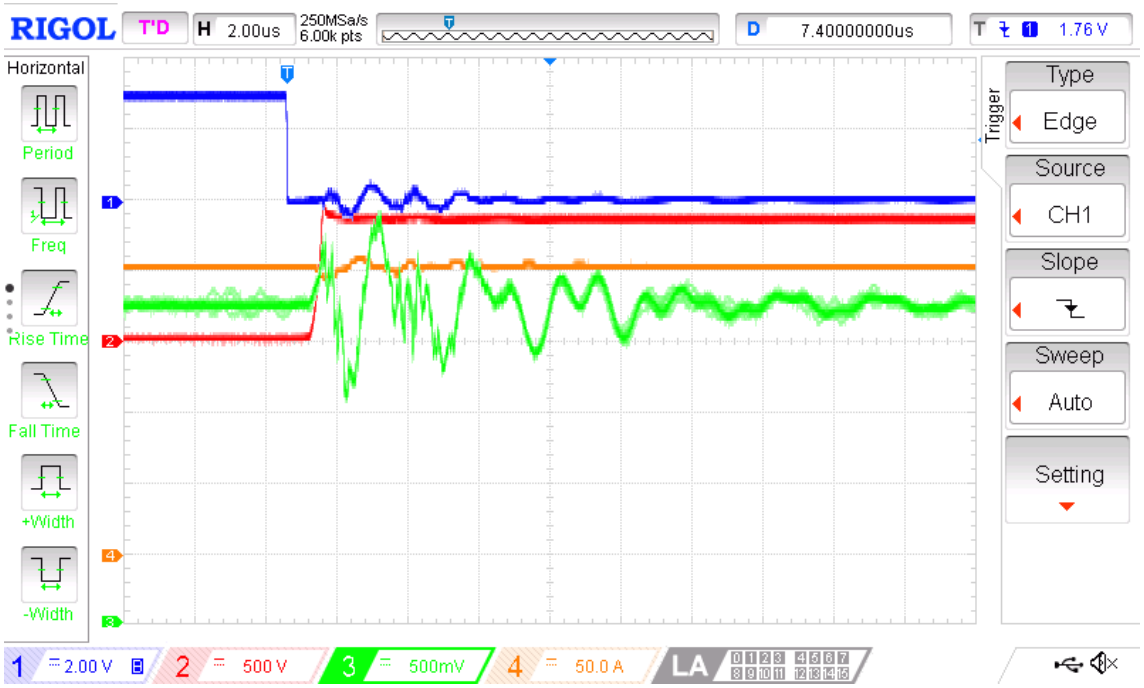

Figure 4.42 H bridge 2 full power test commutation with duty cycle 54% - turning OFF current measurement ripple duration. Blue is the driver command signal, red is the collector-to-emitter voltage, green is the phase current measured by internal system and orange is the phase current measured by external measurement system.

So, after any switching event, a large disturbance lasting for about 15 µs was recorded during the tests on the voltage corresponding to current measurement.

It cannot be judged if this disturbance is really present inside the adaptation apparatus composed of electronic boards. Such a disturbance is probably picked-up along the experimental setup due to the long connection cables between the adaptation board and the oscilloscope and due to the different grounding arrangement (the ground of the scope is connected to the distribution ground of the electrical system, while the 0V of the adaptation board is not). In order to avoid any noise, it is recommended to perform the ADC sampling of the phase currents some tenths of µs away of the switching instants.

The last consideration can be done regarding the voltage V_{CE} between the collector and the emitter of the switching IGBT (red trace). As visible in the following figures, there is a little voltage spike during the switch OFF instant. The following figure (Figure 4.43 and Figure 4.44) with 200 ns per division show in detail the overvoltage detected.

Figure 4.43 H bridge 3 full power test commutation with duty cycle 54% - overvoltage spike during the switch OFF. Blue is the driver command signal, red is the collector-to-emitter voltage, green is the phase current measured by internal system and orange is the phase current measured by external measurement system.

Figure 4.44 H bridge 3 full power test commutation with duty cycle 54% - details of the overvoltage spike during the switch OFF. Blue is the driver command signal, red is the collector-to-emitter voltage, green is the phase current measured by internal system and orange is the phase current measured by external measurement system.

Conversely, no overvoltage has been detected during switch turn ON, as visible in following figures (Figure 4.45 and Figure 4.46).

Figure 4.45 H bridge 3 full power test commutation with duty cycle 54% - VCE during the switch ON. Blue is the driver command signal, red is the collector-to-emitter voltage, green is the phase current measured by internal system and orange is the phase current measured by external measurement system.

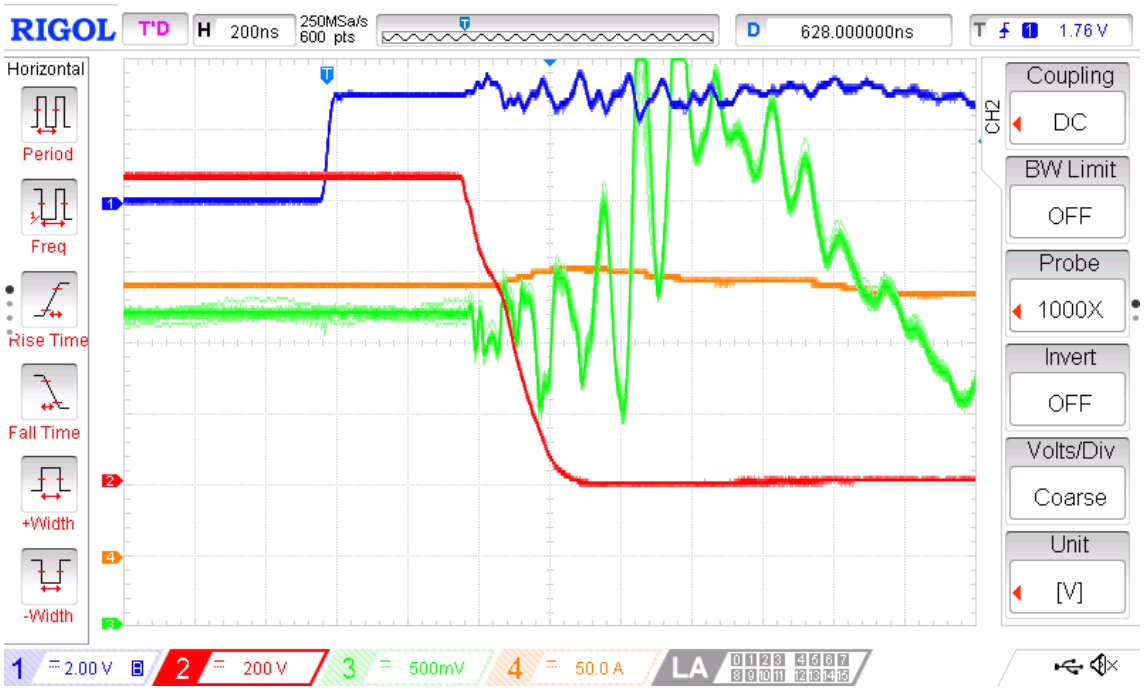

Figure 4.46 H bridge 3 full power test commutation with duty cycle 54% - details of VCE during the switch ON. Blue is the driver command signal, red is the collector-to-emitter voltage, green is the phase current measured by internal system and orange is the phase current measured by external measurement system.

Last pictures also show the already discussed current measurement oscillations.

While testing the H bridge 2, thermal measurements have also been recorded. H bridge 2 is the most thermally stressed due to its central position. The cooling system (the ceiling fan and the fans per each H bridge) has been kept ON for the whole duration of the test. A thermocouple sensor has been placed on the IGBTs heatsink between two IGBT modules, as shown in Figure 4.47.

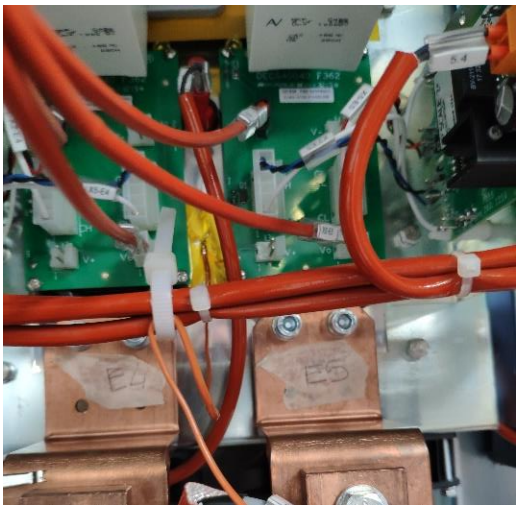

Figure 4.47 Thermal sensor position (yellow) in the middle of two IGBT modules of B bridge.

Figure 4.48 reports the temperature trend [°C] vs time [min]. Since the cooling system has been designed for a maximum admissible heatsink temperature of 85°C, safety is respected since the maximum recorded temperature with a constant current of 200 A constantly applied is about 60°C.

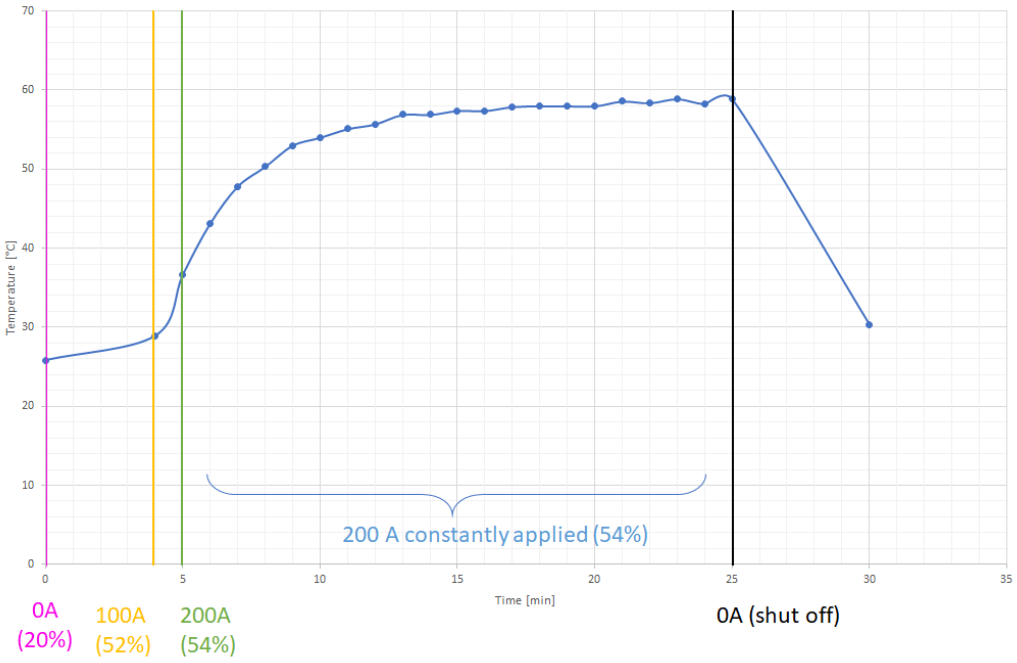

Figure 4.48 B bridge full power test temperature monitoring, current values and corresponding duty cycle vaues are reported.

The thermal images of some parts of the systems have been acquired and they are reported in Figure 4.49 - Figure 4.55.

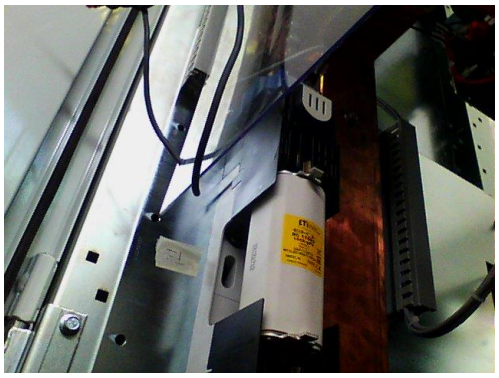

(a)

(b)

Figure 4.49 DC fuse picture (a) and thermal image (b).

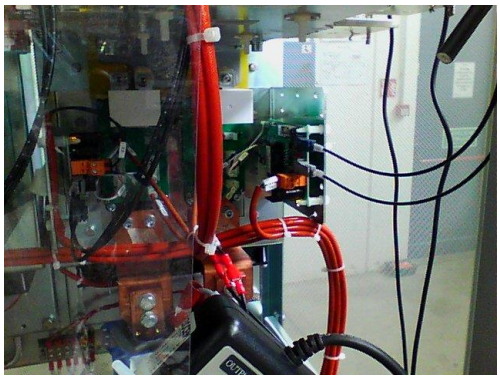

(a)

(b)

Figure 4.50 Driver board picture (a) and thermal image (b).

(a)

(b)

Figure 4.51 Switching IGBT module picture (a) and thermal image (b).

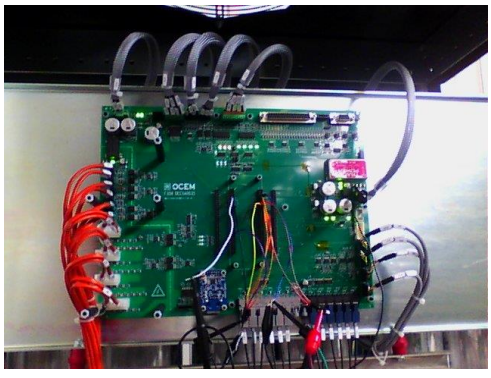

(a)

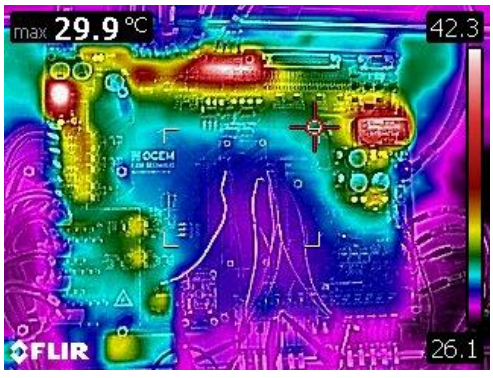

(b)

Figure 4.52 Control adaptation board picture (a) and thermal image (b).

(a)

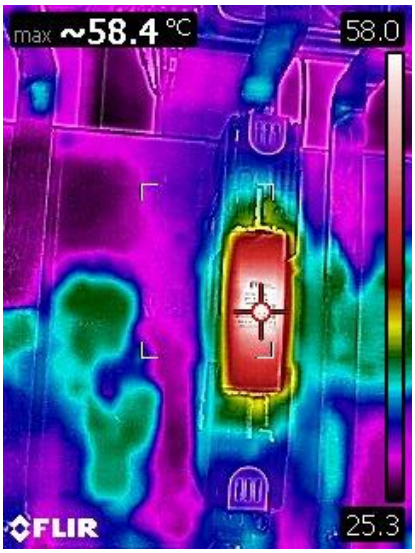

(b)

Figure 4.53 Phase fuse picture (a) and thermal image (b).

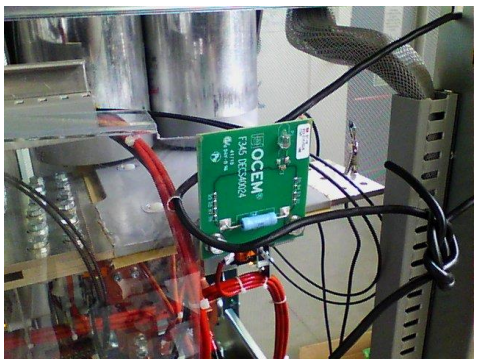

(a)

(b)

Figure 4.54 DC voltage detection light picture (a) and thermal image (b).

(a)

(b)

Figure 4.55 Inductive load picture (a) and thermal image (b).

4.8 Conclusion

Some tests on power electronic converter have been carried out and correctly passed.

First, low voltage tests to verify the correct behavior of the machine and to spot any building mistakes have been done. The behaviors of the IGBTs during the commutation have been driven with a constant DC bus voltage of 40 V and a measurement load of 500 Ω. Switching ON delay time has also been verified and the safety systems have been tested too, including the overcurrent detection system.

Some insulation tests have then been done according to standard IEC 61439. Insulation resistance has been measured at 150 V: 1 MΩ has been found, higher than 230 kΩ value suggested by the standard.

Moreover, the leakage current has been verified both in AC (2 kV) and DC (2.7 kV). The resulting value of 7.5 mA is lower than the 100 mA limit set by the standard.

The ground resistance tests have been performed too.

By switching ON and OFF the IGBTs of the main diagonal for each H bridge, with 850 V of DC link, full voltage tests have been performed, using a 900 Ω resistive load.

Finally, using an ohmic-inductive load of 0.35 Ω and 53 mH, some full-power tests have been done. First, PLECS simulations have been completed to predict the behavior of the system.

With a duty cycle lower than 50%, no significant current has been detected, while with 54% duty cycle, a current of 200 A corresponding to the average current in the real application has been measured.

Since it is not possible to perfectly simulate a real system with stray parameters (capacitances, inductances, resistances and switching ON OFF time delays), differences between simulation and reality are justified. In general: if the duty cycle is lower than 50%, the current is low, while beyond a duty cycle of 50%, current starts increase and it reaches 200 A at a duty cycle of 54%.

Also the evaluation of thermal load has been done for the most stressed H bridge (the central one) by monitoring the temperature and the thermal pictures of all the cabinet have been taken.

Moreover, two kind of IGBTs (Semikron SEMiX603GB17E4p and Infineon FF600R17ME4) have been tested and their behavior has been verified in parallell in order to ensure greater spare parts availability for future development of the project.

Chapter 5 Conclusion

SEA TITAN project started in April 2018 and, after three years, it has been concluded in September 2021, showing the expected results in every sector involved: from the theoretical modelling of the machine to the laboratory dry tests of the overall system.

The project has been developed by many partners from all over Europe in the framework of EU Horizon 2020 and it required many efforts, knowledge and great vision toward the future.

5.1 SEA TITAN project

In a world with growing energy demand, new energy sources are investigated and, obviously, one single answer is not enough.

There are different problems, such as the waste of resources, the bad management of available energy, the inequal distribution of energy sources and the growing world population.

For these reasons, there is the necessity to differentiate the available pool of exploitable energy sources, in order to both guarantee the power extraction in every condition possible (of time and space, thereby enhancing an equal distribution of the energy around the world) and to promote alternative renewable energy sources, instead of traditional sources often based on fossil fuels such as oil, gas or coal.

Alongside the well-known renewables as wind, photovoltaic, geothermal, biomass, another energy source has been studied since the ‘70s: the wave power.

5.1.1 THE AIM OF THE PROJECT

Despite its low level of diffusion, wave power has many advantages: constancy, predictability and large diffusion all over the world. Unfortunately, these advantages do not match with a satisfactory power extraction technology.

Since other renewables have already found their optimized configuration (for example the three blade shape for large wind turbines), the aim of SEA TITAN project has been the search for a solution easily adaptable to different WEC configurations, with the purpose to open the

path for future research to the scientific world and to intensificate efforts toward this kind of energy source by focusing the studies on a commonly accepted configuration.

With a not-consolidated technology, indeed, there are many problems caused by the diversification of approach and the development time is stretched for too long. The introduction of a precise starting point which is robust, cost-effective, versatile and economically viable can give a relevant boost to the entire research sector, thereby promoting contribution from different research centres toward a common idea and starting to create a dedicated supply chain (the lack of which is nowadays reflected in high initial costs).

Keywords of the entire project have been crosscuttingness, robustness, adaptability, versatility and cost-effectiveness. Due to the aim of SEA TITAN, namely "to open the path to further optimization of the wave energy extraction technology", the solution presented is as general as possible, fully exploitable in any conditions and easy adaptable to already existent projects, in order to become a standard answer.

5.2 Phases of the work

The starting point has been the W1 prototype with the W200 PTO already deployed and tested near Gran Canaria in 2014. It has been possible to start from collected real data, from which the optimization for the new AMSRM configuration has begun.

The overall workload has been divided among different partners and the various portion have been then united. Collaboration with different partners from all over Europe has been an effective way to exchange opinions and ideas and to ampliated the resonance of the project.

5.2.1 SIMULATIONS STUDY

In order to complete the design of the power electronics, a simulation model of the system has been studied, including a little bibliographic research on the particular type of machine used (AMSRM PTO), which is not very common and with a very short history in the scientific research. Many studies on the model as well as on the parameters optimization for the machine have been omitted in the thesis. A MATLAB Simulink simulation has been implemented including the overall system developed to analyse the power electronics converters with PLECS.

5.2.2 POWER ELECTRONICS DESIGN

The main focus of the PhD has been the power electronics design. Together with OCEM Power Electronics, a company specialized in power electronics solutions for physics laboratories applications and high technology innovation fields, the power electronics cabinet for SEA TITAN has been designed. Although the power electronics design is not innovative, the idea to adapt a well-known system traditionally made for land-based laboratories to a ocean environment, with many different situation to be taken into account, has been very challenging. A configuration which is modular, compact, easy adaptable to different shapes has been designed.

The typical external mechanical configuration for a wave energy harvesting systems is the cylindrical one. Even if the power electronics section has been shaped in order to make a system suitable for dry laboratory test, thanks to the division of the whole GSC in three different H bridges, it can be organized easily in different configurations.

Components have been chosen in order to have high reliability, with good safety margins and considering any fault possible.

The control electronics adaptation board has been designed with safety margins too, considering also a redundancy in protection intervention to enhance reliability.

Also, the easiness of maintenance has been taken into account, as well as the choice of largely diffused components, in order to make the maintenance as easy as possible for an apparatus which is typically difficult to be reached in case of fault.

5.2.3 POWER ELECTRONICS TESTS

Once the power electronic system has been built, it has been tested associated whit the grid-connected active front end commercially purchased. In the occasion, also the control electronic board has been tested. Tests have been performed at full voltage and full power, reaching heating conditions very similar to those of the real application, thereby validating also the cooling system. Before starting, every caution has been taken in order to ensure integrity of the system to prevent any disruptive consequence in case of failure and to guarantee the safety of the personnel involved in the testing process, according to related standards.

5.3 Drawbacks

The main drawback of any kind of WEC is related with the harsh marine environment, where maintenance is often difficult and materials can suffer from corrosion and strong mechanical stresses. To prevent failures and interventions, robustness is a key feature in the design of a WEC, and the simplicity of SEA TITAN project, as well as the choice for a switched reluctance generator with a robust hysteresis control and a simple power electronics converter, is in line with this necessity.

Another disadvantage of wave energy conversion systems is the environmental impact, already deeply discussed. In any case, especially when dealing with arrays composed by more WECs, also an environmental impact analysis is necessary.

Regarding the solution of the direct-drive PTO for a WEC, the main drawback is the low velocity of the translator (in case of a linear machine like SEA TITAN project) with respect to the stator. This is due to the low velocity in rising and falling of ocean waves (meaning a low frequency of the waves). Even with a machine designed to extend its range of velocity (as for SEA TITAN), required forces are high to reach a certain output power level.

Higher forces mean higher currents in the generator (in a linear relation) with an important increase in losses (in a square relation) and in attractive forces between stator and translator.

Also the power electronics section has been designed to manage such currents and safety systems and measurement systems have been chosen to match these high requirements.

5.4 Conclusion

The present thesis focuses on the design of a modular power converter suitable for wave energy harvesting purposes, associated with an innovative linear switched reluctance electrical machine and showing a new azimuthal mechanical configuration. Although many innovations and peculiar design strategies have been adopted, the result maintains the purpose to be crosscutting in order to establish a standard for future marine energy development. Thanks to the robustness, adaptability, versatility and the easiness of construction, the project has reached its scope.

Future developments include the dissemination of results in an open-hardware vision so that other research centers as well as ocean wave energy companies can bring optimizations and new ideas to establish standard choices and solid paths to make ocean wave renewable energy a sustainable alternative for the future.

References

[1] A. Pecher and J. P. Kofoed, Handbook of Ocean Wave Energy, Springer International Publishing, 2017.

[2] F. Blaabjerg, H. Liu and P. C. Loh, "Marine Energy Generation Systems and Related Monitoring and Control," *IEEE Instrumentation & Measurement Magazine*, vol. 17, no. 2, pp. 27 - 32, April 2014.

[3] A. Muetze and J. Vining, "Ocean Wave Energy Conversion - A Survey," in *IEEE IAS Annual Meeting*, Tampa, FL, USA, 8-12 Oct. 2006.

[4] B. Czech and P. Bauer, "Wave Energy Converter Concepts," *IEEE Industrial Electronics Magazine*, June 2012.

[5] J. Cruz, Ocean wave energy_current status and future perspectives, Springer, 2008.

[6] R. Bhattacharyya and M. E. McCormick, Wave Energy Conversion, Elsevier Academic Press, 2003.

[7] M. Lafoz, M. Blanco, G. Navarro, P. Moreno-Torres and C. Vasquez, "Laboratory tests before sea trial of a wave energy converter," in *IEEE ICIT 2015*, Seville, Spain, 17-19 March 2015.

[8] Z. Liu, R. Zhang, X. H. and X. Wang, "Survey of the mechanisms of power take-off (PTO) devices of wave energy converters," *Acta Mechanica Sinica,* vol. 36, pp. 644-658, 2020.

[9] A. Têtu, in *Power take-off systems for WECs*, 2017, pp. 203-220.

[10] R. Ahamed, K. McKee and I. Howard, Advancements of wave energy converters based on power take off (PTO) systems: A review, Perth, Australia: Department of Mechanical Engineering, Curtin University, 2020.

[11] D. Greaves and G. Iglesias, Wave and Tidal Energy, Wiley, 2012.

[12] M. Folley, Numerical Modelling of Wave Energy Converters. State-of-the-Art Techniques for Single Devices ans Arrays, Academic Press, 2016.

[13] A. Chen, R. Nilssen and A. Nysveen, "Performance Comparisons Among Radial-Flux, Multistage Axial-Flux, and Three-Phase Transverse-Flux PM Machines for

Downhole Applications," *IEEE Transactions on Industry Applications,* vol. 46, pp. 779-789, 2010.

[14] P. Khatri and W. X., "Comprehensive review of a linear electrical generator for ocean wave energy conversion," *IET Renewable Power Generation,* no. 14, pp. 949-958, 2020.

[15] A. LiVecchi, A. Copping, D. Jenne, A. Gorton, R. Preus, G. Gill, R. Robichaud, R. Green, S. Geerlofs, S. Gore, D. Hume, W. McShane, C. Schmaus and H. Spence, Exploring opportunities for marine renewable energy in meritime markets, U.S. Department of Energy (DOE), 2019.

[16] L. Hai, M. Goteman and L. M., "A Methodology of Modelling a Wave Power System via an Equivalent RLC Circuit," *IEEE Transactions on Sustainable Energy,* vol. 7, pp. 1362-1370, 2016.

[17] M. Blanco, G. Navarro and M. Lafoz, "Control of Power Electronics driving a Switched Reluctance Linear Generator in Wave Energy Applications".

[18] D. V. Evans and A. F. O. d. Falcão, "Hydrodynamics of Ocean Wave-Energy Utilization," in *IUTAM Symposium,* Lisbon/Portugal, 1985.

[19] M. Blanco, M. Lafoz, G. Navarro, J. Torres, J. Najera, M. Mantellini and R. Morici, "Design and Control of a Modular Power Electronics Back-to-Back Converter for Wave Energy Harvesting Applications," in *EPE ECCE 2020*, Lyon, France, 7-11 Sept. 2020.

[20] M. Blanco, J. Torres, M. Santos-Herrán, L. García-Tabarés, J. Nájera, D. Ramírez and M. Lafoz, "Recent Advances in Direct-Drive Power Take-Off (DDPTO) Systems for Wave Energy Converters Based on Switched Reluctance Machines (SRM)," in *Ocean Wave Energy Systems*, Springer, Cham, 2021, pp. 487-532.